Centre for Ore Deposit and Exploration Studies

# Proterozoic sediment-hosted base metal deposits

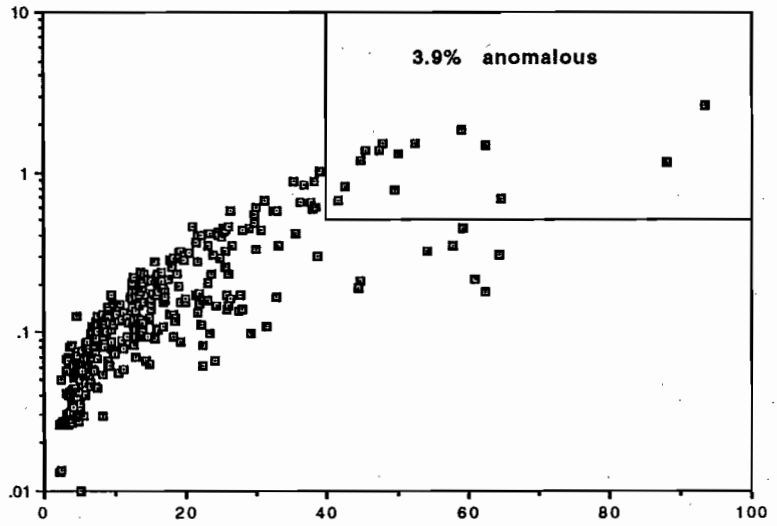


**AMIRA/ARC Project P384**
**Report No. 5**

UNIVERSITY OF TASMANIA

June 1994

Centre for Ore Deposit and Exploration Studies

# Proterozoic sediment-hosted base metal deposits

AMIRA/ARC Project P384
Report No. 5

UNIVERSITY OF TASMANIA

June 1994

# Contents

# Introduction

## Project Objectives: P384

1. To determine the primary geological, geochemical and structural controls on the location and timing of hase metal deposits in sedimentary basins.

2. To understand the chemical and hydrological evolution of metalliferous brines in selected Proterozoic sedimentary basins of Australia.

3. To develop basin metallogenic models and specific ore deposit models that may be used in the exploration for large-tonnage base-metal ore deposits.

## Research framework

This research project involves a multi-disciplinary approach using regional geological, geophysical and structural studies, brine chemical modelling and geochemical and isotopic halo studies to provide a foundation of which to build a network of exploration criteria and ore deposit models for major sediment-hosted base metal deposits.

The project consists of three research modules as outlined below:

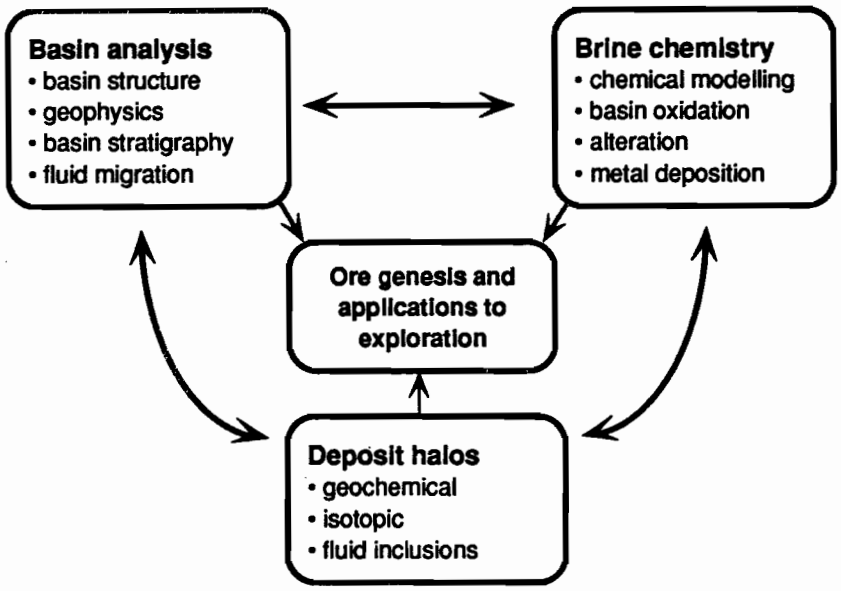

## This report

This is the fifth major report on the project and comes at the end of just over two years of research. In this report emphasis is given to further development of the lithogeochemical halo studies and their application to exploration for stratiform lead–zinc deposits. In this regard a database of lithogeochemistry for the McArthur Basin sediments has been established and background distributions for alteration vectors have been determined for the major stratigraphic units. The alteration index approach to exploration has been tested in a number of case studies; including several subbasins in the McArthur Basin and the Kamarga Prospect on the Lawn Hill Platform. The results of this work are very exciting and confirm the importance of lithogeochemistry in exploration for sedex deposits.

In parallel with our applied studes on alteration vectors we report on the results of more fundamental research on iron carbonate formation and its relationship to ore genesis, and fluid flow studies along the Tawallah Fault.

This work will be presented at the mid-year field meeting in Darwin on 14–15 June followed by a field trip through the McArthur basin to visit areas relevant to the previous and on-going research program.

Particular thanks are extended to AMIRA, the sponsor companies, NTGS and AGSO for their continued support in the planning and execution of this research program.

Ross Large
Director, CODES

# Summary of Research Findings

## Refinement of the Sedex Alteration Index and $MnO_D$ vectors

— Ross Large and Peter McGoldrick

Refinements to the alteration index defined by Large and McGoldrick (1993) have been undertaken in order to improve its value as an exploration tool for stratiform lead–zinc deposits. By combining alteration index with the manganese content of dolomite (MnOD) in the same graphical plot it has been possible to establish criteria to set priorities on particular data sets from either surface rock samples or drill core samples. Four priority zones have been set up from zone 1 — immediate priority to zone 4 — low priority.

## Background data on Sedex AI and $MnO_D$ for McArthur Basin sediments

— Ross Large

A database for lithogeochemistry of sediments in the McArthur Basin has been established using the previously published data sets, which comprise in total 470 surface samples and 246 drill core samples. Analysis of the data base indicates that the background alteration index varies from 0 to 40 and the background $MnO_D$ varies from 0.02 to 0.5 wt% for samples with CaO > 1 wt%. The dolomite content of the "background" sediments has a considerable influence on the calculated alteration index, such that pure dolomites have a mean of around 10, and weakly dolomitic shales have a mean of around 40. Using AI vs $MnO_D$ plots for the database it has been possible to assess the various stratigraphic units in the McArthur Basin in terms of their potential to host stratiform Pb–Zn deposits. This procedure indicates that, in addition to the Barney Creek Formation, the Lynott Formation has a very high potential to host lead–zinc ore deposits.

## Case Studies: Application of the Alteration Index to selected areas in the McArthur Basin

— Ross R. Large

Application of the refined alteration index procedure to three sub-basins in the McArthur Basin has indicated the potential for further stratiform Pb–Zn deposits remote from the HYC deposit. Two favourable horizons identified in the BMR 2 area, 25 km SW of HYC, are confirmed by our recent sampling, however the AI and $MnO_D$ anomalies are considered to relate to HYC rather than more proximal deposits. Evaluation of previous sampling (Brown et al., 1969) in the Top Crossing area (60 km SW of HYC) indicates the presence of a favourable horizon with high potential for lead–zinc mineralisation, down plunge, adjacent to the Tawallah Fault. In the Glyde Sub-basin (80 km S of HYC), drill hole lithochemical sampling by Shell Metals indicates a favourable horizon with anomalous alteration character intersected in one of the ten drillholes.

## Application of the Alteration Index to the Kamarga zinc–lead deposit: preliminary report

— Peter McGoldrick

This report reviews the geology of the large, low-grade, sub-economic, stratabound Kamarga deposit, and presents an assessment of existing core grind whole-rock geochemical data (Jones, 1986) using the Alteration Index (AI) and $MnO_D$ index developed for Lady Loretta and HYC by Large & McGoldrick (1993). The Kamarga data *do not* have patterns like those from the stratiform deposits. Hence, application of the AI could have substantially down-graded the prospectivity of the deposit at an earlier stage of drilling (the data presented here are from four of eighteen diamond drill holes through the Kamarga mineralisation).

## Progress report: Conditions of formation for siderite and ferroan carbonate — implications for the formation of sediment hosted base metal deposits

— David Cooke, Ross Large and Peter McGoldrick

Our recent research has emphasised the importance of siderite and ferroan dolomite in the halo to stratiform sediment-hosted zinc–lead deposits. Thermodynamic modelling of siderite and ferroan dolomite stability places important constraints on the genesis of these deposits. This work demonstrates that $CO_2$ fluid concentration is probably the dominant control on hydrothermal carbonate formation. Siderite and ferroan dolomite are stabilised at high $\Sigma C$ and low $\Sigma S$ concentrations. Lower temperatures will stabilise siderite at constant $a_{CO2}$. Ferroan carbonates that form under relatively oxidised to oxidised conditions in association with pyrite or hematite are favoured by lower temperatures and/or high $\Sigma S$ concentrations, and have the potential to be associated with base metal-rich solutions.

Our calculations indicate that for siderite to form with lead–zinc by exhalation, then at least 250–500 m water depth is required to prevent fluid boiling. Alternatively siderite can form by sub-surface replacement of dolomitic sediments below the palaeowater table.

## Analysis of fluid flow during late stage wrenching of the Tawallah Fault system, southern McArthur Basin, Northern Territory: a fluid inclusion approach

— Jamie Rogers

A fluid inclusion study of the quartz–hematite hydraulic breccias along the Tawallah Fault system indicates that hot (~210°C), saline, oxidised fluids passed through the fault during late-stage wrench movements associated with post-Roper deformation. Enthalpy–chlorite plots suggest that the hot fluids were boiling, and mixing with colder fluids during hematite–quartz deposition. High-heat-producing granites are proposed as a heat source for the fluids, as the system was active well after rifting and volcanism had ceased.

The presence of hot, saline, oxidised fluids lend great potential for mineralisation throughout the entire history of the southern McArthur Basin along the Tawallah Fault and similar fault systems where reduced (graphite and/or pyrite bearing) sediments are juxtaposed against the structure. The results may also provide an insight into processes that occurred along the Emu Fault system during the formation of base metal mineralisation at McArthur River.

## Alteration vectors applied to the Mount Isa Pb–Zn system: a review of existing data

— Peter McGoldrick

This presentation will review some of the published available whole rock geochemical data for the Mount Isa mineralised sequence and associated Mount Isa Group sedimentary rocks.

# Refinement of the Sedex Alteration Index and $MnO_D$ Vectors

**Ross Large and Peter McGoldrick**
*CODES Key Centre*

## Summary

Refinements to the alteration index defined by Large and McGoldrick (1993) have been undertaken in order to improve its value as an exploration tool for stratiform lead–zinc deposits. By combining alteration index with the manganese content of dolomite ($MnO_D$) in the same graphical plot it has been possible to establish criteria to set priorities on particular data sets from either surface rock samples or drill core samples. Four priority zones have been set up from zone 1 — immediate priority to zone 4 — low priority.

## Introduction

In our previous AMIRA report (No.3, October 1993) we outlined the development of an alteration index which has the potential to be an excellent vector toward stratiform Pb–Zn mineralisation. The alteration index combined with another parameter $MnO_D$ (calculated manganese content of dolomite) defines halos around the Lady Loretta and HYC deposits which extend up to 25 km along strike from economic ore. Our research has defined the basis for a new approach to Sedex exploration which uses lithogeochemical stratigraphic drilling (LSD) to define potential ore horizons followed by lithogeochemical vector drilling (LVD) to target the ore deposit (Large & McGoldrick, 1993: 123–124).

## Factors in the alteration index

The alteration index (AI) as defined by Large & McGoldrick (1993) is

$$AI = \frac{[FeO + 10MnO]}{[FeO+10MnO+MgO+Na_2O]} \times 100$$

for samples with $CO_2$ >1%.

Background values for Proterozoic sediments on the Lawn Hill Platform and McArthur Basin vary from 0 to 40, while sediments in the halo to Pb–Zn mineralisation increase from 40 to 100 approaching mineralisation. The factors which control the index are discussed below:

FeO — increases in Fe content of carbonates, or pyrite development in the sediments, will lead to increases in the AI value approaching ore.

MnO — increases in the Mn content of carbonate cause increases in the AI index approaching mineralisation.

MgO — decreases approaching mineralisation due to substitution of Fe and Mn for Mg in dolomite, and/or replacement of dolomite by siderite.

$Na_2O$ — decreases towards ore at Lady Loretta due to replacement of dolomite by siderite (Large & McGoldrick 1993: Fig. 8). However, an opposite trend of increasing $Na_2O$ in the

footwall approaching ore is observed in the HYC sediments.

CaO — shows a marked decrease towards ore in the footwall at HYC due to an increase in the ratio of shale facies to dolomite facies. At Lady Loretta, on the other hand, CaO decreases toward ore due to replacement of dolomite ($CaMg(CO_3)_2$) by siderite ($FeCO_3$).

It is strongly recommended that the AI should not be applied to sediments with less than 1% $CO_2$, as these contain insufficient carbonate to give meaningful results. In dolomitic rocks 1% $CO_2$ is equivalent to about 1% CaO.

## Refinement of the alteration index

Due to the variable correlation of $Na_2O$ with the alteration index as outlined above it has been decided to delete this parameter. We now define the Sedex alteration index as:

$$\text{Sedex AI} = \frac{[FeO + 10MnO]}{[FeO+10MnO+MgO]} \times 100$$

for samples with $CO_2 > 1\%$.

As shown in Figure 1, the effect of deleting $Na_2O$ from the AI is minimal. On graphs of Zn vs AI for both the Lady Loretta and HYC halos, the patterns are virtually identical for AI *with* $Na_2O$ and AI *without* $Na_2O$.

## Combining Sedex AI and $MnO_D$

Although the Sedex AI and $MnO_D$ vectors have similar and related elemental factors they measure different geochemical/lithological variations in the rock.

- $MnO_D = \frac{MnO \times 30.41}{CaO}$

is the calculated percentage of MnO in dolomite within the rock.

- Sedex AI is also affected by the MnO content of dolomite, but is related to other factors including:
  - Fe content of dolomite
  - pyrite content of the sediment
  - dolomite/shale ratio of the sediment.

Thus a dolomitic sediment with a high FeMn dolomite mineralogy, including pyrite and a low ratio of dolomite to shale will produce a high Sedex AI value.

By combining Sedex AI and $MnO_D$ in a graphical manner (Fig.2), it is possible to get maximum information from these two vectors. In Figure 2, the $MnO_D$ vs AI plot is divided into four priority zones:

Zone 1 — Immediate priority: $MnO_D > 2\%$, AI > 80 (close to ore)

Zone 2 — Very High Priority: $MnO_D > 1\%$, AI > 60.

Zone 3 — High Priority: $MnO_D > 0.5\%$, AI > 40.

Zone 4 — Low Priority: $MnO_D > 0.2\%$, AI > 20 (potential horizon but very distal from ore).

Drill hole or surface outcrop samples consistently plotting in zones 1 to 3 require follow-up, whilst zone 4 is merging with the background data and indicates a potential horizon but the need for lower priority follow-up.

## Elements to analyse, and assessment procedure

In order to apply the Sedex AI and $MnO_D$ vectors to exploration drilling, the following procedures need to be followed.

1. Select sediment samples at 10 m intervals down the full length of the drill hole. Samples should be about 20 cm in length, of half core.

2. Analyse samples for FeO, MnO, CaO, MgO, Zn, Pb, Cu, S and $CO_2$. ICP is suitable for all elements except $CO_2$.

3. Determine the dominant type of carbonate present by plotting the following graphs:
   - FeO vs $CO_2$ → siderite present?
   - MgO vs CaO → identify dolomite, calcite.
   - CaO vs $CO_2$ → identify dolomite, calcite, siderite.

4. Divide data-base into two groups:
   Group A — samples with CaO ≥ 1%.
   Group B — samples with CaO < 1%

5. Group A (CaO ≥ 1%)
   - Calculate Sedex AI
   - Calculate $MnO_D$
   - Plot Sedex AI vs Zn
   - Plot Sedex AI vs $MnO_D$
   - Plot Sedex AI vs meterage down hole
     Plot Zn vs meterage down hole
     Plot $MnO_D$ vs meterage down hole
   - Identify anomalous horizons from drill hole plots.
   - Identify anomalous sample sub-set with AI > 40 and $MnO_D$ > 0.5%.

6. Group B (CaO < 1%)
   - Determine if siderite is present by plotting FeO vs $CO_2$
     - if no siderite, discard this group
     - if siderite present, then continue
   - Calculate Sedex AI
   - Calculate $MnO_S$
   - Plot Sedex AI vs Zn
   - Plot Sedex AI vs $MnO_S$
   - Plot Sedex AI vs meterage down hole
     Plot Zn vs meterage down hole
     Plot $MnO_S$ vs meterage down hole
   - Identify anomalous siderite horizons from drill hole plots
   - Identify anomalous siderite sample set with AI > 40 and $MnO_S$ > 0.5%.

## Reference

Large, R.R. & McGoldrick, P., 1993: Primary geochemical halos related to Proterozoic sediment-hosted Pb-Zn deposits, and applications to exploration. AMIRA P384, unpublished report 4: 63–126.



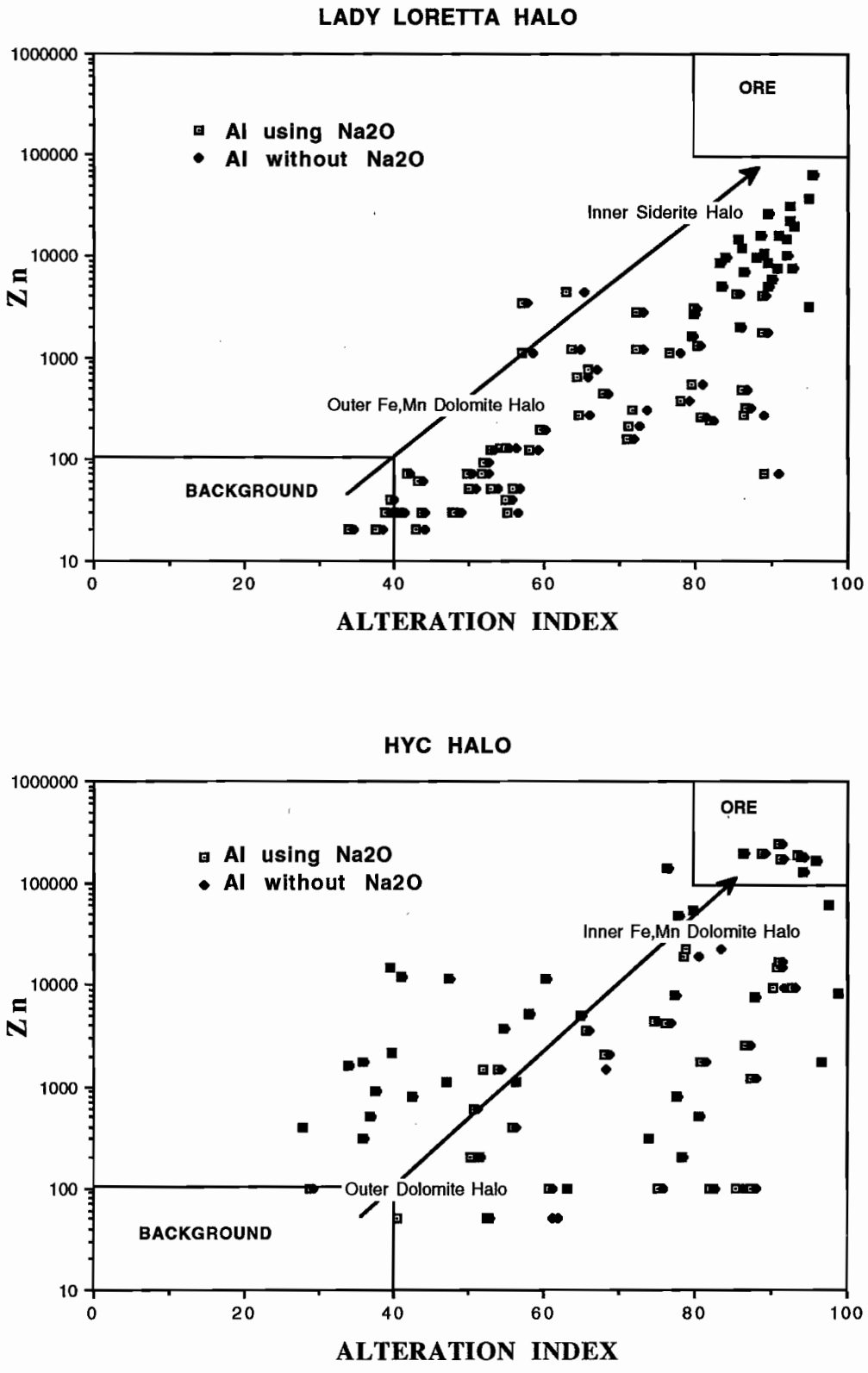


*Figure 1 — Variation in alteration index (AI) with zinc content in the haloes to Lady Loretta and HYC. The AI varies from 30 to 100 approaching the orebody in both deposits. Note the minimal effect of $Na_2O$ in the value of AI in both cases.*

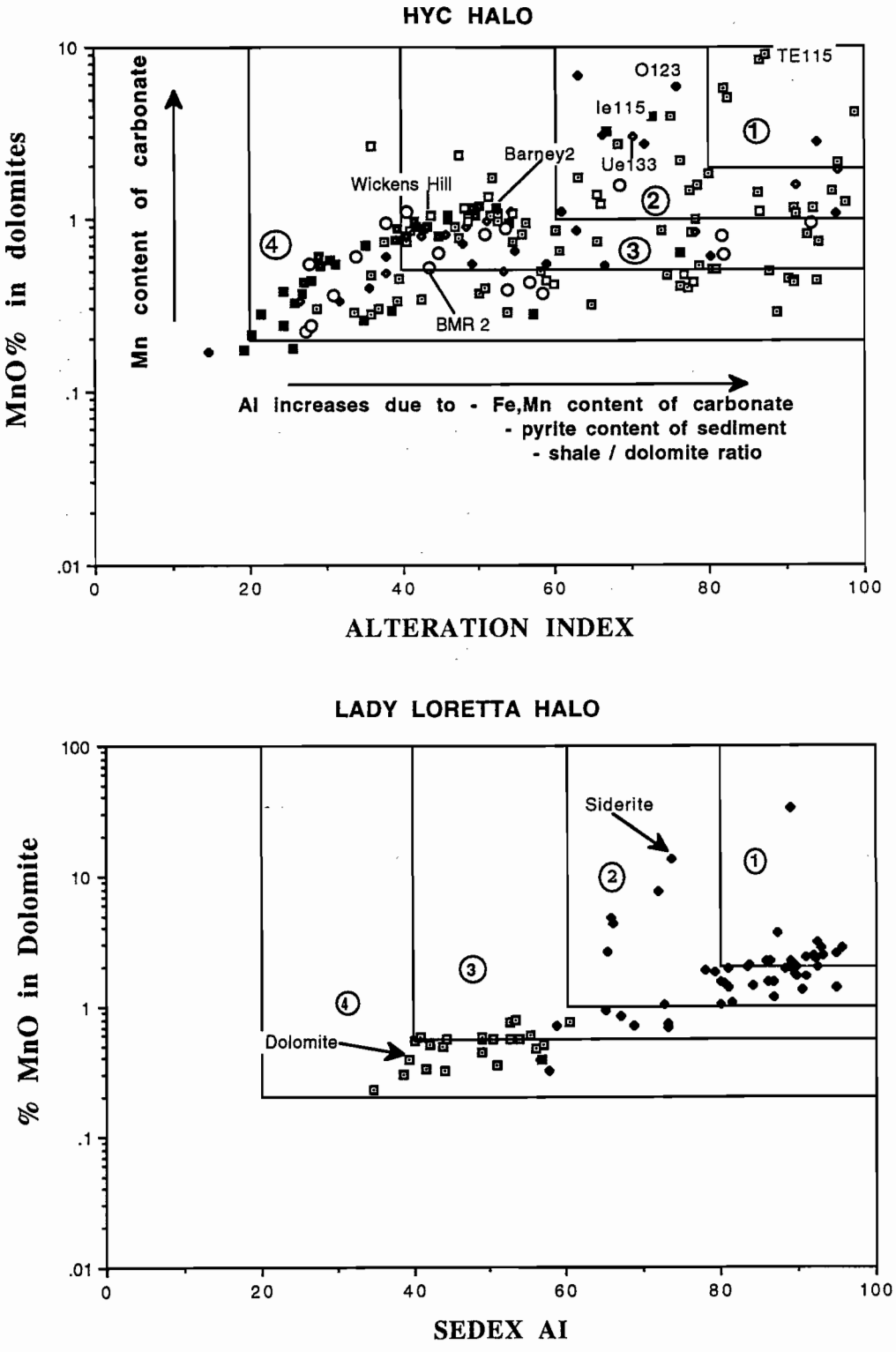


*Figure 2 — Priority zones defined on an AI vs $MnO_D$ plot for the HYC and Lady Loretta haloes. Zone 1: immediate priority (adjacent to ore). Zone 2: very high priority. Zone 3: high priority (distal position). Zone 4: low priority (very distal, >50 km).*

# Background Data on Sedex AI and $MnO_D$ for McArthur Basin Sediments

**Ross Large**
*CODES Key Centre*

## Summary

A database for lithogeochemistry of sediments in the McArthur Basin has been established using the previously published data sets, which comprise in total 470 surface samples and 246 drill core samples. Analysis of the data base indicates that the background alteration index varies from 0 to 40 and the background $MnO_D$ varies from 0.02 to 0.5 wt% for samples with CaO > 1 wt%. The dolomite content of the "background" sediments has a considerable influence on the calculated alteration index, such that pure dolomites have a mean of around 10, and weakly dolomitic shales have a mean of around 40. Using AI vs $MnO_D$ plots for the database it has been possible to assess the various stratigraphic units in the McArthur Basin in terms of their potential to host stratiform Pb–Zn deposits. This procedure indicates that, in addition to the Barney Creek Formation, the Lynott Formation has a very high potential to host lead–zinc ore deposits.

## Introduction

In order to successfully apply and interpret the Sedex AI and $MnO_D$ vectors, it was recognised at the previous AMIRA P384 meeting that there was a need to acquire a comprehensive database of sediment geochemistry for the McArthur Basin and Lawn Hill platform. Our immediate objective was to compare samples in the halo of HYC and Lady Loretta to "background" or "barren" sediments that are well removed from mineralisation. A second consideration was to evaluate the use of the AI and $MnO_D$ vectors on surface rock samples compared to unweathered drill core samples.

## Lithogeochemical data for the McArthur Basin

Fortunately for this project, there have been three previous studies of rock geochemistry in the McArthur Basin.

- Brown, M.C., Claxton, C.W. and Plumb, K.A., 1969: The Proterozoic Barney Creek Formation and some associated carbonate units of the McArthur Group, Northern Territory. BMR Record No. 1969/145.

- Large, D.E., 1979: Rock geochemistry study. McArthur Basin Project. Federal Institute for Geosciences and Natural Resources (BGR), Hanover, Archiv. Nr. 82032.

- Plumb, K.A., Wyborn, L.A.I. & Ryburn, R.J., 1992: McArthur Basin and Murphy Inlier Rockchem data set documentation. BMR Record 1992/37.

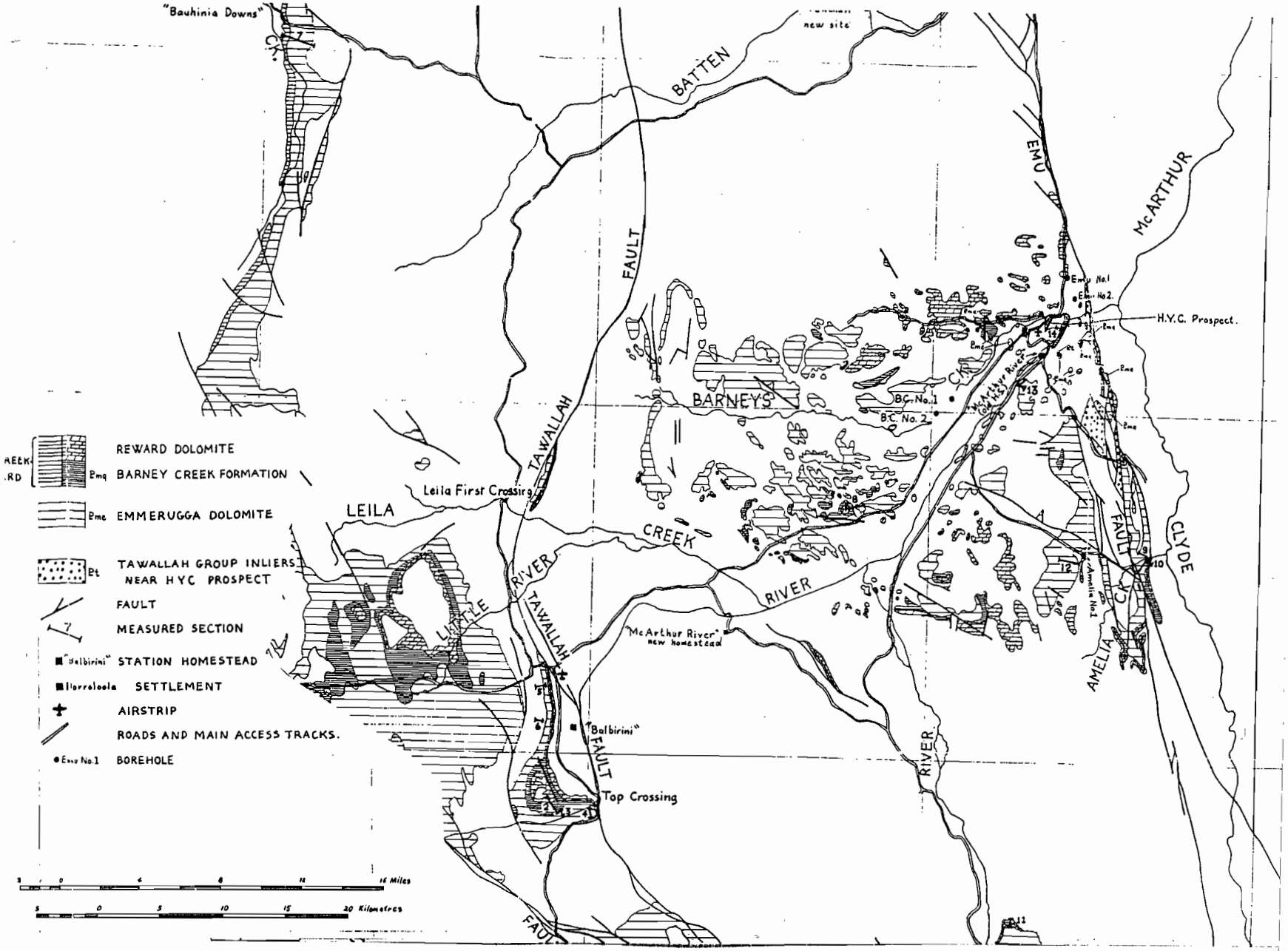


*Figure 1 — Sample traverse locations for the Brown et al. (1969) data set. Traverses are highlighted in yellow.*

From these studies a database of partial geochemical analyses has been established, which includes 771 sediments from both surface outcrop and drill core. Because different geochemical methods were used for each data set they will be discussed separately below.

## The Brown et al. (1969) data set

Brown et al. collected a total of 360 surface samples from 14 separate measured sections in the McArthur Basin. Locations of the sections are shown in Figure 1. Samples were collected from the following formations in the McArthur Group

Reward Dolomite
Barney Creek Formation
Teena Dolomite
(incl. Coxco Dol. member)
Emmerugga Dolomite
(incl. Mara Dolomite and Mitchell Yard Dolomite members)
Myrtle Shale
Tooganinie Formation

Figure 2 provides a stratigraphic column for reference.

The samples were analysed for Ca, Mg, K, Fe, Mn, P, Zn, Pb, Cu, Ni, Co and acid insoluble residue. Details of analytical techniques are given in Brown et.al. (1969: 39-41).

### Discussion of the data

The plot of MgO vs CaO in Figure 3a shows that dolomite is the dominant carbonate mineral in the great majority of sediments sampled. Four samples show high CaO/MgO ratios, suggesting a significant component of calcite in the carbonate sediments.

Plots of Sedex AI vs Zn and Sedex AI vs $MnO_D$ (Figs 3b and 3c) indicate that the background AI values are concentrated in the interval 0 to 20 with a spread of samples up to AI = 75. Zinc values are commonly less than 50ppm and $MnO_D$ varies from 0.01 to 2.65 wt% with the majority of samples from 0.03 to 0.3 wt%. Based on the priority zones defined by Large & McGoldrick (1994) 3.9% of the samples have both anomalous AI and $MnO_D$ at a level indicative of proximity to stratiform Pb–Zn mineralisation.

### Breakdown of analysis by formation/member

The data set has been divided into Formation, or Member where appropriate, and Sedex AI, $MnO_D$ relationships are plotted in Figure 4. The following comments are relevant to this breakdown:

- Reward Dolomite — shows a background distribution with no anomalous samples.

- Barney Creek Formation — 24% of the samples are anomalous in both AI and $MnO_D$. This is expected in light of the fact that the Barney Creek Formation is host to the HYC deposit. The one sample (no. 1503) which plots in high priority zone 1 (AI > 80, $MnO_D$ > 2%) was taken from an outcrop situated 490m SSW of the HYC V121 prospect shaft.

- Coxco Dolomite member (Teena Dolomite Formation) — most samples give a background pattern with AI < 20. One sample is anomalous (Priority 3).

- Teena Dolomite — no anomalous samples.

- Mitchell Yard Member (Emmerugga Dolomite Formation) — the samples plot as a classic background curve indicating relatively pure dolomite with little shale or pyrite enrichment.

- Mara Dolomite Member (Emmerugga Dolomite Formation) — no anomalous samples.

- Myrtle Shale — no anomalous samples.

- Tooganinie Formation — no anomalous samples. Samples with AI > 20 probably contain an increased shale component.

## BRG database

Large (1979) reports major and trace element analyses from 210 surface rock samples taken from various stratigraphic formations in the McArthur Group; in particular, the Barney Creek Formation, Teena Dolomite, Tooganinie Formation, Amelia Dolomite and the Mallapunya Formation. Selected graphs of the data with CaO > 1% are shown in Figures 6 and 7.

### Discussion of the data

The samples are principally dolomitic siltstones (Fig. 6a) with a few outliers due to presence of calcite or magnesite (5% of samples). The majority of samples give AI values of 5 to 40 with 8.4% of the samples plotting in the anomalous field. Zinc values are generally less than 100ppm with a high proportion of samples recording 1ppm. Such low values are not reported in the other two data sets and indicate the possibility of analytical error in Zn for the BRG samples.

### Breakdown by Formation (Fig. 7)

The Barney Creek Formation and Mallapunya Formation show the highest percentage of anomalous samples (14% and 17% respectively). The Teena Dolomite and Tooganinie Formation show background distributions with no anomalous samples, supporting the same result from the Brown et.al. data set. The Amelia Dolomite has one anomalous sample in the priority 3 zone.

The Barney Creek Formation is the only unit sampled which contains data in the very high priority zones 1 and 2 (Fig. 7a).

### Relationship between lithofacies and alteration index

The BRG data-set was divided into four lithofacies based on calculated dolomite content.

- Shales with <25% dolomite component.
- Dolomitic shales with 25-50% dolomite component.
- Shaley dolomites with 50-75% dolomite component.
- Dolomites with 75-100% dolomite component.

These groups, plotted in Figure 8, indicate a gradual increase in AI and $MnO_D$ values passing from the dolomite lithofacies through to the shale lithofacies. The dolomites have a mean AI of around 10, the shaley dolomites about 20, the dolomitic shales about 25 and the shales about 40. Thirty-one percent of the shales have both anomalous AI and $MnO_D$, while less than 2% of the dolomites are anomalous.

## Rockchem database

The Rockchem data-base for the McArthur Basin and Murphy Inlier (Plumb et.al., 1992) contains 607 samples. A subset of 246 samples of chemical sediments with CaO > 1 wt% was selected for this particular study of the McArthur Basin lithochemistry. The samples are drill core from a series of holes remote from the HYC deposit — Amoco 82-5, Amoco 82-6, Mant 78-1 and Leila Yd 1 (Fig.8). Formations intersected by these drill holes are

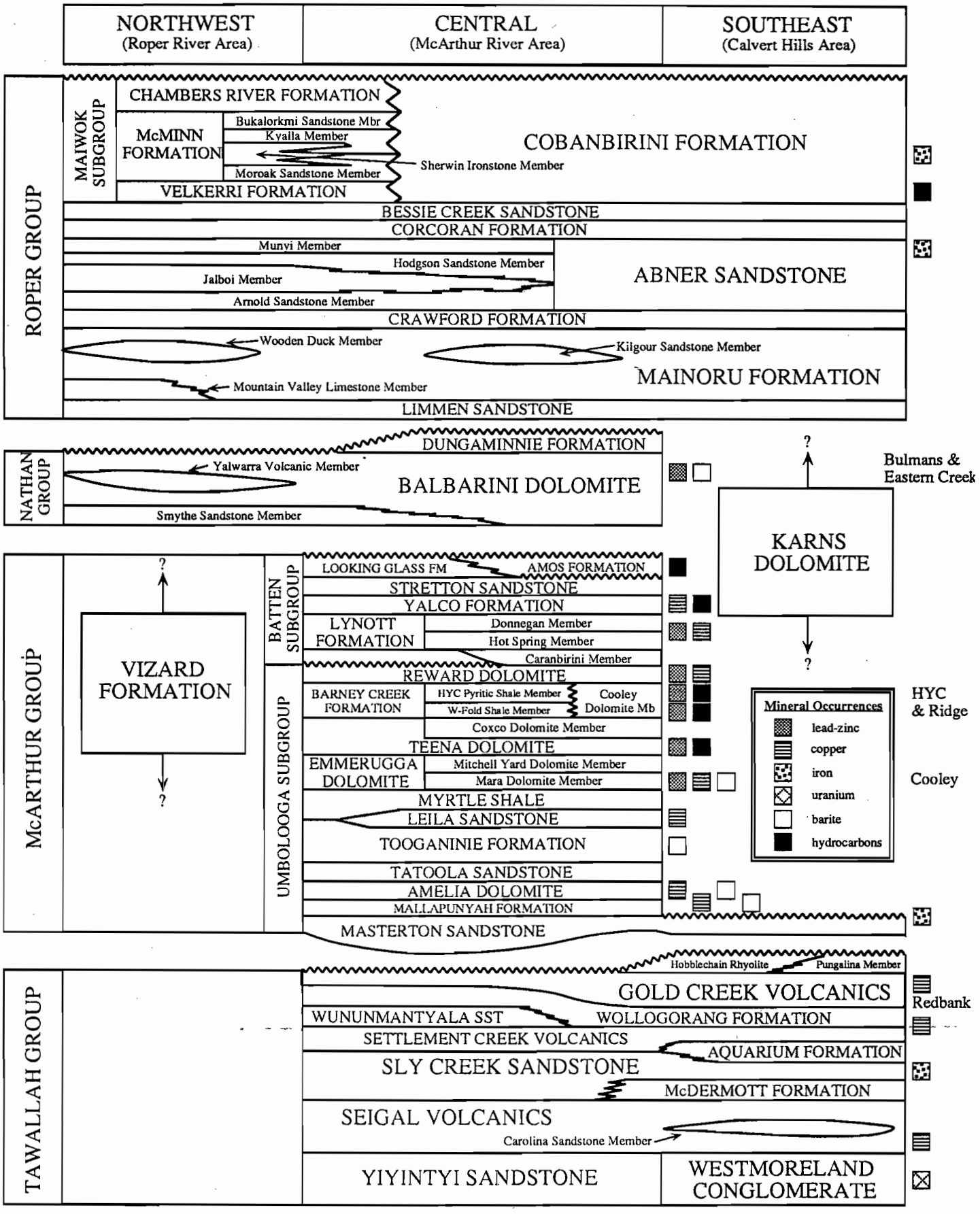


*Figure 2 — Stratigraphic column for the McArthur Basin.*

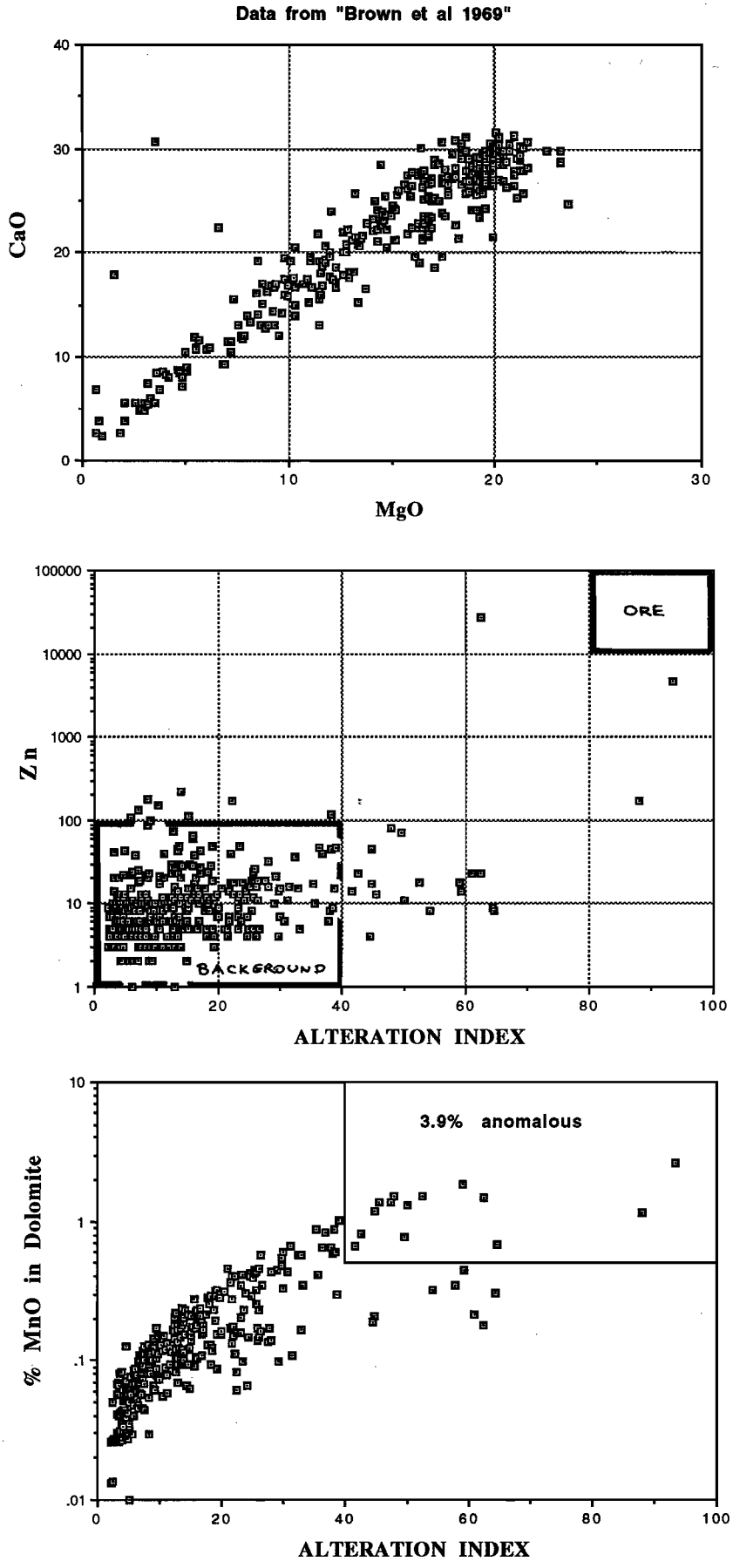


*Figure 3 — Lithogeochemical plots for the Brown* et al. *(1969) data set of McArthur Basin sediments.*

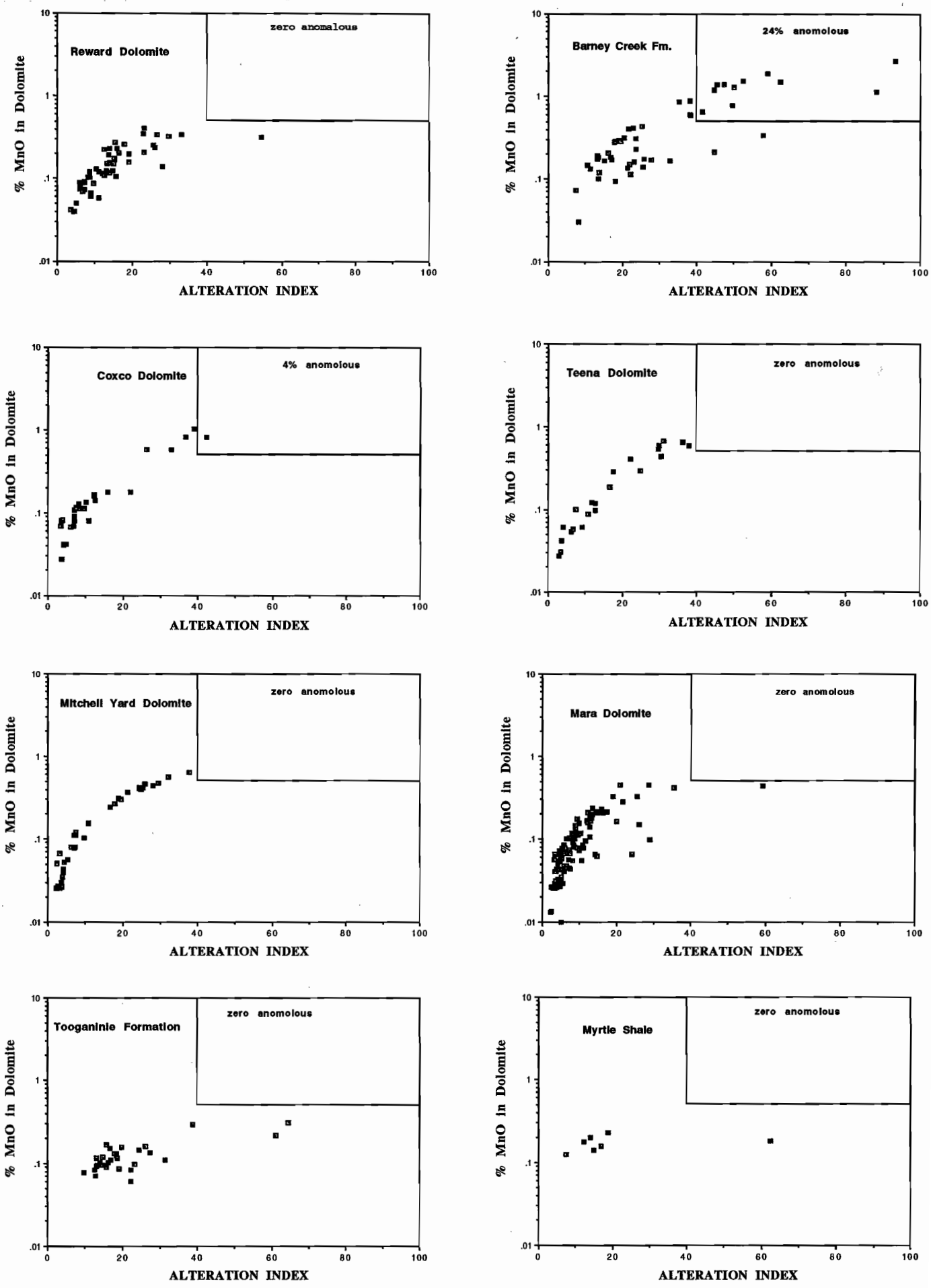


*Figure 4 — Set of alteration index plots for the Brown* et al. *(1969) data set divided according to formation or member. The box in the top right corner of each plot defines the priority 3 zone (high priority; AI > 40, $MnO_D$ > 0.5%).*

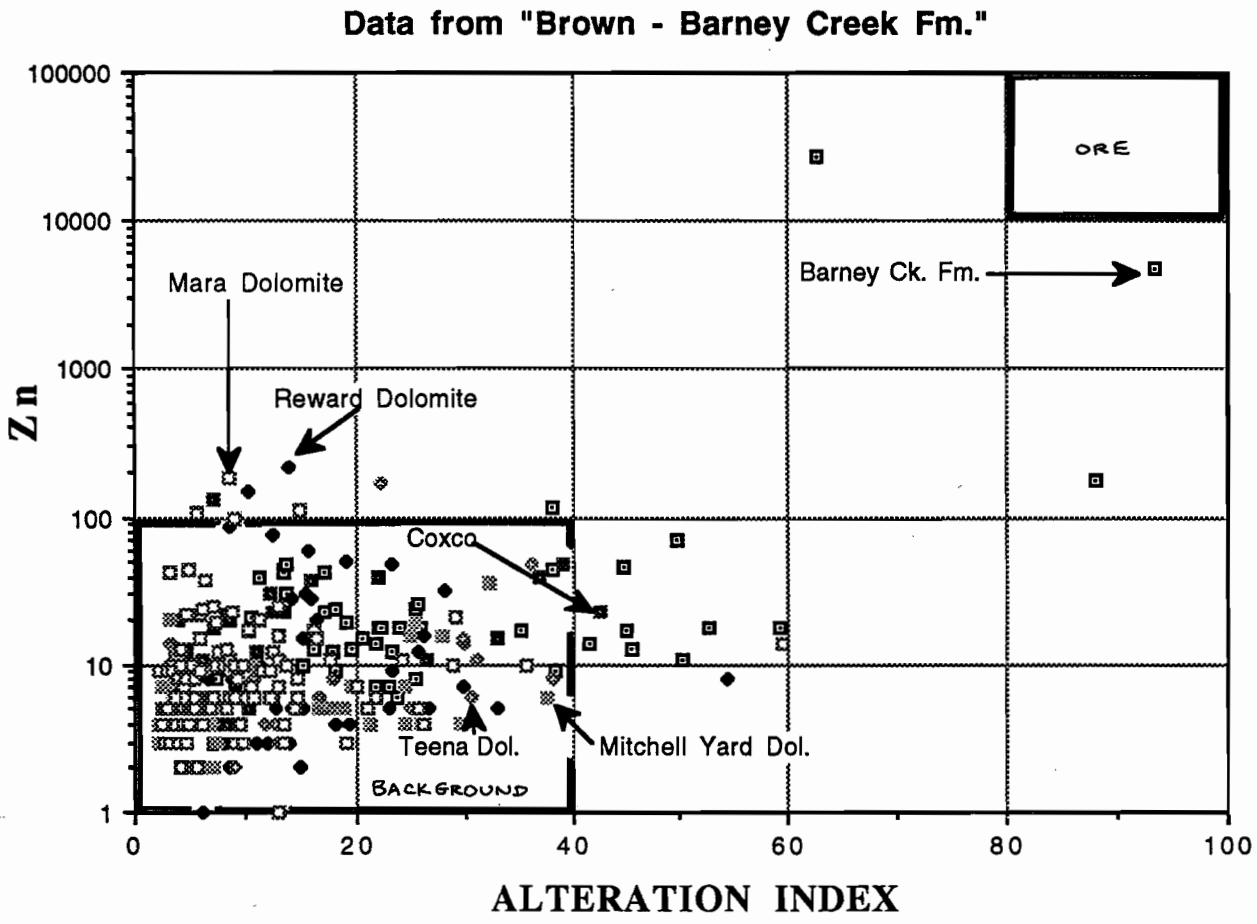


*Figure 5 — AI vs Zn plot showing breakdown of data based on stratigraphic unit.*

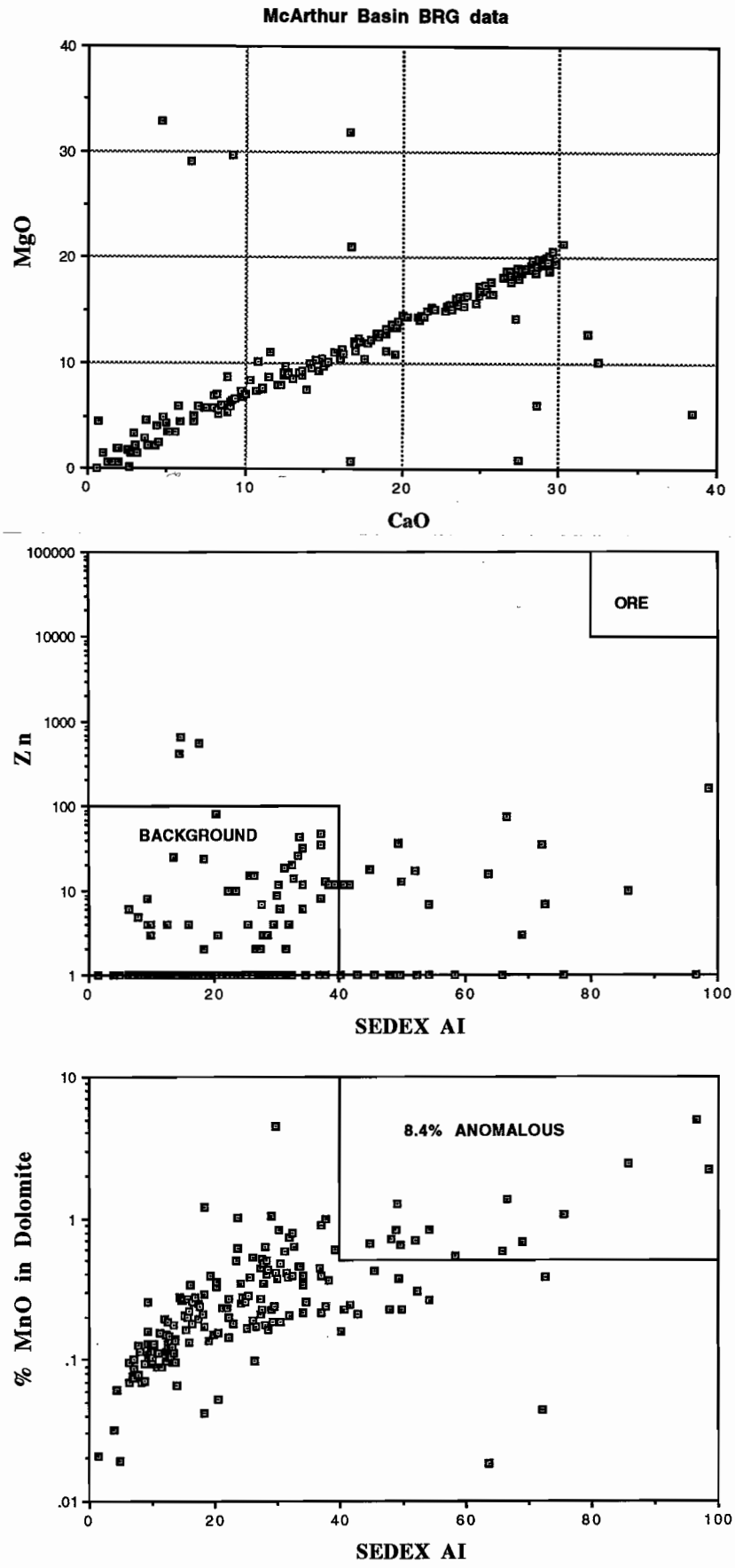


*Figure 6 — Lithogeochemical plots for the BRG data set (Large, 1979).*

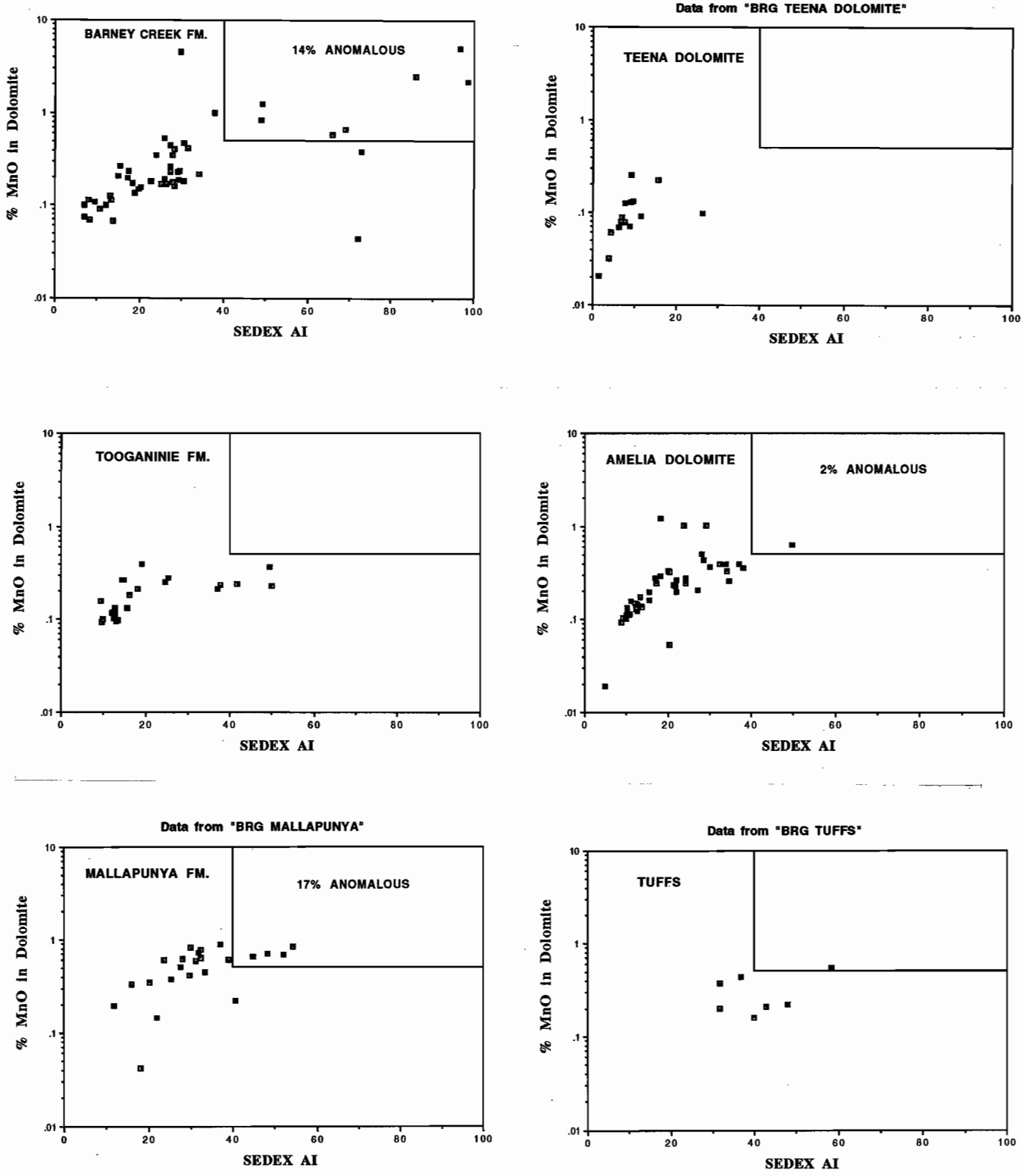


*Figure 7 — Set of alteration index plots for the BRG data divided according to formations. The box in the top right corner of each plot defines the priority 3 zone (high priority; AI > 40, $MnO_D$ > 0.5%).*

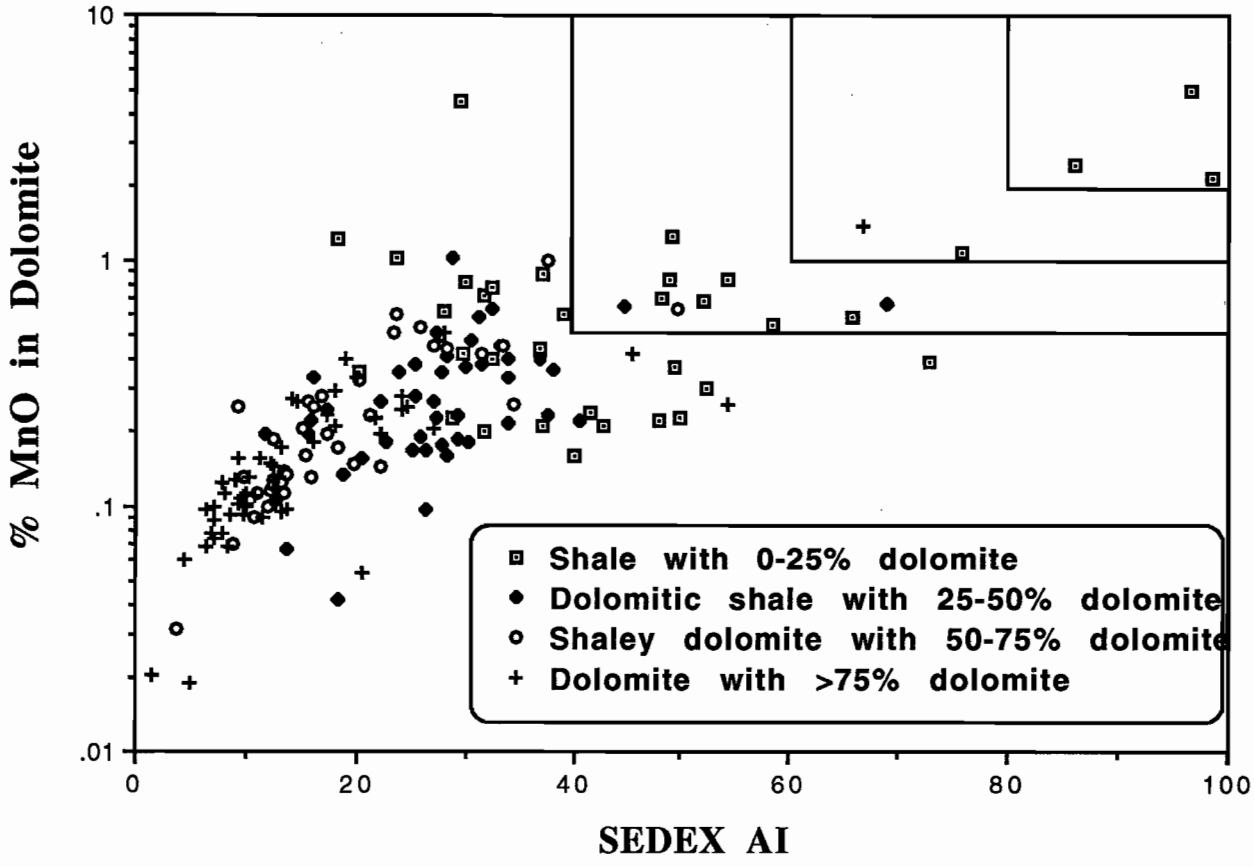


*Figure 8 — Variation in alteration index and $MnO_D$ with lithofacies for the BRG data set. Note: dolomite mean AI ≈ 10, shaley dolomite mean AI ≈ 20, dolomitic shale mean AI ≈ 25, shale mean AI ≈ 40.*

stratigraphically above the Barney Creek Formation (HYC host rocks) and include the Lynott Formation and Yalco Formation in the Batten Subgroup and the Balbarini Dolomite in the Nathan Group (Fig.2).

### Analysis of Al and $MnO_D$ Patterns

The MgO vs CaO plot in Figure 9 indicates that the majority of samples are dolomitic; however, high MgO/CaO ratios in a significant number of samples must be due to the presence of a second Mg-bearing mineral such as magnesite or chlorite. All samples with MgO/CaO above the dolomite line come from the Yalco Formation. Over 90% of the samples plot within the Al background box with values of 10 to 40 (Fig. 9b). Samples with elevated Zn (above 100ppm) all come from the Lynott Formation. Overall 7.7% of the samples are anomalous and require follow-up (Fig. 9c).

### Breakdown by Formation (Fig. 10)

- Lynott Formation shows a spread of Al and $MnO_D$ values with 8% of the samples anomalous. Two samples plot in the top priority zone 1 and a further four in the very high priority zone 2 (Fig. 10). These priority samples come from drill holes Amoco 82-5, Mant 78-1 and Leila Yd 1, and indicate the potential for stratiform Pb–Zn deposits in the Lynott Formation.

- Yalco Formation shows a fairly tight cluster of background Al/$MnO_D$ with only three samples in the priority 3 category. These anomalous samples are from Amoco 82-6.

- Balbirini Formation — there are too few samples for a meaningful pattern. Two of the eight samples are anomalous priority 3.

## The Presence of siderite

It was not possible to determine the presence or absence of siderite in these data sets due to the lack of $CO_2$ analyses. Samples with less than 1% CaO were deleted from the interpretation and consequently sideritic sediments may have been overlooked. It is recommended that $CO_2$ analyses be undertaken on the Brown et.al. (1969) and AGSO Rockchem data-bases in order to evaluate the presence of sideritic sediment in the McArthur Basin.

## Comparison of data sets

A comparison of the alteration index vs $MnO_D$ plots for the three data sets (Fig. 11), indicates that background values in the Rockchem data set are significantly higher in both Al and $MnO_D$ than the Brown et.al. or BGR data sets. This appears to be due to sampling bias. The AGSO Rockchem data set is biased toward the shales lithofacies (<10% CaO) with few pure dolomites (>25% CaO) while the Brown et.al. data set is dominated by pure dolomite samples (>25% CaO). The variation in CaO amongst the three data sets is shown in Figure 12.

## Conclusions

Analyses of the three data sets available on sediment geochemistry of stratigraphic formations in the McArthur basin indicate that background values of alteration index vary from 0 to 40 and background $MnO_D$ varies from 0.02 to 0.5 wt% for sediments with CaO > 1 wt%. The alteration index varies with dolomite content of the lithofacies from about 10 for pure dolomites to about 40 for shales with <25% dolomite. Plots of Al vs $MnO_D$ for all the major stratigraphic units allow the following assessment of potential to host stratiform Pb–Zn deposits (Figs 4, 7, 10):

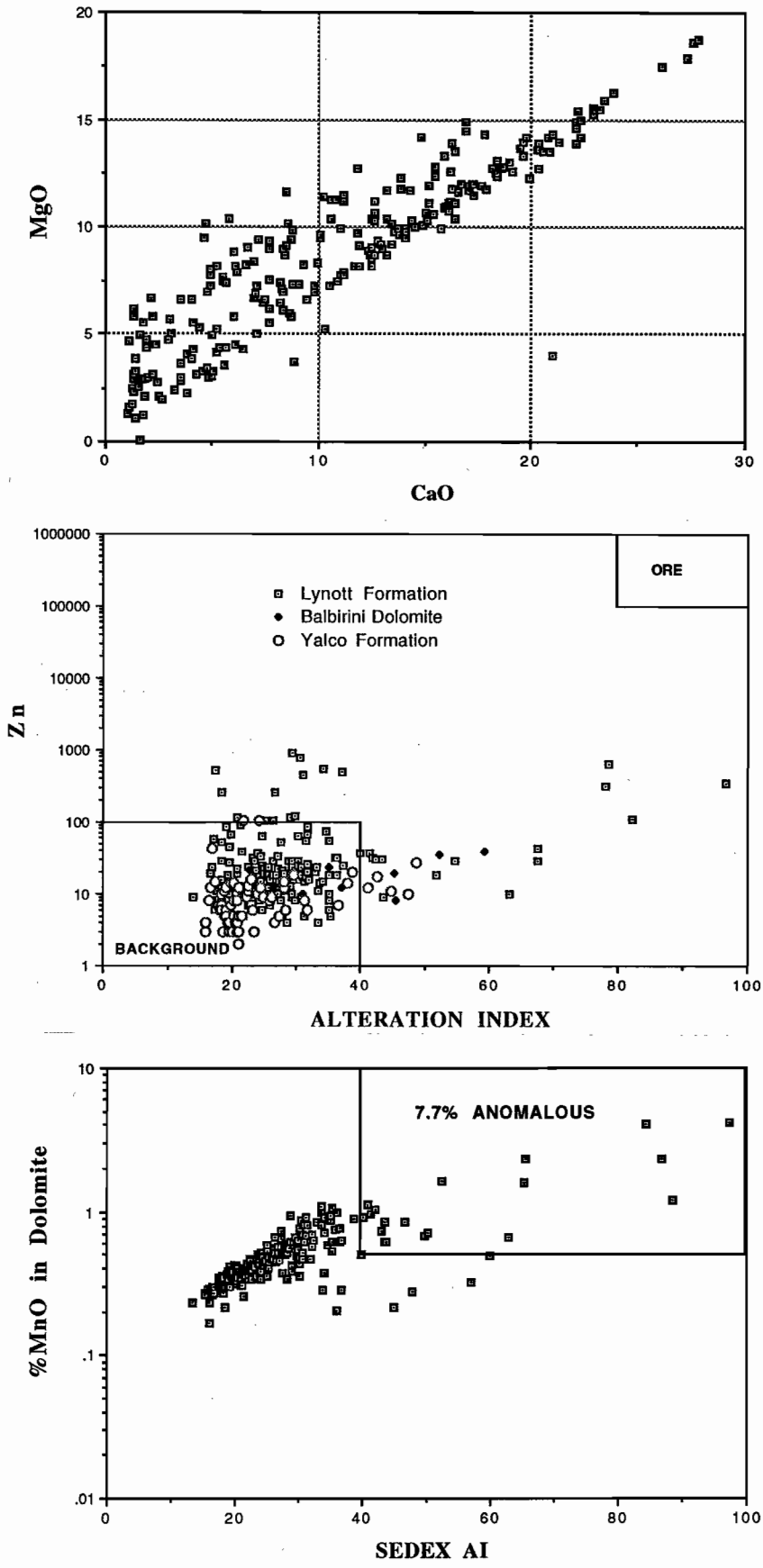


*Figure 9 — Lithogeochemical plots for the AGSO Rock chem data set.*

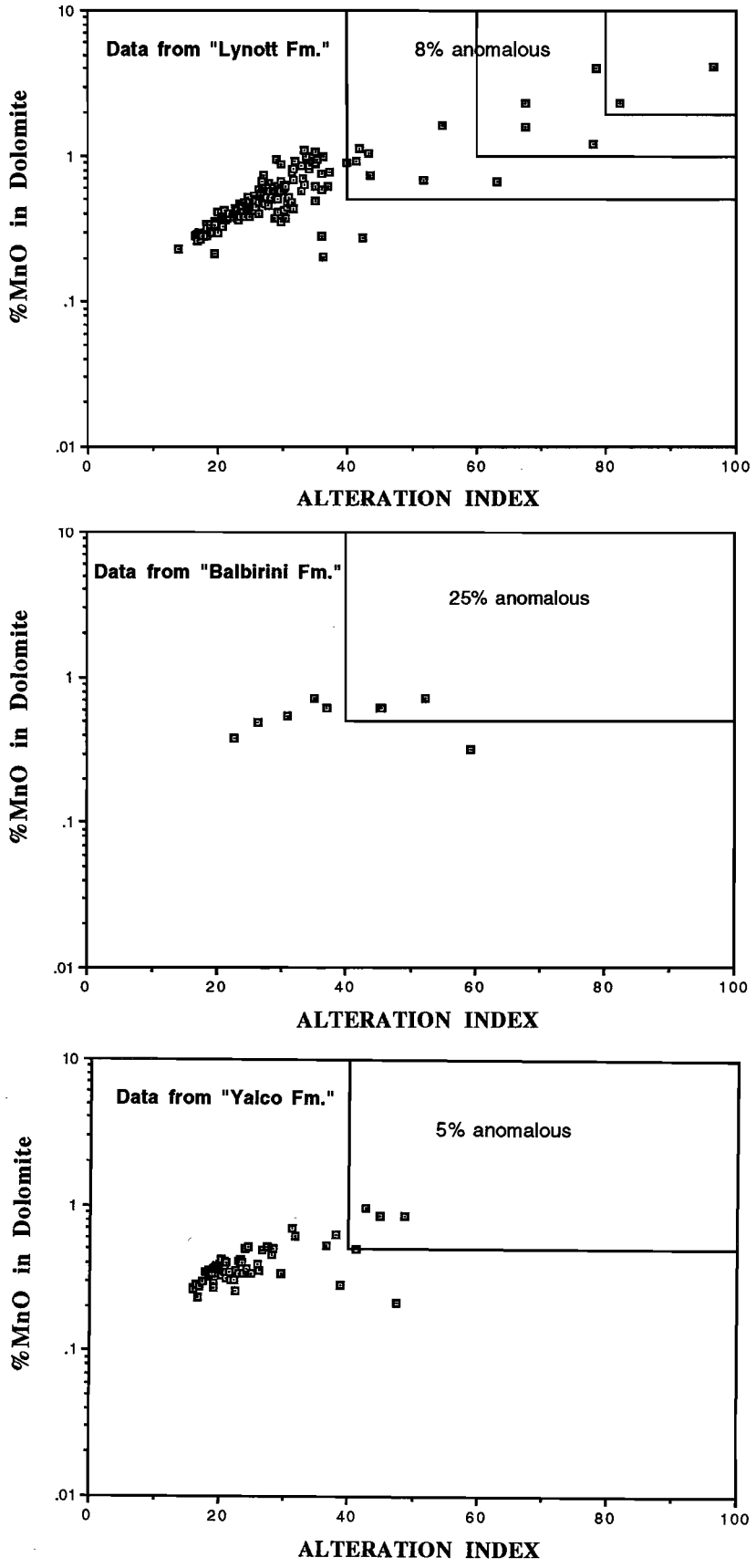


*Figure 10 — Set of alteration index plots for the Rockchem data set divided according to formations. Note the zone 1 "immediate priority" samples from the Lynott Formation.*

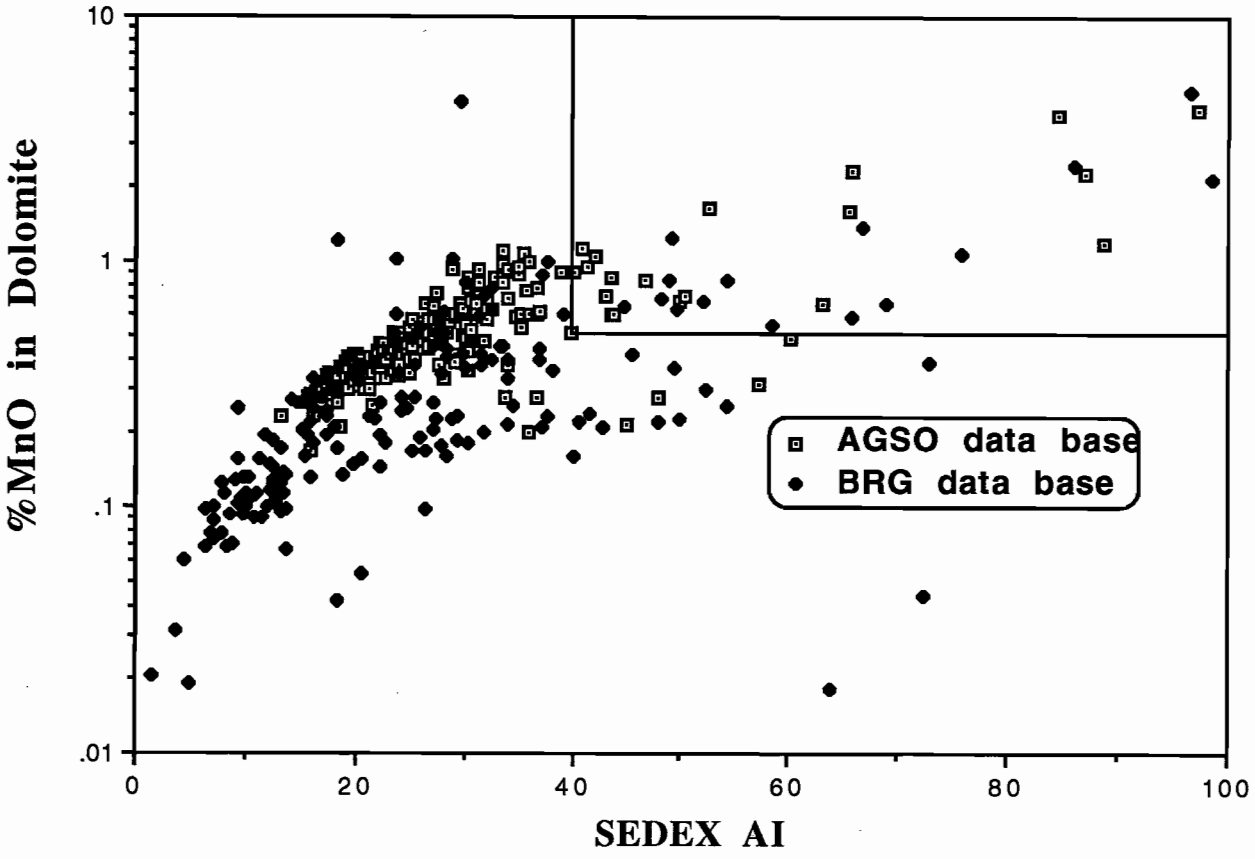


*Figure 11 — Comparison of alteration patterns in AGSO Rockchem data set and BRG data set. Note the BRG data set has a lower mean AI and $MnO_D$, compared to the AGSO data set, due to a bias towards pure dolomite samples.*

Very High Potential

- Barney Ck Formation
- Lynott Formation

Moderate Potential

- Mallapunya Formation
- Yalco Formation
- Amelia Dolomite
- Balbirini Formation

Low Potential

- Reward Dolomite
- Coxco Dolomite
- Teena Dolomite
- Mitchell Yard Dolomite
- Mara Dolomite
- Myrtle Shale
- Tooganinie Formation

Background Zn values in the sediments concentrate in the interval 20–40ppm with a spread of <1% of samples up to 200ppm Zn. Anomalous samples with 100–1000 ppm Zn fall into two populations (Fig.13).

Population A:

Zn 100–1000 ppm, AI <40; probably relates to minor Zn–Pb veins which may, or may not, be related to Sedex mineralisation.

Population B:

Zn 100–10,000 ppm, AI>40; considered to be the favourable horizon for Sedex mineralisation.

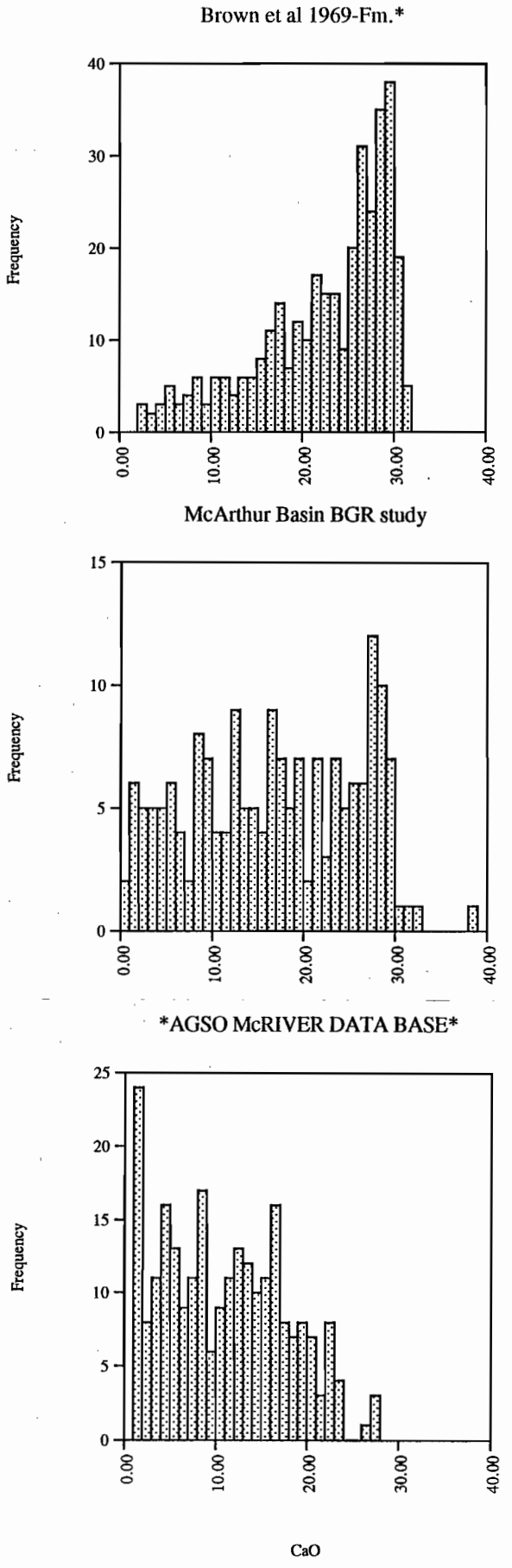


*Figure 12 — Comparison of CaO histograms for the three McArthur Basin sediment data sets. The high mean CaO in the Brown data set, compared with the other two data sets, indicates a bias towards pure dolomites.*

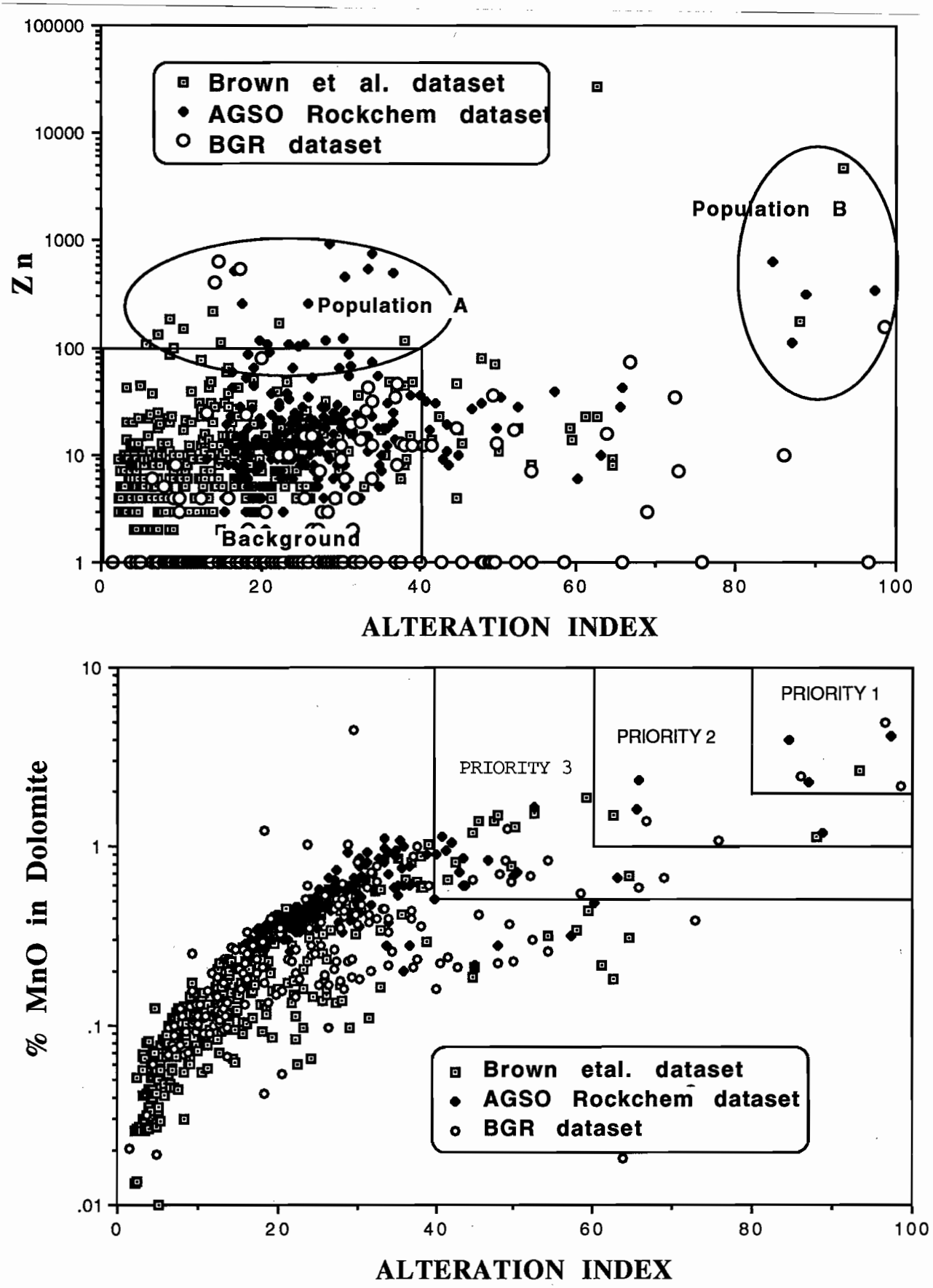


*Figure 13 — Comparison plots for the three McArthur Basin data sets.*

## Acknowlegements

Special thanks to Lesley Wyborn for locating the Brown et al. (1969) report and data set.

## References

Brown, M.C., Claxton, C.W. & Plumb, K.A., 1969. The Proterozoic Barney Creek Formation and some associated carbonate units of the McArthur Group, Northern Territory. BMR Record No. 1969/145: 59 pp.

Large, D.E., 1979. Rock geochemistry study McArthur Basin project. Federal Institute for Geosciences and National Resources (BGR).

Large, R.R. & McGoldrick, P., 1993. Primary geochemical halos related to Proterozoic sediment-hosted Pb-Zn deposits, and applications to exploration. AMIRA P384, unpublished report 3: 63–126.

Plumb, K.A., Wyborn, L.A.I. & Ryburn, R.J., 1992. McArthur Basin and Murphy Inlier Rockchem data set documentation. BMR Record 1992/37: 34 pp.

# Case Studies: Application of the Alteration Index to Selected Areas in the McArthur Basin

**Ross R. Large**
*CODES Key Centre*

## Summary

Application of the refined alteration index procedure to three sub-basins in the McArthur Basin has indicated the potential for further stratiform Pb–Zn deposits remote from the HYC deposit. Two favourable horizons identified in the BMR 2 area, 25 km SW of HYC, are confirmed by our recent sampling, however the AI and $MnO_D$ anomalies are considered to relate to HYC rather than more proximal deposits. Evaluation of previous sampling (Brown et al., 1969) in the Top Crossing area (60 km SW of HYC) indicates the presence of a favourable horizon with high potential for lead–zinc mineralisation, down plunge, adjacent to the Tawallah Fault. In the Glyde Sub-basin (80 km S of HYC), drill hole lithochemical sampling by Shell Metals indicates a favourable horizon with anomalous alteration character intersected in one of the ten drillholes.

## Introduction

The alteration vectors defined by Large & McGoldrick (1993) have been applied to three sub-basins in the McArthur Basin that are remote from HYC:

- Glyde Sub-basin, 80 km south of HYC
- Top Crossing Area, 60 km SSW of HYC
- BMR 2 Area, 25 km SW of HYC

These areas where selected on the basis of availability of lithogechemical data on the Barney Creek Formation.

## Glyde Sub-Basin

The Glyde Sub-Basin is a fault bounded depocentre adjacent to the Emu Fault, 80 km south of HYC (Fig. 1) (Davidson and Dashlooty, 1993). Exploration in the period from 1977 to 1982 by Amoco, Kennecott and Billiton included drilling 10 vertical diamond drill holes through the Barney Creek Formation (Fig. 2). Limited lithochemical data is available on selected intervals of each hole, representing the major rock units. Twenty-eight samples were analysed for major & trace elements by Billiton (Dashlooty, 1982).

### Results of vector analysis

The graphical plots shown in Figure 3 indicate that anomalous values of AI and $MnO_D$ are present in the data set. Two samples, GR73 and GR74 plot within the priority 2 zone (Fig. 3b) and are worthy of follow-up. Both these samples are form the W-fold Shale intersected in DDH GR7 in the northern sector of the Glyde Sub-basin about 1km west of the Emu fault (Fig .2). The closest other drill holes to GR7 are over 3 km distant (GR 2, 5 and 10).

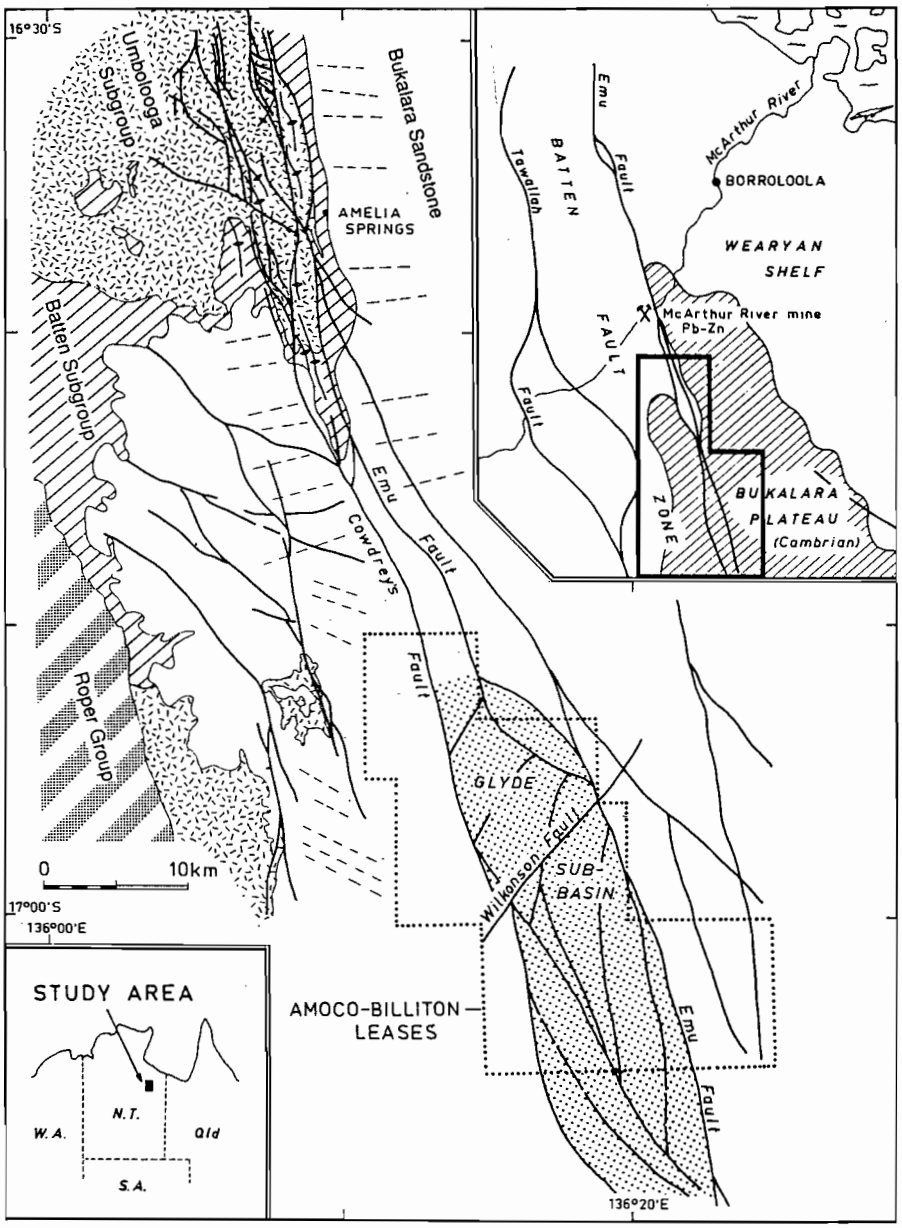


*Figure 1 — Location and regional structure of the Glyde Sub-basin (from Davidson & Dashlooty, 1993).*

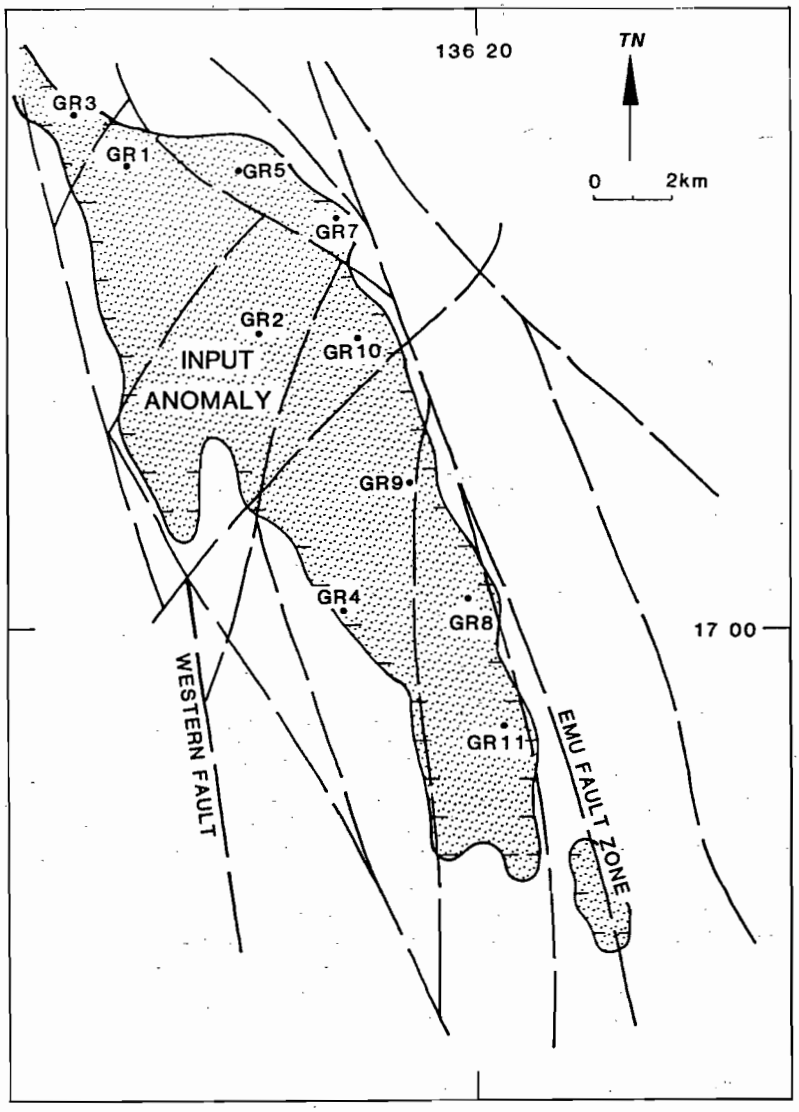


*Figure 2 — Lineament structure and drill hole locations, Glyde Sub-basin (Davidson & Dashlooty, 1993).*

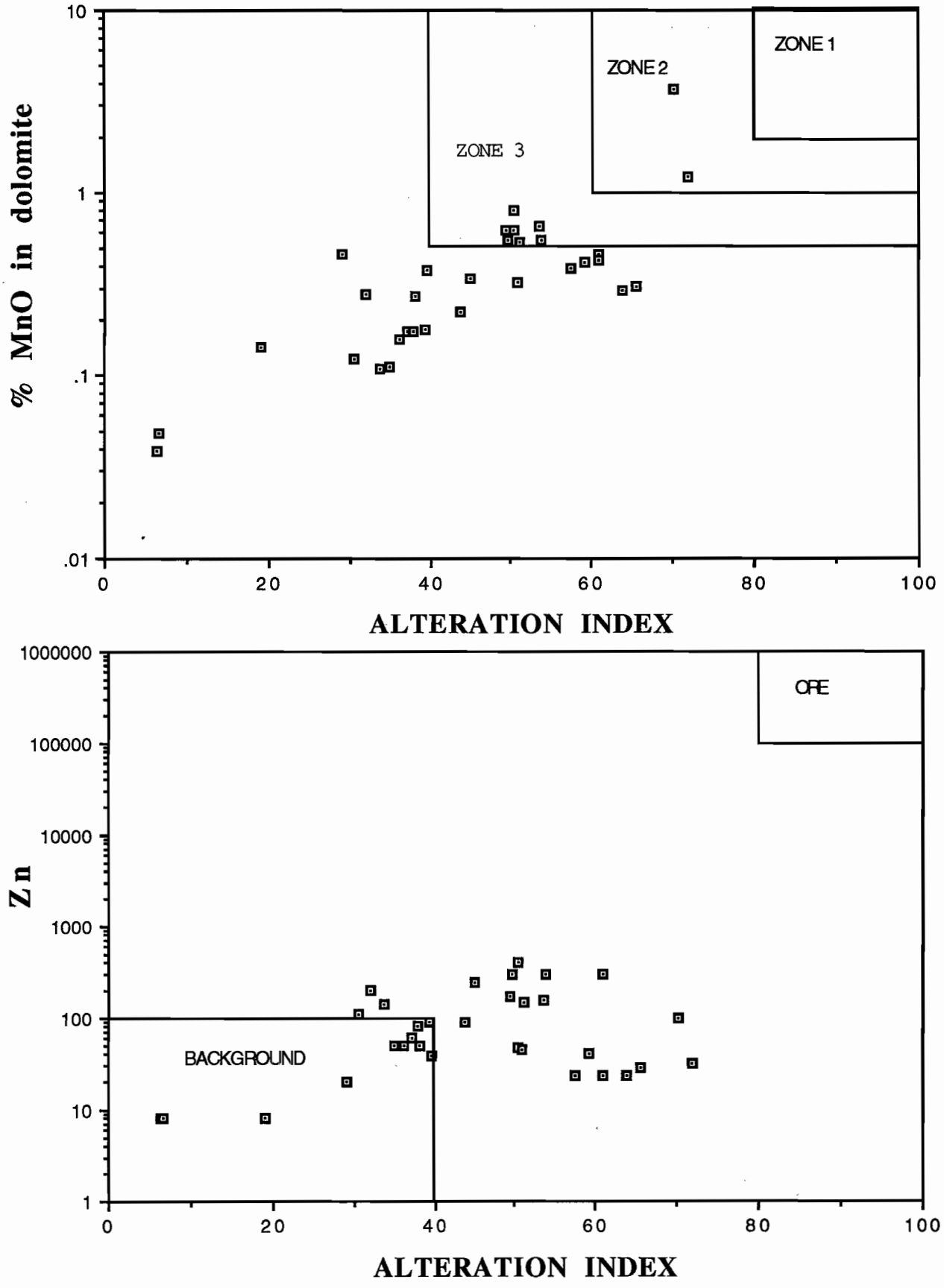


*Figure 3 — Alteration plots for Billiton samples from the Glyde Sub-basin drilling program. The two anomalous samples in the priority zone 2 come from DDH GR7 (fig. 2).*

## Top Crossing Area

The Top Crossing Area was sampled by Brown et al. (1969) as part of their regional study of carbonate sediments in the McArthur Basin. This area was also the subject of a CODES honours mapping project in 1993 (Mathews, 1993) and will be visited on the Sponsors Excursion in June 1994. At Top Crossing, 60 km SW of the HYC deposit (Fig. 4), the Barney Creek Formation is exposed in a broad north east plunging syncline. The syncline limbs are truncated by the Tawallah Fault on the eastern side. The structural/stratigraphic position of the Top Crossing sub-basin is similar to the HYC sub-basin (Fig. 5). Brown et al. (1969) provide a 1.5 km stratigraphic section of the syncline from the Cooley Dolomite, through the BCF to the Reward Dolomite (Fig. 6). Forty-one surface samples were collected along the traverse and analysed for selected major and trace elements (Brown et al., 1969: Appendix 1).

### Discussion of Results

The Top Crossing lithogeochemical data provide an excellent case study for application of AI and $MnO_D$ using oxidised surface samples. From Figure 7 it is apparent that five of the 41 samples plot in the priority 3 zone, suggesting high potential for "remote" stratiform Pb–Zn mineralisation. However, all samples have background zinc values of less than 100 ppm.

A stratigraphic section of Zn ppm, % dolomite in sediments, alteration index and $MnO_D$ is given in Figure 8. Note that the Y-axis to these graphs is sample number rather than metres along traverse. The samples are consecutive along the traverse and located in Figure 6. These plots indicate two favourable horizons in the Barney Creek formation located at sample position 215 and sample position 224. The former (position 215) has $MnO_D$ values >1% and AI >40 and is considered to have the highest potential. From the Dolomite % plot (Fig.4b), it is evident that this favourable horizon corresponds to an interbedded dolomite/shale sequence in the middle of the BCF. The upper favourable horizon corresponds with a shale unit at the top of the BCF. A plot of the raw Mn values in the sediments along the section indicates a strong anomaly related to the lower favourable horizon; however, the upper horizon shows no Mn enrichment (Fig. 9). Further field work and sampling are planned in the current field season to verify these results. This locality will be visited on the field trip in June.

## BMR 2 Area

Our previous interpretation of data from diamond drill hole BMR 2, 25 km SW of HYC, given in AMIRA Project Report 3 (Large & McGoldrick, 1994: 110–112), indicated that two potential ore horizons were identifiably from the alteration index and $MnO_D$ patterns. A further 34 samples were collected by Stuart Bull from the drill hole at the AGSO Core Shed, Canberra, in order to check the previous results and study the correlation between sedimentary facies and alteration index. The samples were analysed for Ca, Mg, Fe, Mn, Zn, Pb, Cu and S by ICP at ALS, Brisbane.

### Discussion of lithogeochemistry

The Sedex AI–$MnO_D$ plot (Fig.10) indicates that two samples (4%) plot in the Priority 2 zone and a further 14 (27%) in the Priority 3 zone.

Both sets of data show a similar pattern. The samples with anomalous AI show Zn values of less than 200 ppm, indicating a very distal position with respect to stratiform Pb–Zn ore. A comparison of the two data sets in the downhole plots (Fig. 11) indicate reasonable agreement. Two favourable



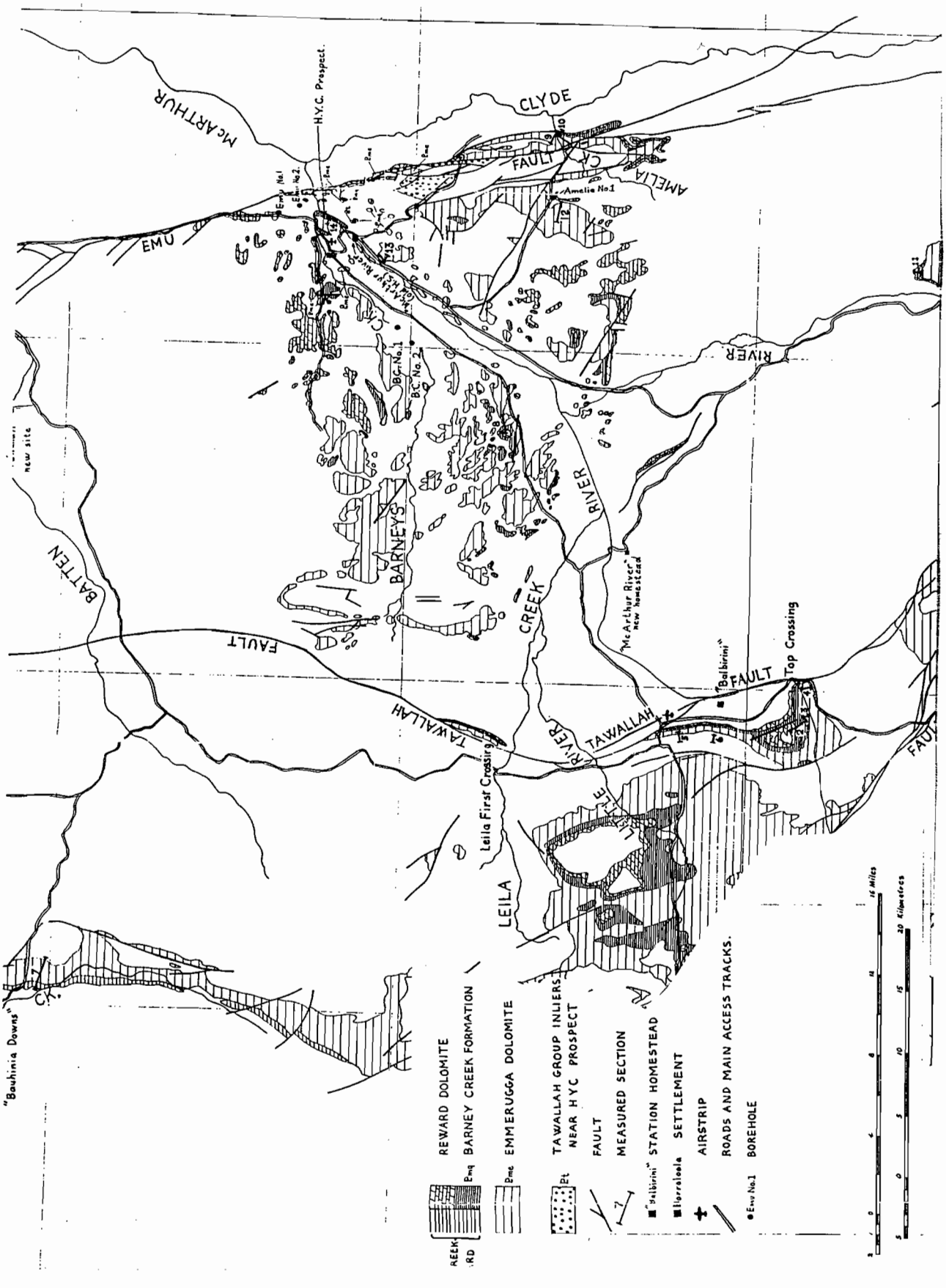


*Figure 4 — Location and geology of the Top Crossing area.*

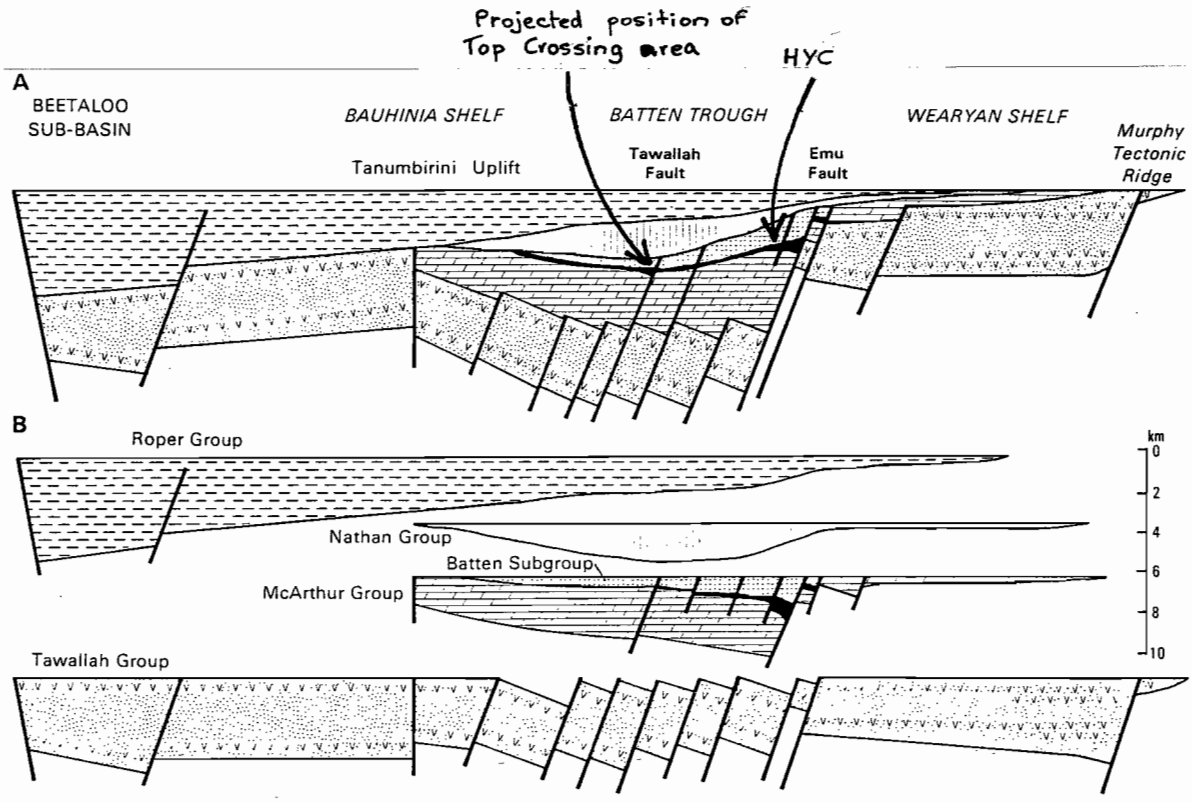


*Figure 5 — Schematic cross section from Plumb (1987) showing projected position of Top Crossing area.*

# Plate 2

## Measured Section 2, About 2½ Miles West of Top Crossing

Measured with 5ft. staff and Abney Level. Legend as on Plate 12

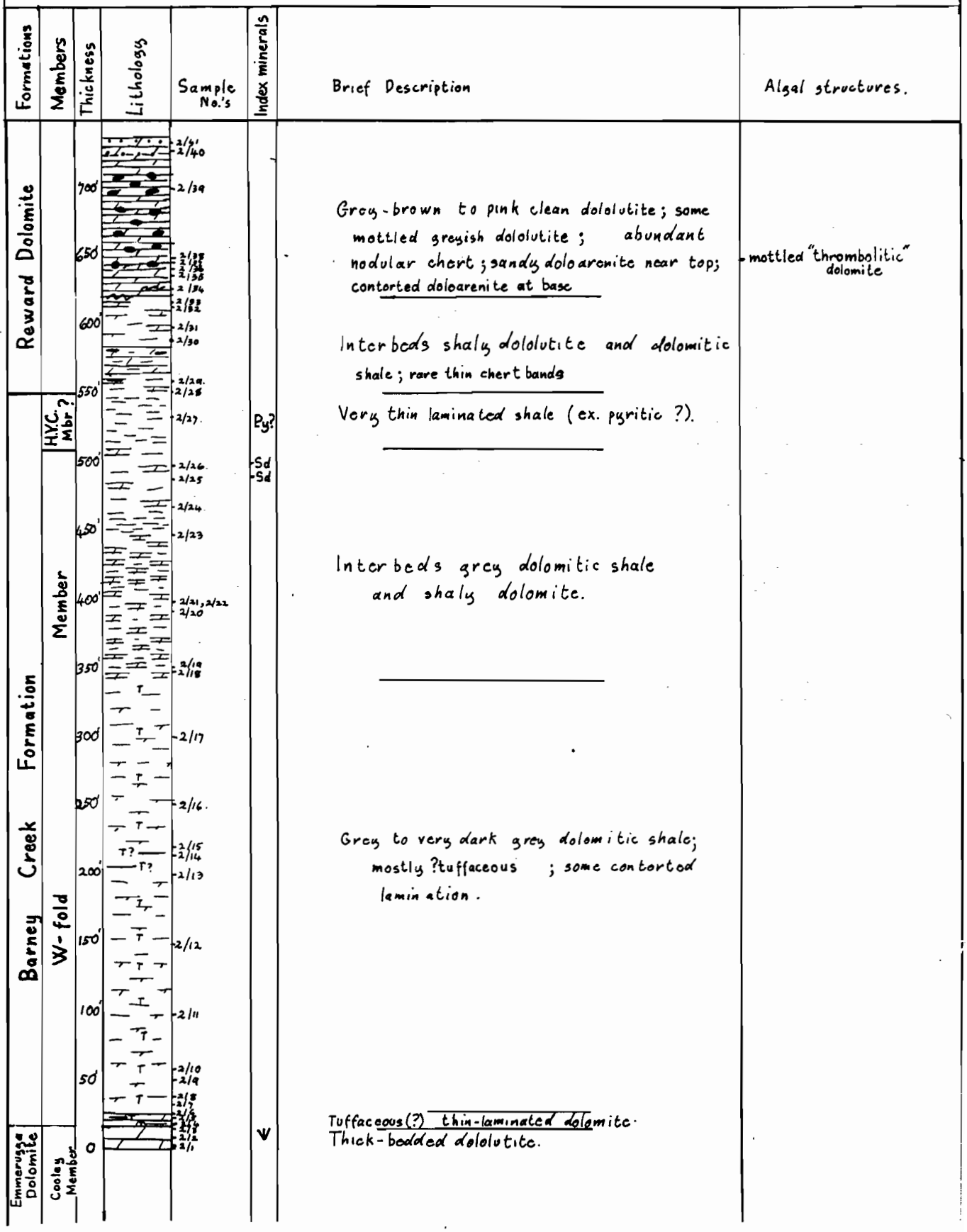


To accompany Record 1969/145

E53/A3/34

*Figure 6 — Measured section with sample locations in the Top Crossing area (from Brown et al., 1969).*

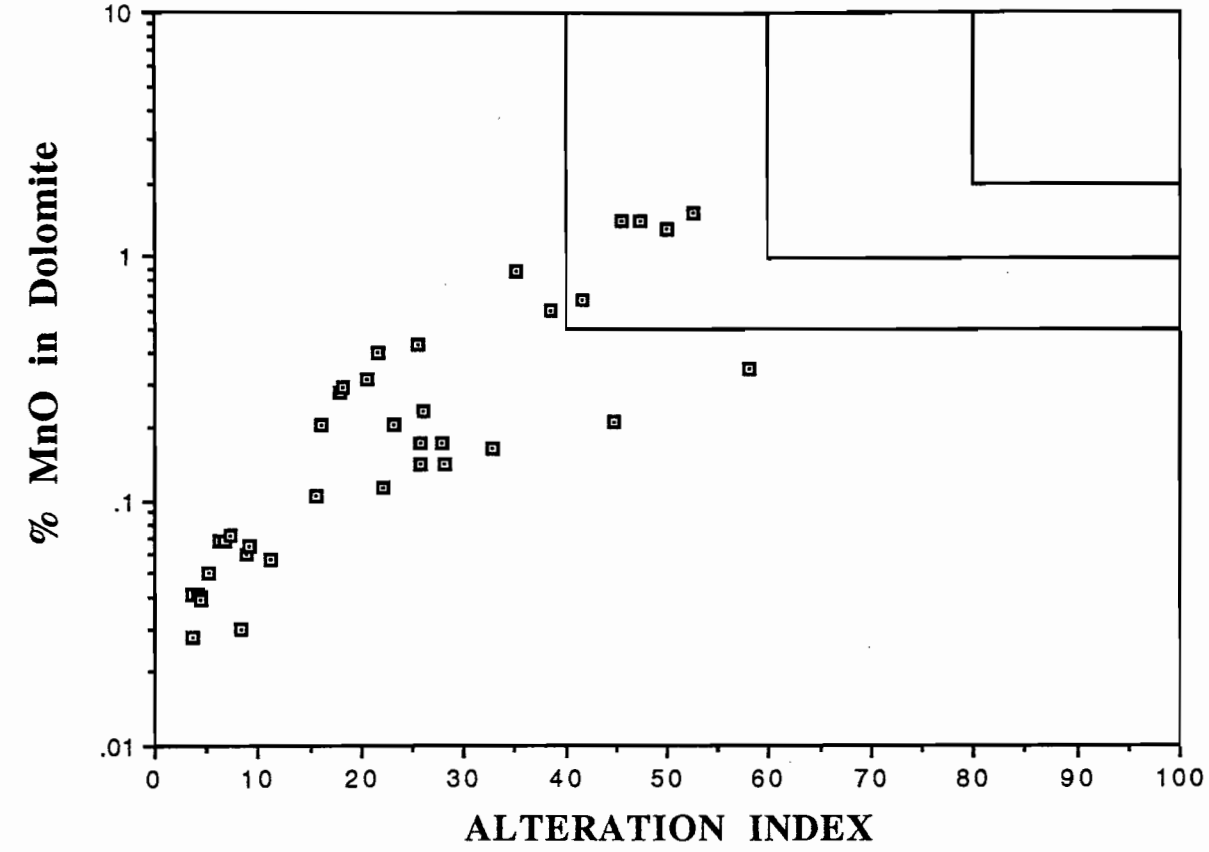


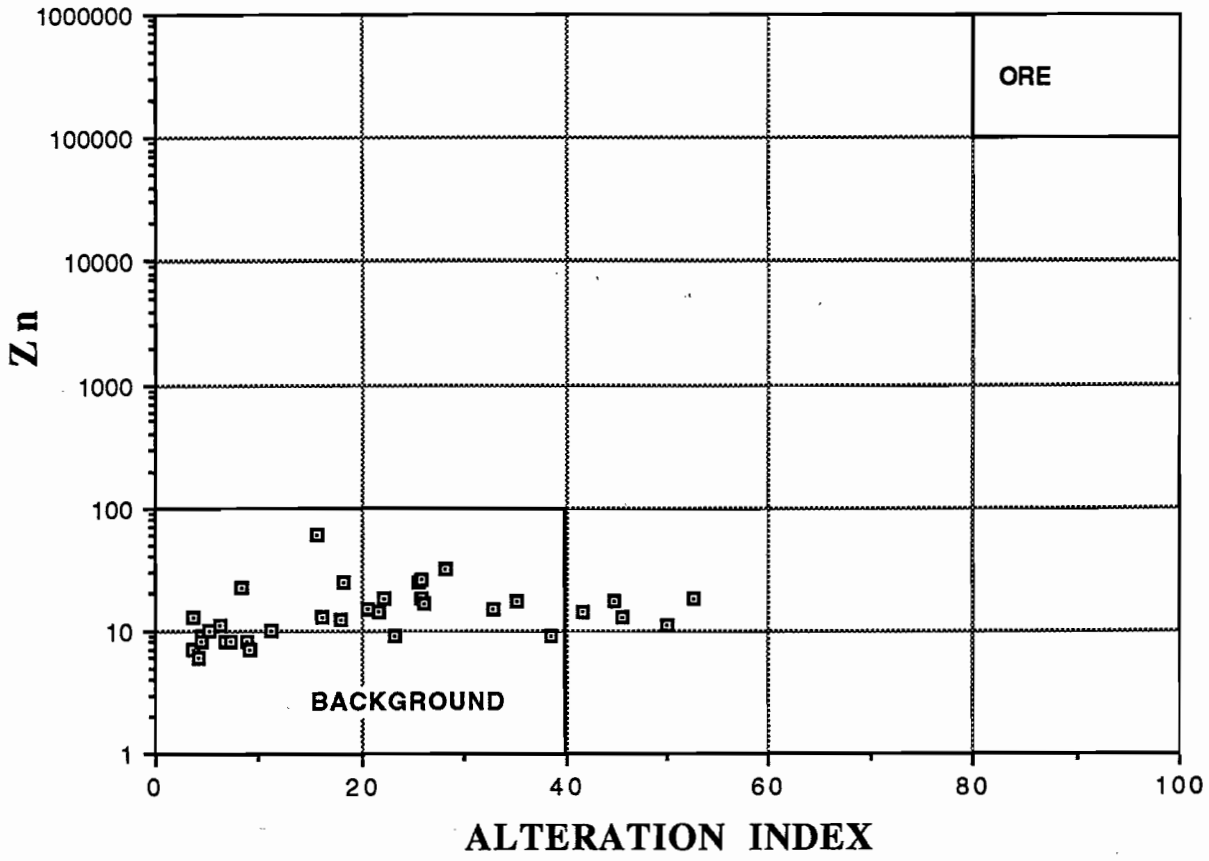


*Figure 7 — Alteration plots for the Top Crossing samples. Five of the 41 samples plot in priority zone 3.*

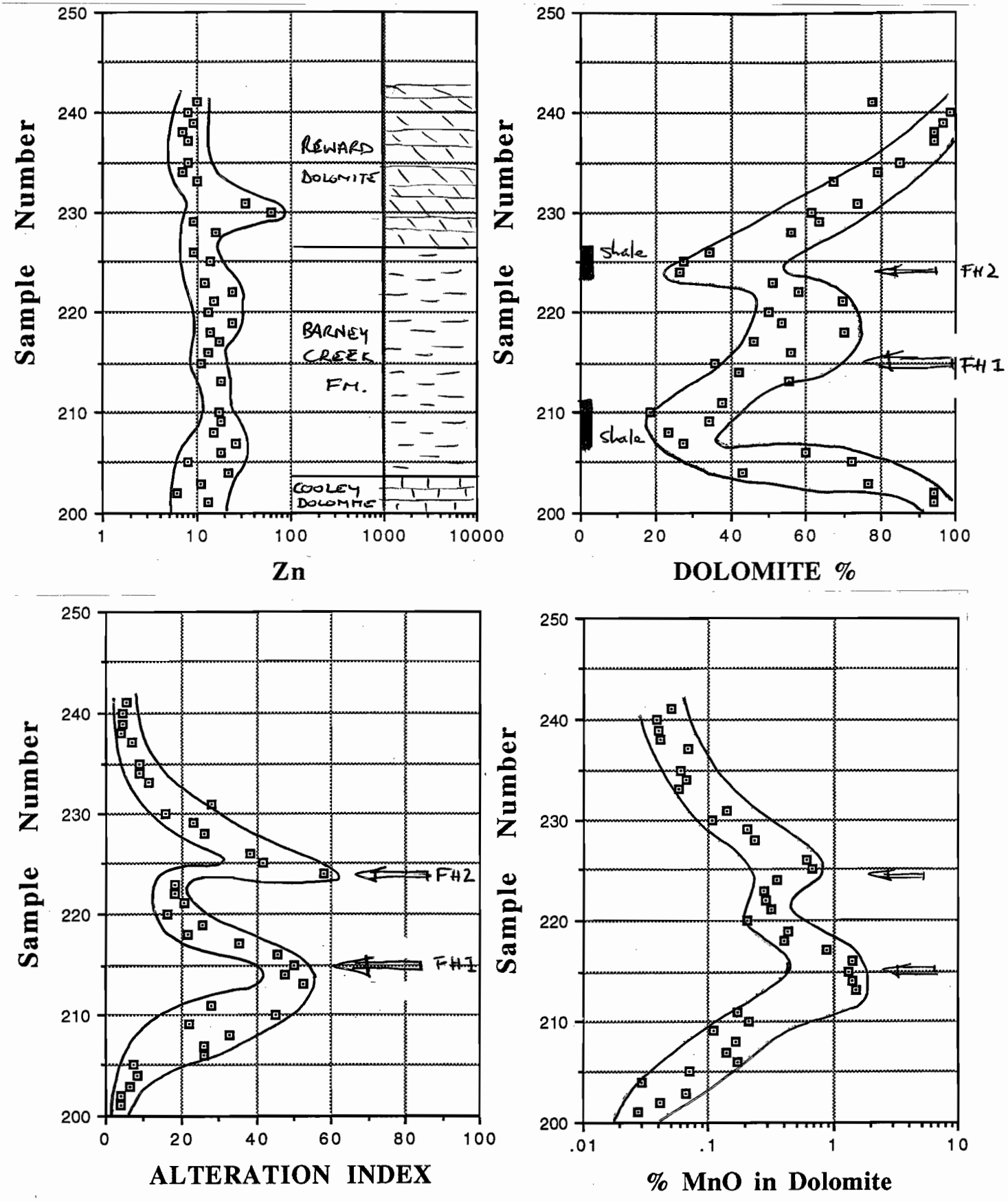


*Figure 8 — Along-traverse plots of Zn, dolomite %, alteration index and $MnO_D$ for the Top Crossing area. The Y-axis is sample numbers, with position shown in figure 6. Favourable horizons (FH) for stratiform Pb–Zn are indicated at sample positions 215 and 224.*

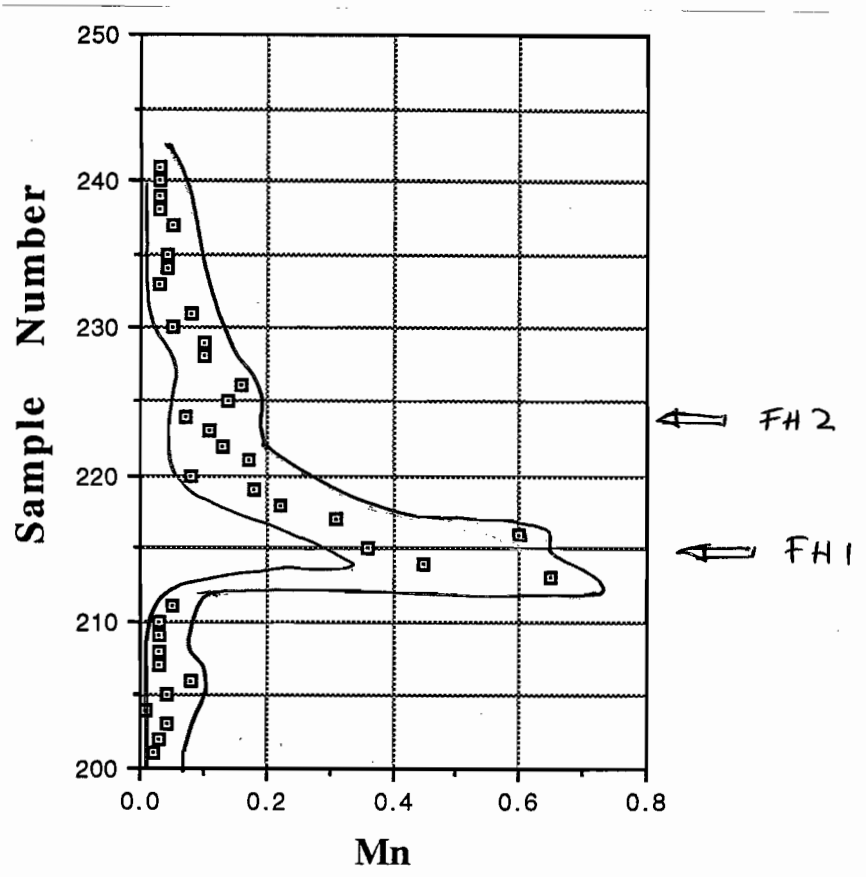


*Figure 9 — Raw Mn variation along the traverse at Top Crossing. The lower favourable horizon (FH1) is clearly anomalous.*

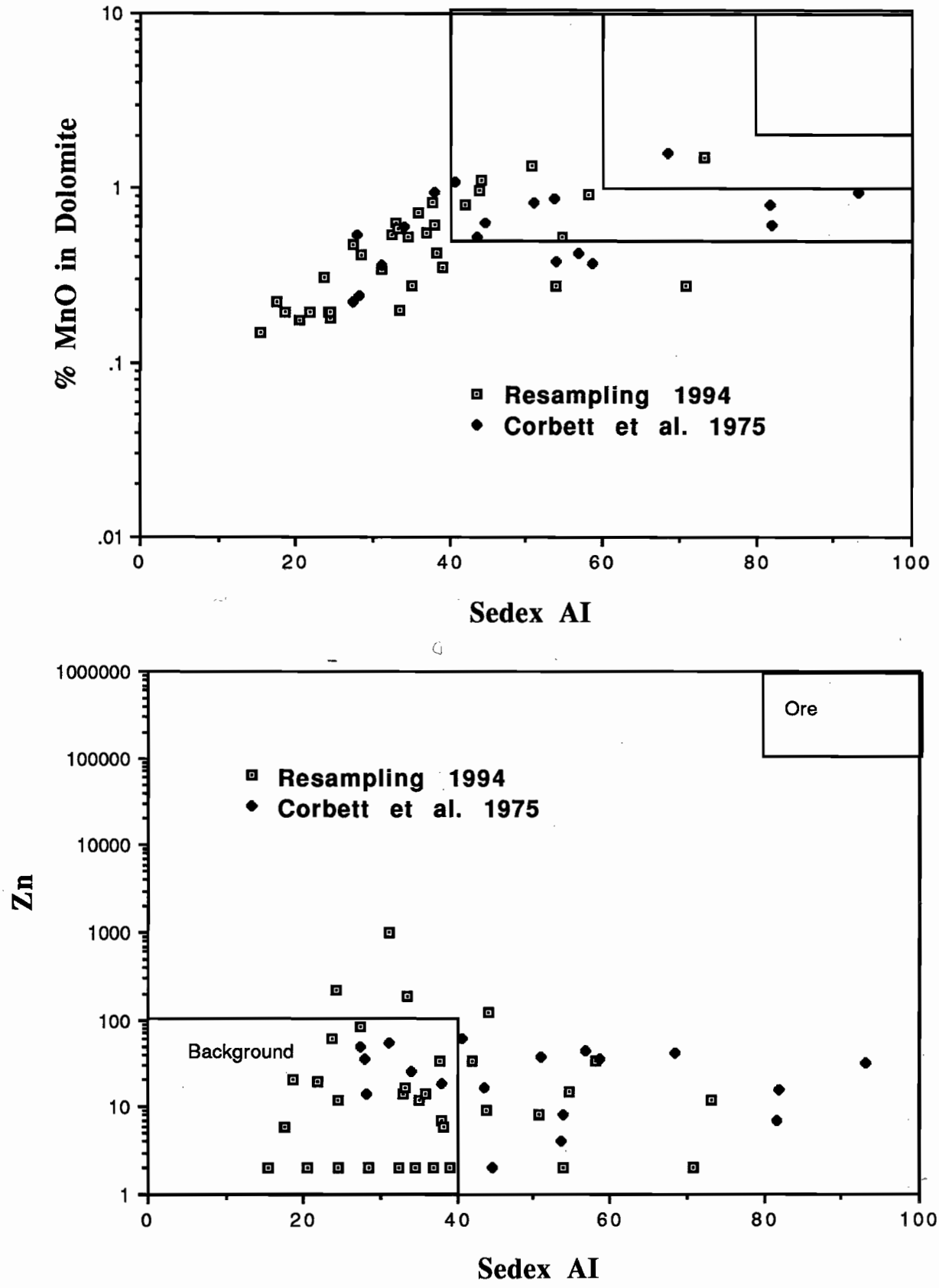


*Figure 10 — Alteration plots for the old and new data from DDH BMR2. Two samples (one from each data set) plot in the very high priority 2 zone.*

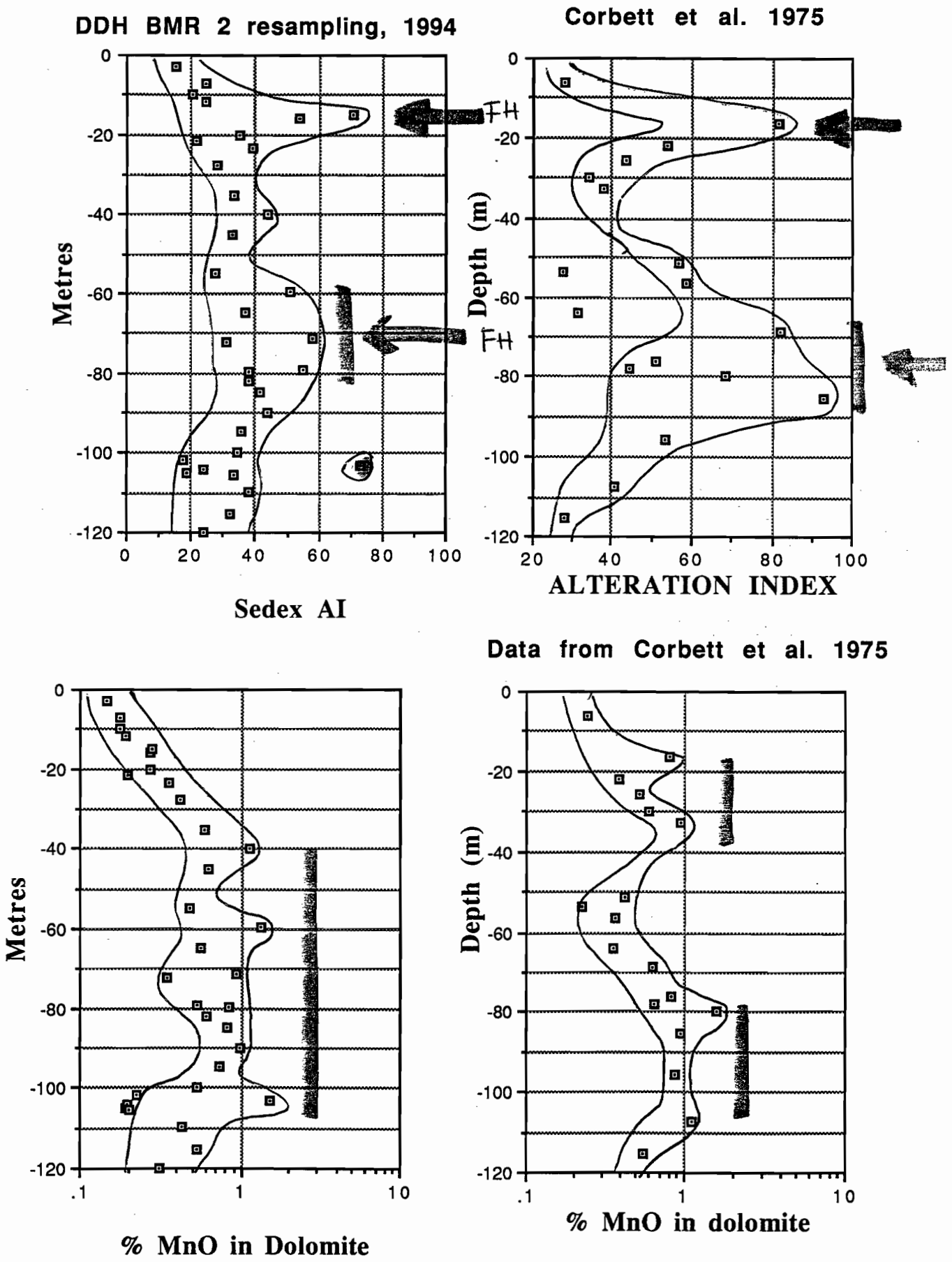


*Figure 11 — A comparison of downhole alteration index and $MnO_D$ plots for the original Crobett data and our 1994 resampling. The AI plot shows two favourable horizons at 15 m and 60–90 m downhole.*

horizons for distal Pb–Zn are suggested in both data sets:

- 10 - 20m where AI > 40, but $MnO_D$ < 1%.
- 60 - 90m where AI > 40 and $MnO_D$ up to 1.5%.

Based on the higher $MnO_D$ values, the lower horizon is considered to have the greater potential.

Further work will be undertaken on the samples to study the correlation between sediment facies, lithogeochemistry and carbon/oxygen isotopes of the carbonates.

## Conclusions

Application of the lithogeochemical vectors, Sedex AI and $MnO_D$, have enabled the identification of favourable horizons for mineralisation with the Barney Creek Formation in all three areas studied: Glyde Sub-basin, Top Crossing Area and BMR2 area. The alteration pattern in DDH BMR2 is probably a response to the ore deposit 25 km distant at HYC. However, the anomalous pattern along the surface traverse in the Top Crossing area is unlikely to be related to HYC but may indicate the potential for a closer Pb–Zn deposit. The anomalous pattern of samples from the W-fold member in DDH GR7 at the northern end of the Glyde Sub-basin is worthy of follow-up.

## References

Brown, M.C., Claxton, C.W. & Plumb, K.A., 1969. The Proterozoic Barney Creek Formation and some associated units of the McArthur Group, N.T. BMR Record No. 1969/145: 59 pp.

Dashlooty, S.A., 1982. 1981/1982 Annual Report, Exploration Licences 1330;Shell Metals Division, Report No. 08.1252.

Davidson, G.J. & Dashlooty, S.A., 1993. The Glyde Sub-basin: A volcaniclastic-bearing pull-apart basin coeval with the McArthur River base metal deposit, Northern Territory. *Aust. J. Earth Sci.* 40: 527–543.

Large, R.R. & McGoldrick, P., 1993. Primary geochemical halos related to Proterozoic sediment-hosted Pb-Zn deposits, and applications to exploration. AMIRA P384, unpublished report 3: 63–126.

Mathews, K., 1993. Geology of the Top Crossing area, Cape Crawford, NT. Unpublished BSc Hons thesis, University of Tasmania.

## Appendix — Analyses of BMR 2 drill core samples conducted by ALS.

**AUSTRALIAN LABORATORY SERVICES P/L**
A.C.N. 009 936 029

**Brisbane Head Office and Laboratory**
32 Shand Street, Stafford, Q. 4053
P.O. Box 66, Everton Park, Q. 4053
Telephone (07) 352 5577
Facsimile (07) 352 5109

# ANALYTICAL REPORT

CENTRE FOR ORE DEPOSIT

Attention: MR R LARGE
YourOrder: LETTER
SampleType: PULP

Page-no: 1
STAFFORD
Batch-no: 8695
Sub-batch: 0
No-samples: 34
Received: 16/05/94
Checked:

| Element | Cu | Pb | Zn | Fe |
|---|---|---|---|---|
| Unit | ppm | ppm | ppm | % |
| Method | IC587 | IC587 | IC587 | IC587 |
| 1 | 13 | 43 | <5 | 1.86 |
| 2 | 19 | 49 | <5 | 3.53 |
| 3 | 12 | 31 | 12 | 1.70 |
| 4 | 13 | 26 | <5 | 1.34 |
| 5 | 17 | 35 | <5 | 1.47 |
| 6 | 11 | 31 | 19 | 1.39 |
| 7 | 11 | 15 | 101 | 1.42 |
| 8 | 9 | 19 | <5 | 0.98 |
| 9 | 12 | 37 | <5 | 2.24 |
| 10 | 10 | 31 | 12 | 1.51 |
| 11 | 13 | 15 | <5 | 1.43 |
| 12 | 8 | 10 | 83 | 1.42 |
| 13 | 6 | 10 | 14 | 1.48 |
| 14 | 14 | 34 | 8 | 2.32 |
| 15 | <5 | 9 | 33 | 1.56 |
| 16 | 7 | 19 | 9 | 1.83 |
| 17 | <5 | 17 | 125 | 1.72 |
| 18 | 6 | 21 | 17 | 1.42 |
| 19 | 8 | 23 | <5 | 1.77 |
| 20 | 6 | 22 | 6 | 0.61 |
| 21 | 15 | 38 | 185 | 2.14 |
| 22 | 8 | 19 | 21 | 1.15 |
| 23 | 12 | 20 | 226 | 1.56 |
| 24 | 34 | 95 | 12 | 5.40 |
| 25 | 12 | 34 | <5 | 1.76 |
| 26 | 5 | 13 | 6 | 1.02 |
| 27 | 10 | 25 | <5 | 1.74 |
| 28 | 8 | 22 | 33 | 1.71 |
| 29 | 18 | 37 | 34 | 3.53 |
| 30 | 17 | 43 | 989 | 1.82 |
| 31 | 33 | 71 | 15 | 3.94 |
| 32 | <5 | 9 | 59 | 1.57 |
| 33 | <5 | 13 | 14 | 1.63 |
| 34 | 14 | 36 | 7 | 2.29 |
| Limit of Detection | 5 | 5 | 5 | 0.01 |

AUSTRALIAN LABORATORY SERVICES P/L
A.C.N. 009 936 029

Brisbane Head Office and Laboratory
32 Shand Street, Stafford, Q. 4053
P.O. Box 66, Everton Park, Q. 4053
Telephone (07) 352 5577
Facsimile (07) 352 5109

# ANALYTICAL REPORT

CENTRE FOR ORE DEPOSIT

Attention: MR R LARGE
YourOrder: LETTER
SampleType: PULP

Page-no: 3
STAFFORD
Batch-no: 8695
Sub-batch: 0
No-samples: 34
Received: 16/05/94
Checked:

| Element | Mn | Ca | Mg | S |
|---|---|---|---|---|
| Unit | ppm | % | % | ppm |
| Method | IC587 | IC587 | IC587 | IC587 |
| 1 | 241 | 2.48 | 1.39 | 1.84% |
| 2 | 211 | 2.12 | 1.18 | 3.50% |
| 3 | 757 | 10.99 | 5.86 | 8790 |
| 4 | 642 | 10.30 | 5.93 | 992 |
| 5 | 534 | 8.41 | 4.80 | 550 |
| 6 | 703 | 10.06 | 5.77 | 9080 |
| 7 | 994 | 10.49 | 9.33 | 9700 |
| 8 | 587 | 11.15 | 6.64 | 255 |
| 9 | 824 | 6.59 | 3.68 | 1.91% |
| 10 | 519 | 5.33 | 2.90 | 1.19% |
| 11 | 1470 | 10.00 | 5.68 | 6780 |
| 12 | 2170 | 12.78 | 7.37 | 5250 |
| 13 | 2510 | 11.16 | 6.29 | 6160 |
| 14 | 4670 | 9.77 | 5.25 | 1.51% |
| 15 | 3400 | 11.41 | 6.34 | 6110 |
| 16 | 3440 | 9.77 | 5.26 | 1.12% |
| 17 | 4360 | 10.93 | 5.98 | 8060 |
| 18 | 1990 | 9.47 | 5.32 | 6910 |
| 19 | 2220 | 11.59 | 6.47 | 7830 |
| 20 | 375 | 2.46 | 1.23 | 4260 |
| 21 | 546 | 7.69 | 4.14 | 2.04% |
| 22 | 771 | 11.24 | 6.45 | 6020 |
| 23 | 668 | 9.69 | 5.43 | 1.17% |
| 24 | 2470 | 4.53 | 2.22 | 5.41% |
| 25 | 2100 | 11.13 | 5.70 | 1.15% |
| 26 | 1050 | 13.10 | 7.60 | 4320 |
| 27 | 2170 | 10.96 | 5.15 | 1.24% |
| 28 | 2400 | 8.20 | 4.43 | 1.09% |
| 29 | 1940 | 5.84 | 3.06 | 3.15% |
| 30 | 1120 | 9.13 | 5.05 | 1.38% |
| 31 | 1120 | 5.98 | 3.22 | 3.76% |
| 32 | 1550 | 14.07 | 7.76 | 4840 |
| 33 | 3010 | 11.63 | 6.41 | 7660 |
| 34 | 2250 | 10.27 | 5.72 | 1.75% |
| Limit of Detection | 5 | 0.01 | 0.01 | 10 |

# Application of the Alteration Index to the Kamarga zinc–lead deposit: preliminary report

**Peter McGoldrick**
*CODES Key Centre*

## Summary

This report reviews the geology of the large, low-grade, sub-economic, stratabound Kamarga deposit, and presents an assessment of existing core grind whole-rock geochemical data (Jones, 1986) using the Alteration Index (AI) and $MnO_D$ index developed for Lady Loretta and HYC by Large & McGoldrick (1993). The Kamarga data ***do not*** have patterns like those from the stratiform deposits. Hence, application of the AI could have substantially down-graded the prospectivity of the deposit at an earlier stage of drilling (the data presented here are from four of eighteen diamond drill holes through the Kamarga mineralisation).

## Introduction

The Kamarga deposit is a large low grade Zn–Pb resource hosted in evaporitic sediments of the Gunpowder Creek Formation. It is located about 200 km north of Mount Isa on the southern flanks of the Kamarga Dome (Fig. 1).

## History

The Kamarga mineralisation was discovered in the early 1970s by CRAE and Newmont. The area was extensively drilled (18 diamond drillholes) by these companies between 1973 and 1980. This work established a resource of approximately 50 million tonnes of mineralisation at a grade of about 3% Zn + Pb in a triangular area of about 2.5 $km^2$ (Fig. 2). A higher grade zone (5–10% Zn+Pb) of about 10 million tonnes is present within this lower grade resource (Jones, 1986).

## Geology

### Sedimentology

The Gunpowder Creek Formation together with the underlying Torpedo Creek Quartzite are a terrestrial to shallow marine sequence at the base of the McNamara Group (Cavaney 1975) Hutton var.). At Kamarga, Jones (1986) distinguished three subfacies of the Torpedo Creek Quartzite and eight separate members within the Gunpowder Creek Formation (Table 1).

Jones (1986) interpreted depositional environments for the Torpedo Creek Quartzite and Gunpowder Creek Formation to represent a transition from a terrestrial to marginal marine (or lacustrine) setting. Torpedo Creek Quartzite sedimentation commenced with fluviatile conglomerates and sandstones deposited from braided ephemeral streams (Facies 1 and 3). Facies 2 of the Torpedo Creek Quartzite represents a palaeoregolith. Wave ripples become

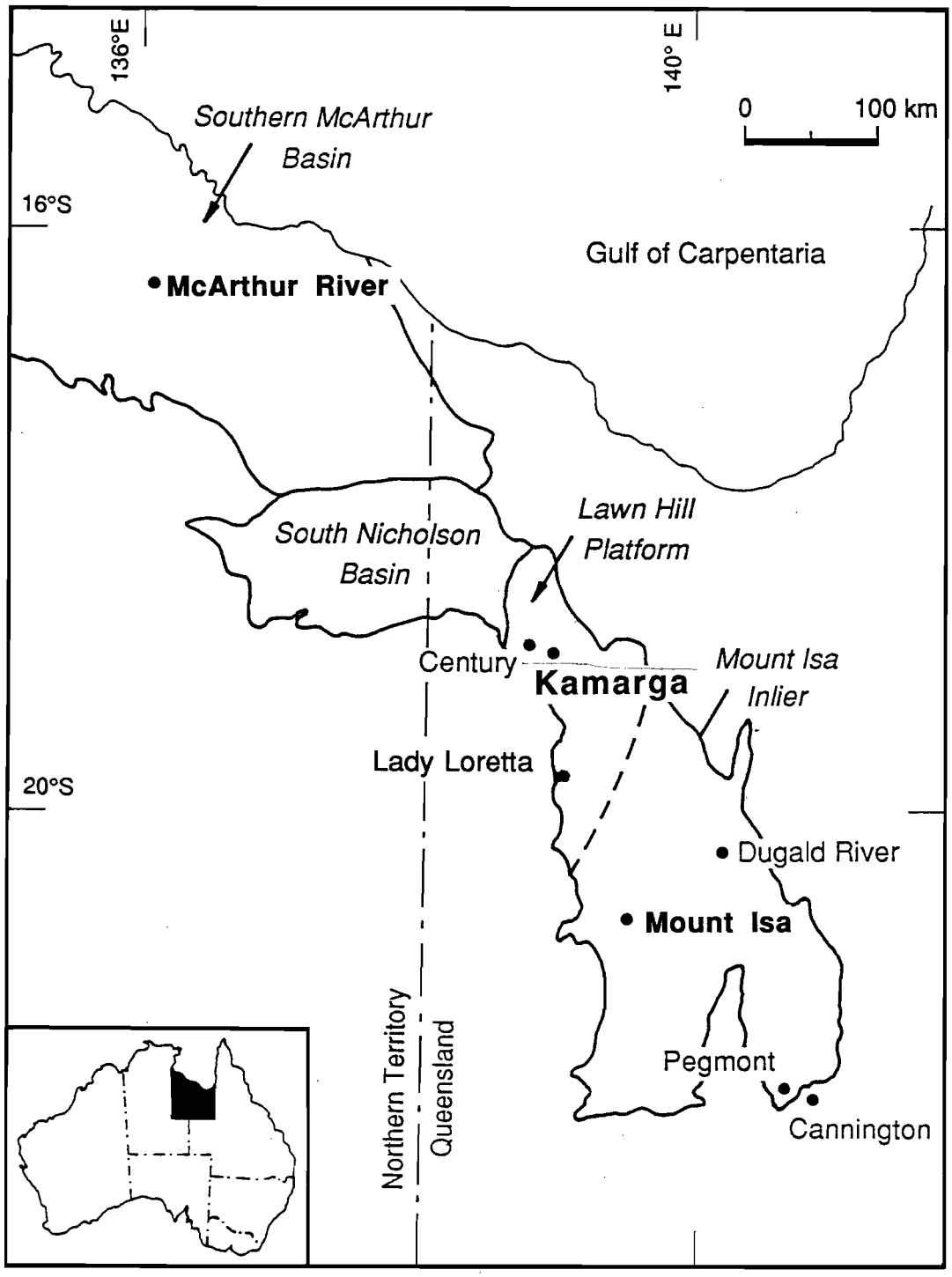


*Figure 1 — Major geological subdivision of northwest Queensland and eastern Northern Territory showing the location of the Kamarga deposit.*

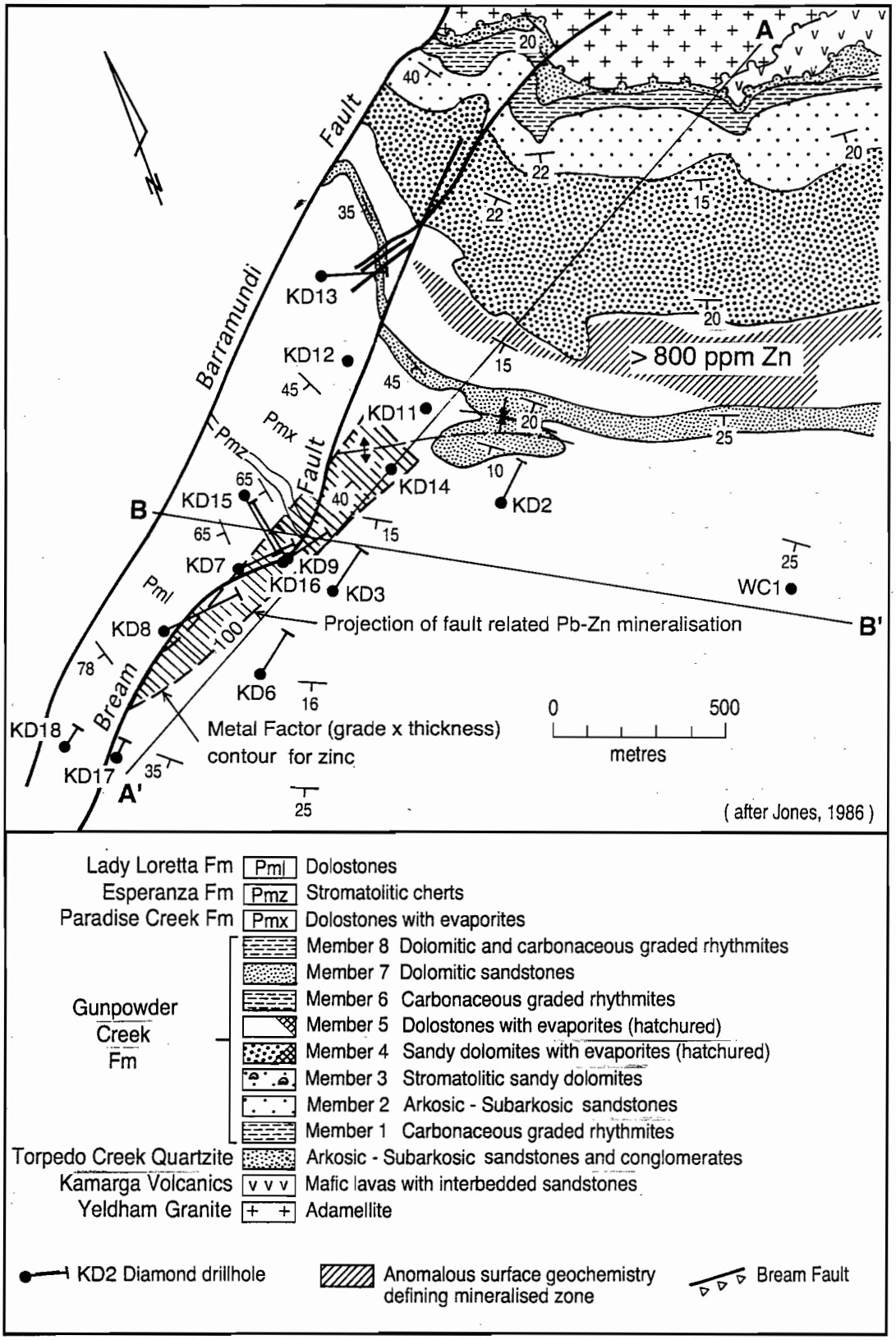


*Figure 2 — Plan view of the geology of southern edge of the Kamarga Dome east of the Barramundi Fault with DDH localites. The surface Zn anomaly and the projection of the mineralisation to the surface ('Grade-Thickness Contours') are also displayed.*

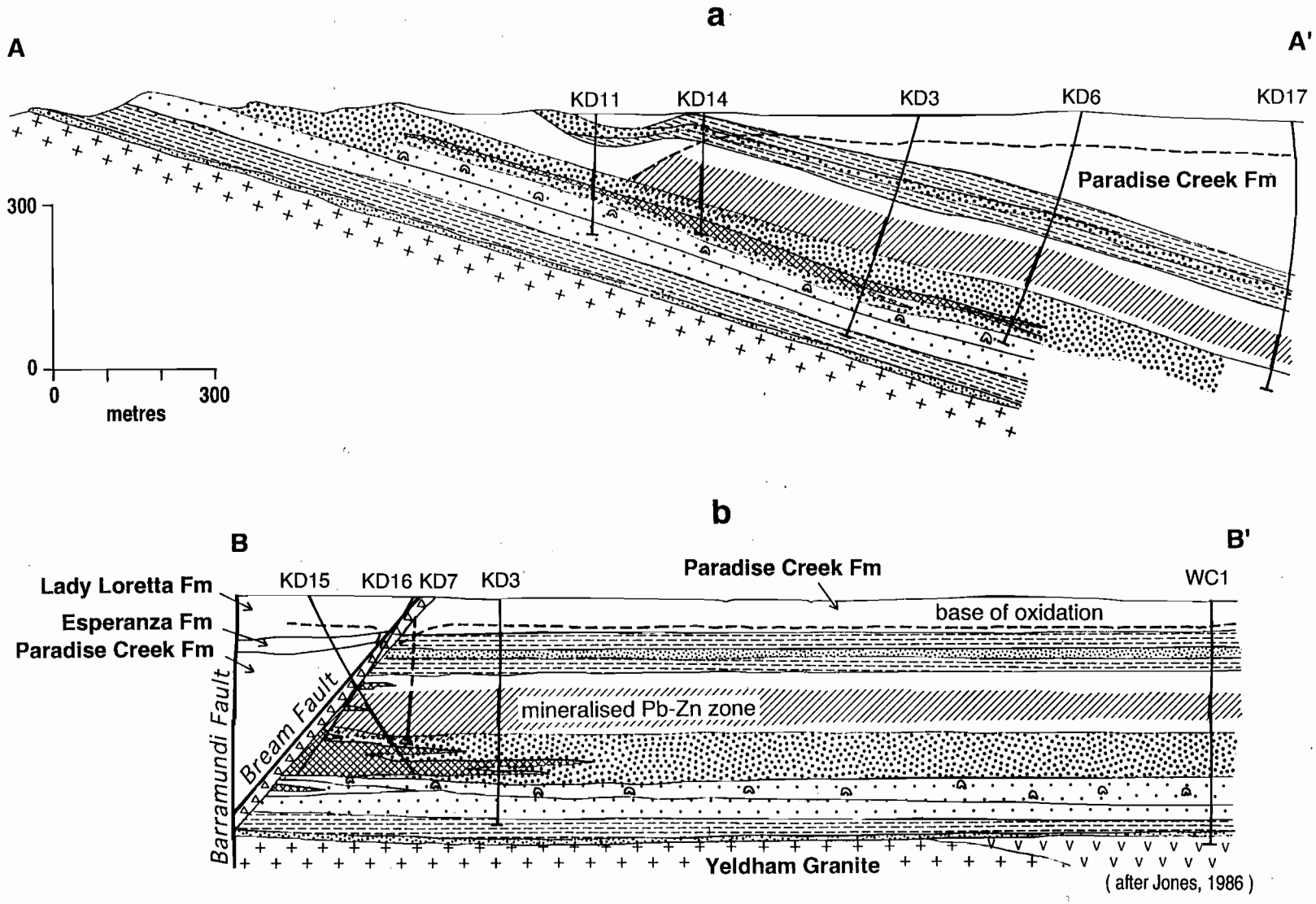


*Figure 3 — Geological cross-section (a) and long-section (b) of the Kamarga deposit (legend as for Figure 2).*

## TABLE 1 SUMMARY OF CHARACTERISTICS OF TORPEDO CREEK QUARTZITE AND GUNPOWDER CREEK FORMATION

| FACIES/MEMBER | LITHOLOGY | TEXTURAL COMMENTS | BEDDING CHARACTERISTICS | SEDIMENTARY STRUCTURES |
|---|---|---|---|---|
| FACIES T1 | Granule to boulder grade, polymictic conglomerate. Arkosic to subarkosic sand matrices. | Framework supported angular to submounded clasts. Clean sand matrices. | Thick to very thick bedded. Localised within lenses up to 100 m wide x 8 m thick. Lens out on edges to single pebble horizons. Abrupt lower surfaces-scour? | Massive, structureless occasional oriented pebbles. Ungraded, poorly sorted. |
| FACIES T2 | Granule to boulder grade, monomict to polymict breccia. Arkosic to subarkosic sand matrices. | Framework supported very irregularly shaped clasts. Sand matrices. | Widespread, thin sheet ranging from less than a metre to ~5 metres in thickness mantling uncontormity surface, minimal transport - possibly *in situ*. | Massive, structureless, very poorly sorted, ungraded. |
| FACIES T3 | Fine to medium, rarely coarse grained arkose and subarkose. Occasional pebble horizons. Silty intercalations common in upper sections. | Framework supported, matrix free, moderate to good sorting. Quartz > dolospar cement. | Planar, parallel-wavey thin to thick bedded. Gradational upper contact. | Massive-parallel laminated occasional planar cross-lamination. Current ripples. Symmetrical and assymmetrical wave ripples. Rare dessication polygons. Graded silty horizons. |
| MEMBER 1 | Graded fine grained sandstone - carbonaceous siltstone rhythmites. Minor evaporite mush facies. | Mostly framework supported, minor-matrix, poorly sorted. Dolospar >> quartz cement. | Thin- to very thin-bedded 1-5 cm graded couplets. Planar to slightly wavey bedding. Gradational upper and lower contacts. | Abundant synaeresis cracks. Planar to wavey laminated, minor planar, trough and ripple cross-lamination. Well developed grading within couplets, with sharp based sandstone lamina grading up to carbonaceous siltstone. Occasional slumped bedding. |
| MEMBER 2 | Fine to medium grained subarkose and arkose, with minor quartzites. Subordinate interbedded siltstone and evaporite mush facies. | Framework supported, well sorted, matrix free. Dolospar > quartz cement. | Thin to thick bedded, planar, parallel sided beds with abrupt contacts. Top and bottom of member gradational. | Massive to laminated. Mainly horizontal lamination, occasional planar cross lamination and graded lamination towards base of unit. Ripple marked. Convolute lamination developed in some silty horizons. |
| MEMBER 3 | Stromatolitic dolomite. Dolomitic siltstone, silty to sandy dolomite, dolomitic sandstone, nodular and minor mush facies evaporites. | Dispersed to framework supported, moderately to well sorted sands micrograded silts. Dolospar >> quartz cement. | Appears to form lensoidal bodies 100's-1000's m wide x 10-50 m thick - mounds or banks. Top and bottom of member gradational. | Algal laminated, stromatolitic, intraclastic, planar to wavey and contorted lamination in fine grained lithologies. Massive to laminated sandstones. Minor nodular and mush textured evaporites. |
| MEMBER 4 | Dolomitic sandstone, sandy and intraclastic dolarenite, laminated dolomitic siltstone and dololutite. Sandy mush facies evaporites and nodular evaporites. | Framework supported, moderately sorted sands, poorly sorted intraclastic gravels. Dispersed, matrix supported, sands. Dolospar >> quartz cement. | Medium to thin bedded. Extensive interfingering of facies, abrupt contacts. Top and bottom of member gradational. | Massive to laminated sandstone and gravels, algal planar to wavey lamination in fine grained lithologies. Stromatolites. Intraclastic breccias. Abundant nodular and mush textured evaporites. Rare cross lamination and ripples. |
| MEMBER 5. | Micritic dolostone, silty and sandy dolomite, dolarenite. Intraclastic dolomite. Nodular and mush textured evaporites. | Micritic and microsparry dolomite. Framework supported, fine to medium grained, poorly sorted to bimodal sandy matrices to intraclastic dolomites. Micrograded silts. | Thick to very thin bedded. Fine interbedding of various facies with generally abrupt contacts. Bottom of member gradational, top relatively sharp. | Massive to laminated, cross laminated, micrograded. Algal laminations and stromatolitic. Intraclastic breccias, oolites, fenestral fabrics.? Grumeleuse structures. Nodular and mush textured evaporites. Halite casts. |
| MEMBER 6 | Graded fine grained sandstone - carbonaceous siltstone rhythmites. | Mostly framework supported, minor matrix, poorly sorted. Dolospar cements. | Thin to very thin bedded, 1-5 cm graded couplets. Planar to slightly wavey bedding. Top and bottom of member sharp. | Abundant synaeresis cracks. Planar to wavey laminated, minor cross lamination well developed grading within couplets from sharp based sands up to carbonaceous silts. Rare nodular evaporites. |
| MEMBER 7 | Dolomitic sandstones, sandy dolomites, dolomitic siltstones. | Fine to medium grained dispersed to framework supported, moderately sorted. Dolospar cement - largely recrystallised from micritic matrix. | Thin to thick bedded, planar to parallel sided beds. Top and bottom of member sharp. | Planar laminated, rare cross lamination. Intraclastic breccia and stromatolitic horizons. |
| MEMBER 8 | Graded sandstone - carbonaceous siltstone rhythmites. | Dispersed to framework supported, poorly poorly sorted fine sands. Dolospar cements and matrices. | Thin to very thin bedded. 1-5 cm graded couplets. Planar to slightly wavey bedding. Top and bottom of member sharp. | Graded couplets with planar to wavey lamination, minor cross lamination and convolute lamination, intraclastic breccias, algal lamination and stromatolitic structures. Minor nodular evaporites. |

(Jones, 1986)

common and palaeocurrent directions are more diverse toward the top of the Torpedo Creek Quartzite suggesting a change to a marginal marine or lacustrine environment. The graded rhythmites of Member 1 of the Gunpowder Creek Formation mark the culmination of this transgressive phase. Fine and medium grained arkoses and quartz sandstones of Member 2 were deposited in an ephemeral stream environment indicating a return to emergent conditions. Microbial laminated dolomites and dolomitic clastic sediments of Member 3 are interpreted as a mound-forming subtidal stromatolitic facies.

Members 4 and 5 of the Gunpowder Creek Formation are a mixed facies representing the transition from siliciclastic to carbonate (dolomite) dominated sedimentation. Member 4 contains four main facies:

(i) dolomitic sandstones and intraclastic sandy dolomites
(ii) algal laminated dolomitic siltstones and dololutites with nodular evaporites
(iii) stromatolitic dolomites identical to Member 3
(iv) evaporite mush facies

Member 5 is similar to Member 4 but lacks the siliciclastic component and thick evaporite mush of the latter. Jones (1986) interprets both Members to have been deposited in a sabkha setting with the different facies forming in the sub-tidal, intertidal and supratidal parts of the sabkha. Jones (1986) also notes a small-scale (1–5 m) cyclicity in Members 4 and 5. In DDH WC1 these cycles commence with coarse sands and intraclast conglomerates and pass upwards into massive and (cryptalgal?) laminated dolomites and dolomite after sulphate evaporite. The top of the cycles are usually marked by carbonaceous laminites which may contain chert nodules (after displacive anhydrite). Shoaling upwards cycles on this scale are necessary to conclusively demonstrate a sabkha setting in ancient evaporite sequences (Bull, pers. comm. 1994; Warren, 1989).

Member 6 contains fine sandstone and carbonaceous siltstone rhythmites similar to Member 1 and records the onset of a second major transgressive cycle. Member 7 comprises thin and thick bedded plane laminated dolomitic sands and is interpreted to be a (?subtidal) sabkha margin sandflat. Member 8 is similar to Members 1 and 6 but lacks synaeresis cracks.

### Structure

In the Kamarga area lower McNamara Group sediments dip gently off the flanks of the Kamarga Dome (Fig. 3, see page 44). Near the deposit the southern margin of the dome is displaced by a regional scale, northeast trending, fault with a dextral offset of about 6 km (the Barramundi Fault). Mineralisation is localised against a smaller fault (the Bream Fault) which forms a splay or scissors fault about 200 m east of, and sub-parallel to, the Barramundi Fault (Fig. 2).

### Mineralisation

The Kamarga mineralisation occurs in Members 4 and 5 of the Gunpowder Creek Formation. It forms a zone at least 100 m thick and extends east from the Bream Fault for at least 1.5 km, and for about the same distance down-dip. Pyrite – base metal mineralisation occurs as veins, breccia cements, irregular disseminated and massive zones, open space fillings and late stage open veins. Pyrite and sphalerite are the most abundant sulphides with lesser amounts of galena, chalcopyrite and jordanite. Pyrite and chalcopyrite are most abundant near to the Bream Fault and decrease eastward. There are several non-sulphide minerals commonly associated with the mineralisation (in order of decreasing abundance): dolospar, quartz, bitumen and fluorite.

Jones (1986) argues that the sulphide–sediment relationships and the discordant nature of the mineralisation indicate that it post-dates the deposition of the host sediments, and, furthermore, because diagenetic fabrics are overprinted, post-dates early stages of diagenesis.

## Formation of the mineralisation

### Fluid inclusions

Studies of fluid inclusions in sphalerite, carbonate, quartz and fluorite from the Kamarga mineralisation were reported in Jones (1986) and Wilkins (1979). Salinities of between 16 and 22 wt% NaCl were measured in primary inclusions. Pressure corrected trapping temperatures for sphalerite, dolospar and quartz, and fluorite are 270°–320°C, 230°–335°C, and 160°–260°C, respectively (Jones, 1986: 113). Pressure estimates are constrained between about 130 bar hydrostatic and 330 bar lithostatic. Jones (1986) agued that the presence of $CO_2$-rich fluid inclusions was evidence that an immiscible $CO_2$ phase was generated in the mineralised zone during the mineralising event.

### Lead and sulphur isotopes

Lead in galena from Kamarga is non-radiogenic and homogeneous indicating a 'well mixed crustal source' for the lead in the deposit (Jones, 1986). In contrast, Pb in syndiagenetic pyrite is radiogenic and inhomogeneous, and interpreted by Jones (1986) to derive more locally (from McNamara Group sediments). Lead in epigenetic pyrite is a mixture of these two types.

Light S is present in syndiagenetic pyrite of Member 1, indicating a biogenic origin (Jones, 1986). In contrast, sulphides from the main mineralised zone have $\partial^{34}S$ values between 12 and 27 ‰, consistent with the mineralising fluid having a $\partial^{34}S$ of about 20 to 25 ‰. Jones (1986 p.136) concluded that this indicated that the bulk of the S in the deposit was sourced from sulphate derived from dissolution of evaporites within the lower McNamara Group (?during diagenetic dolomitisation of primary sulphates). Two sphalerite-galena mineral pairs indicated temperatures of formation of 270°C and 330°C comparable to mineralising temperatures suggested by fluid inclusions.

### Genetic model

Jones (1986) proposed a genetic model for the Kamarga deposit that envisages the incorporation of sulphate-rich, connate brines into a hydrothermal convection system formed in response to elevated geothermal gradients in an extensional tectonic regime. Circulation through the 'basement' caused high temperature water–rock interaction which reduced sulphate to $H_2S$ and extracted metals from the rocks. Subsequently, this fluid (salinity about 5 molar, temperature about 300°C, moderately acid (pH of 3 to 4), and moderately reduced (pyrite stable, $H_2S>>SO_4^{2-}$)) was expelled up the Bream Fault, where mineralisation formed when the fluid first encountered dolomitic sediments (i.e. Members 4 and 5 of the Gunpowder Creek Formation). The main drive for metal sulphide and dolospar precipitation was neutralisation reactions, with smaller amounts of late stage fluorite and barite deposited in response to declining temperature.

It is noteworthy that Jones (1986) suggested that the Kamarga mineralising fluids were also responsible for sideritic, base metal anomalous horizons higher in the stratigraphy (Lady Loretta Formation) at Kamarga. However, the physico-chemical controls on siderite formation (Cooke, pers comm. 1994) are probably not compatible with siderite formation from Jones' Kamarga fluid.

## The Alteration Index at Kamarga

### The data

Jones (1986) presents total rock analyses for 49 samples from four drill-holes from Kamarga and these data will be used here to examine the Alteration Index (AI = 100(FeO + 10MnO)/(FeO + 10MnO + MgO + $Na_2O$); Large and McGoldrick, 1993) and '$MnO_D$' ($MnO_D$ = (MnOwhole rock × 30.41)/CaOwhole rock (for rocks with >1wt% CaO); Large and McGoldrick, 1993). Samples analysed were continous core grinds of between 2 and 40 m in length from DDH KD7 (which intersects the main mineralised zone), DDH KD2/3 (on the eastern fringe of the main mineralisation), DDH WC1 (about a kilometre east of the mineralisation) and DDH KD 16 (adjacent to the Bream Fault). Elements measured for most samples include the major elements, $CO_2$, Cu, Zn, Pb and Ba. The full analyses are presented in Jones (1986) and a copy of the data on diskette can be made available to sponsors on request.

### Preliminary discussion

Jones (1986) states that his continous core grinds represent uniform rock types or complete individual members of the Gunpowder Creek Formation. Recent inspection of some of the sampled core by the writer indicates that within sample lithological variation can be quite marked. Hence, the long continous grind samples probably represent 'average' analyses of a mixture of rock types, and as such are not directly comparable to the 20 to 30 cm 'grab' samples used for previous geochemical studies in this project (McGoldrick, 1993). There is no *a priori* reason why core grinds would not be appropriate to alteration index studies, but long sample intervals would be expected to reduce 'spiky' anomalies and may disguise more subtle variations. Furthermore, Jones (1986) only briefly describes his analytical techniques (AAS for majors and flame photometry for the alkalis) and does not provide an estimate of precision and accuracy for his data. However, be this as it may, the data can be used to calculate AI and $MnO_D$ and have important implications for the status of the Kamarga mineralisation. Further geochemical work is planned (see below) to confirm the preliminary interpretation presented here.

### Results

Figure 4 displays Zn and AI for all 49 samples. There is a general trend of high Zn with low AI and low Zn with high AI. This is the opposite of the trend shown by host siltstones at Lady Loretta and HYC (Large & McGoldrick, 1993).

The MgO/CaO relationship (Fig. 5) indicates that dolomite is the only important carbonate mineral in all but five of the samples. The $MnO_D$ values have been calculated for these samples and are compared with Zn and AI on Figure 6. There is a general trend of increasing $MnO_D$ with increasing AI, but, many samples have relatively low $MnO_D$ with moderate to high AI. Only one sample has 'anomalous' $MnO_D$ if 1wt% is used as a cut-off (see Large, this volume, for further discussion of 'anomalous' $MnO_D$ ). Furthermore, Zn and $MnO_D$ display a broadly antipathetic relationship.

Downhole plots through the mineralised zone also emphasise a ***lack of correlation*** of Zn-rich intervals with high AI and $MnO_D$ (Figs 7 and 8).

### Discussion and conclusions

Clearly, if it is assumed that the relations described are not an artefact of sampling, then the ***AI/$MnO_D$ signature of*** the stratabound ***Kamarga*** mineral-

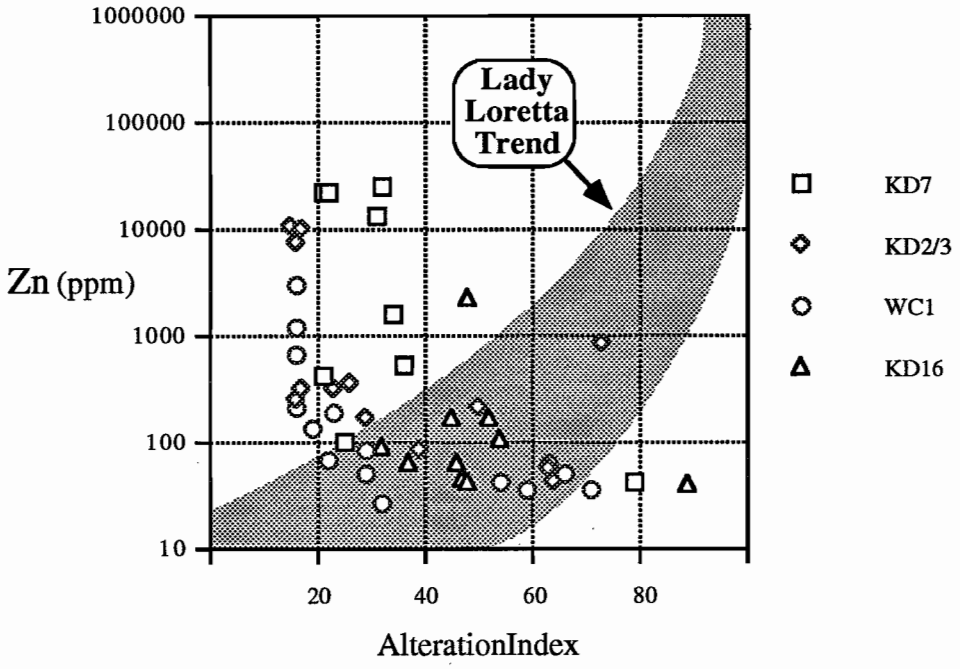


*Figure 4 — Zinc and Alteration Index for 49 samples from Kamarga (data from Jones, 1986).*

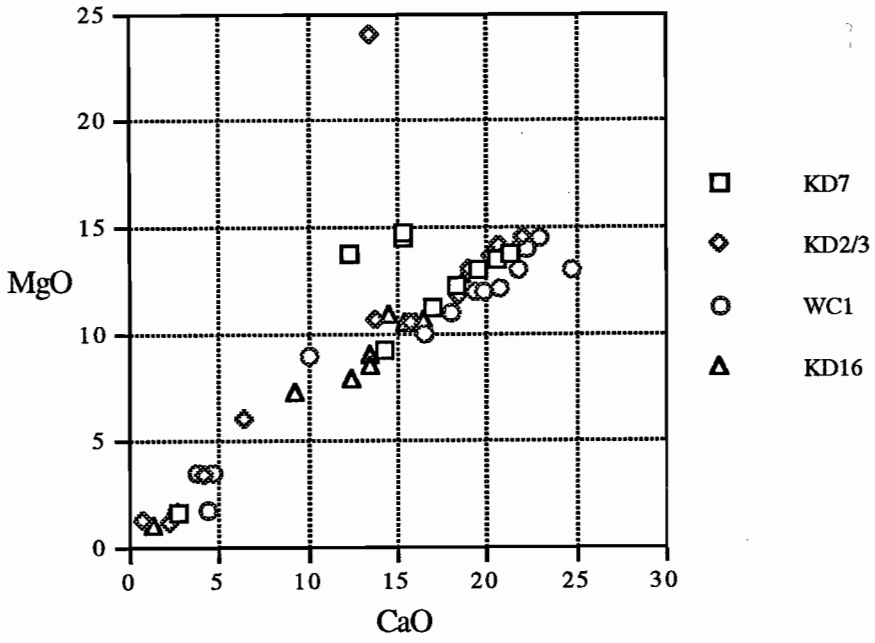


*Figure 5 — MgO and CaO in 49 samples from Kamarga. Most samples lie on a dolomite compositional trend; three MgO-rich samples are from the bottom of DDH KD7 and contain visible siderite.*

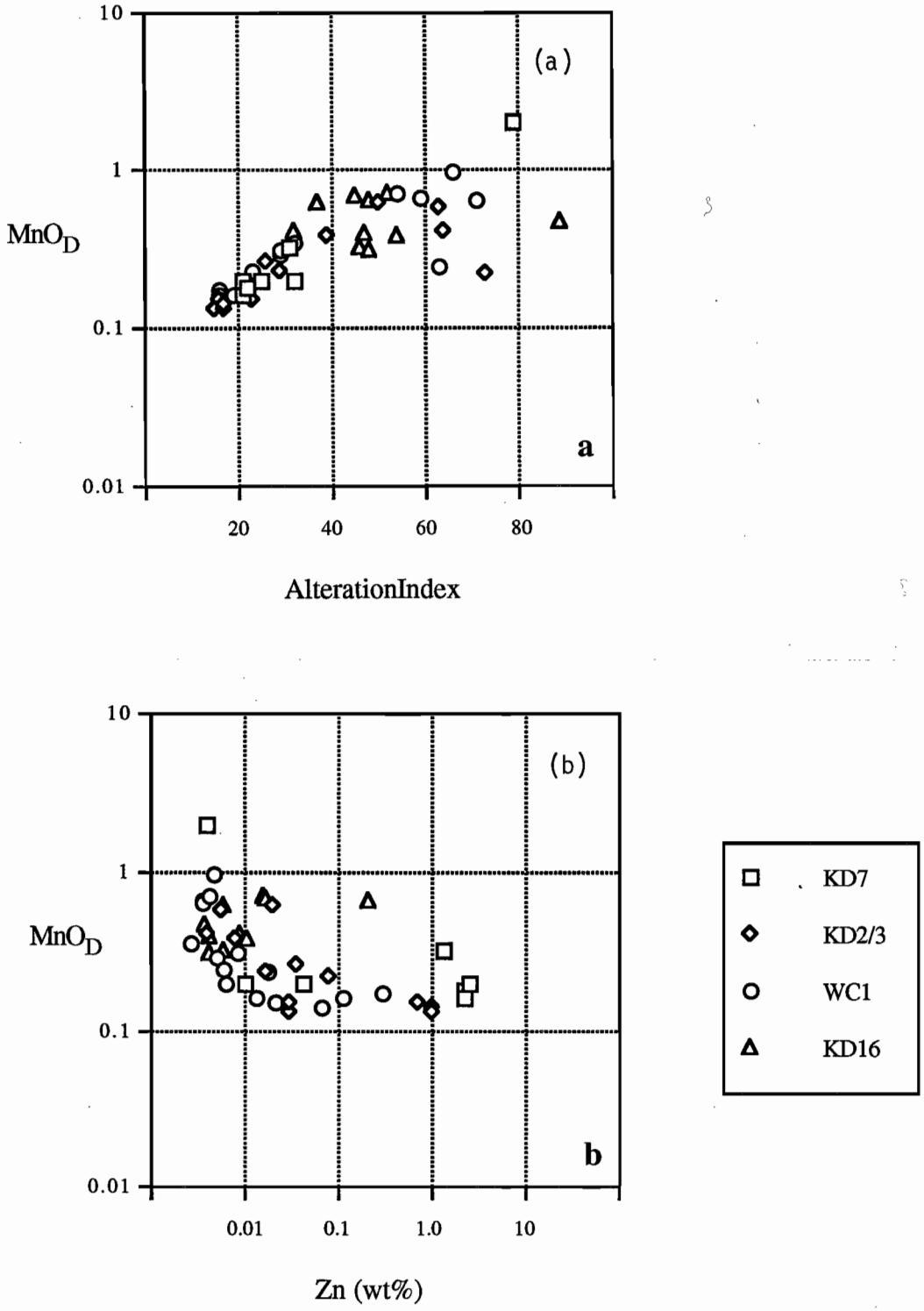


*Figure 6 — (a) $MnO_D$–AI and (b) $MnO_D$–Zn relationship in 44 dolomitic samples from Kamarga.*

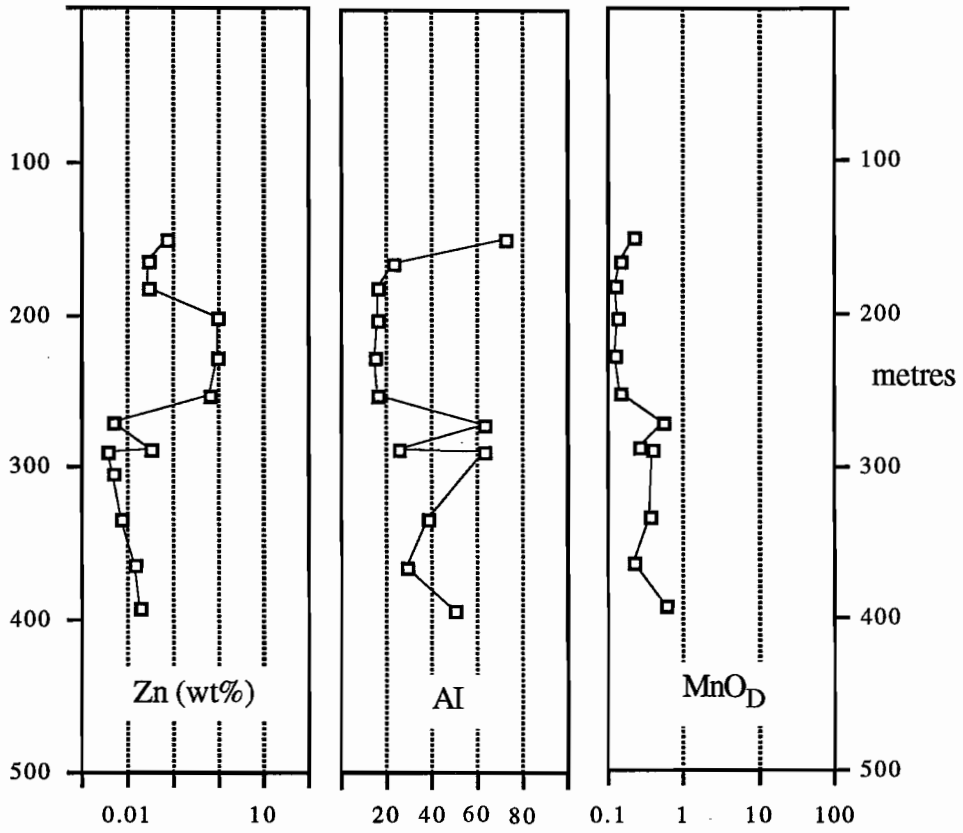


*Figure 7 — The depth–Zn–AI–$MnO_D$ relationship in DDH KD2/3. Note highest Zn values correspond to lowest AI and $MnO_D$.*

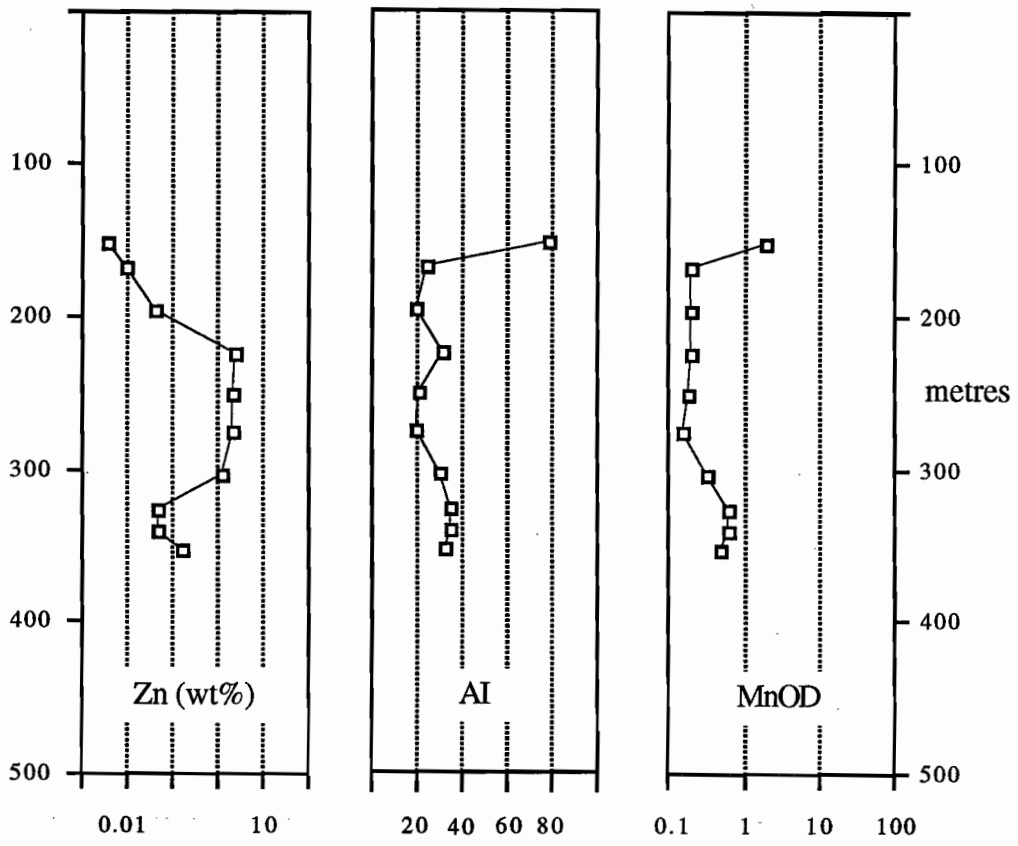


*Figure 8 — The depth–Zn–AI–$MnO_D$ relationship in DDH KD7.*

isation is ***quite distinct from*** that of the stratiform ***Lady Loretta and HYC*** deposits. This difference is interpreted to indicate a fundamentally different mineralising process has operated at Kamarga. Either, the fluids were of a different physico-chemical character to those that formed the stratiform deposits (see Cooke, this volume), or, mineralising fluids were restricted to specific pathways and pervasive rock alteration could not occur, or both. Regardless of the mineralising process, the ***Al/MnO$_D$ analysis substantially down-grades the prospectivity of the Kamarga mineralisation*** and could have been used to argue for cessation of drilling at a much earlier stage of exploration.

## Future work

The writer has recently re-sampled two of the diamond drill-holes from Kamarga. Chemical analyses will be carried out to confirm the trends reported here can be repeated using grab samples. A re-assessment of the available fluid inclusion data (the chief constraint on ore-fluid temperature) will also be undertaken.

## References

Cavaney, R. J., 1975. Stratigraphic and structural controls to copper mineralisation in the Mount Isa — Lawn Hill district, Unpubl. MSc thesis, James Cook University of Northern Queensland: 116 pp.

Hutton, L.J. and I.P. Sweet, 1981. New and revised stratigraphic units, Lawn Hill Platform, northwest Queensland. *Qld. Govt. Mining Journal* 82: 423–434.

Jones, D.A., 1986. The Kamarga Deposit: stratabound zinc–lead mineralisation in the Middle Proterozoic McNamara Group, northwest Queensland, Unpubl. PhD thesis, University of New England: 198 pp.

Large, R.R. and P.J. McGoldrick, 1993. Deposit Halos 5. Primary geochemical halos related to Proterozoic sediment hosted Pb–Zn deposits and applications to exploration, CODES: AMIRA/ARC Project P384, unpublished report no. 3: 31–62.

McGoldrick, P.J., 1993. Deposit Halos 4. Sampling and whole rock analyses for the Lady Loretta deposit, CODES: AMIRA/ARC Project P384, unpublished report no. 3: 63–226.

Warren, J.K., 1989.*EVAPORITE SEDIMENTOLOGY*. Prentice-Hall Books: 310 pp.

Wilkins, R.W.T., 1979. Fluids associated with the origin of the Kamarga carbonate-hosted Pb/Zn prospect. CSIRO Division of Mineralogy, Restricted Investigation Report 1051R: 12 pp.

# Progress report: Conditions of formation for siderite and ferroan carbonate — implications for the formation of sediment-hosted base metal deposits

**David R. Cooke, Ross Large and Peter McGoldrick**
*CODES Key Centre*

Our recent research has emphasised the importance of siderite and ferroan dolomite on the halo to stratiform sediment-hosted zinc–lead deposits. Thermodynamic modelling of siderite and ferroan dolomite stability places important constraints on the genesis of these deposits. This work demonstrates that $CO_2$ fluid concentration is probably the dominant control on hydrothermal carbonate formation. Siderite and ferroan dolomite are stabilised at high ΣC and low ΣS concentrations. Lower temperatures will stabilise siderite at constant $a_{CO2}$. Ferroan carbonates that form under relatively oxidised to oxidised conditions in association with pyrite or hematite are favoured by lower temperatures and/or high ΣS concentrations, and have the potential to be associated with base metal-rich solutions.

Our calculations indicate that for siderite to form with lead–zinc by exhalation, then at least 250–500 m water depth is required to prevent fluid boiling. Alternatively siderite can form by subsurface replacement of dolomitic sediments below the palaeowater table.

## Introduction

Carr (1984) and Waltho & Andrews (1993) reported the presence of siderite in the Lady Loretta and Century sediment-hosted massive sulfide (SHMS) deposits. Lambert & Scott (1973) noted the occurrence of ferroan dolomite (up to 2 wt. % Fe) in the sediments underlying the HYC deposit, and Eldridge et al. (1993) noted the presence of ferroan dolomites $(Ca_{0.50}Mg_{0.33-0.41}Fe_{0.07-0.15}Mn_{0.02-0.03})CO_3$ associated with Pb–Zn mineralisation in the same system. Large & McGoldrick (1993) have emphasised the importance of siderite and ferroan carbonate halos as a potential guide to exploration for SHMS deposits. This preliminary report discusses some of the controls on siderite and ferroan carbonate deposition from low-moderate temperature hydrothermal fluids as a function of temperature and fluid composition, and discusses their implications for the genesis of SHMS deposits.

## Redox state of hydrothermal fluids

Before discussing controls on ferroan carbonate deposition, it is first necessary to briefly consider the redox state of hydrothermal fluids. While some workers advocate using hydrogen fugacity or the ratio of oxidised to reduced sulfur as a means of defining the oxidation state of a system, the most commonly used reference frame remains oxygen fugacity ($f_{(O2)}$). Igneous petrologists commonly use mineral buffers that occur at fixed values of $f_{(O2)}$ (at a given temperature and pressure) to define the redox state of magmatic systems (e.g. Nickel–Nickel Oxide [NNO]; quartz–fayalite–magnetite [QFM]; etc.). In hydrothermal systems, economic geologists



commonly refer to oxidised and reduced fluids without specifically defining what these terms mean. As an initial guide, the mineral assemblage hematite–magnetite can be used to define oxidised (ie. hematite-stable) vs reduced (magnetite-stable) conditions at neutral to alkaline pH (Fig. 1). While hm–mt represents a fixed point buffer that provides a unique value of $f_{(O2)}$ at any given temperature, it is not a stable assemblage in acidic solutions (Fig. 1), except when total sulfur concentrations ($\Sigma S$) are low enough to stabilise magnetite at the expense of pyrite. Instead, hematite–pyrite (hm–py) provides a guide for the transition from 'oxidised' to 'reduced' conditions in acidic solutions. Hm–py is a sliding-scale buffer, providing a unique value of $f_{(O2)}$ only for a given temperature, pH and $\Sigma S$ concentration.

Just as mineral assemblages reflect redox transitions in hydrothermal systems, so too does aqueous species behaviour. Hundreds or even thousands of aqueous species may be present in a hydrothermal solution, but any given species is only *abundant* under a restricted range of physiochemical conditions. Consequently, the *predominance fields* of aqueous species are portrayed on log $f_{(O2)}$–pH diagrams to illustrate where one aqueous species is more abundant than other related species. On Figures 1 and 2, the transition from the predominance of oxidised ($SO_4^=$, $HSO_4^-$) to reduced ($H_2S_{(aq)}$, $HS^-$) sulfur species can be seen to be broadly coincident with the transition from hematite to pyrite (acid) and hematite to magnetite (alkaline). Given the importance of sulfur speciation for the formation of base metal deposits, the correlation between oxidised sulfur species and the hematite field demonstrates that hm–mt and hm–py provide good guides to the redox state of the system. Therefore, in this report, *oxidised* fluids are considered to be those where hematite is stable and oxidised sulfur species predominate. *Reduced* fluids are pyrite-, magnetite- and/or pyrrhotite-stable and contain sulfur primarily as sulfide species. *'Relatively' oxidised* systems are those where pyrite or magnetite is stable, but sulfates are the predominant sulfur species in solution.

## Carbon Speciation

The transition from oxidised ($H_2CO_{3\,(aq)}$, $HCO_3^-$, $CO_3^=$) to reduced carbon-bearing species ($CH_{4\,(aq)}$) occurs several log units below the hm–mt, hm–py and oxidised-reduced sulfur boundaries (Figs 1 and 2). This has important implications for carbonate deposition. Carbonate minerals are stable when conditions favour carbon transport as an oxidised species (i.e. in the +4 valence state). Figures 1 and 2 illustrate how dolomite is stable over a broad range of conditions when oxidised carbon species are predominant, but becomes highly soluble when the transition to aqueous methane ($CH_{4\,(aq)}$) occurs (carbonates are also soluble at low pH, where $\Sigma C$ and cation concentrations control the stability field boundary). Because oxidised carbon species persist to lower $f_{(O2)}$ values than oxidised sulfur species, carbonate minerals can coexist with pyrite, magnetite, hematite or (rarely) pyrrhotite.

Aqueous sulfur- and carbon-bearing species are involved in chemical reactions that control siderite/ferroan carbonate deposition (in contrast to Ca, Mn and Mg-carbonates). The involvement of carbon *and* sulfur allows two distinct regimes for ferroan carbonate deposition in $f_{(O2)}$–pH space. Ferroan carbonates may form when oxidised sulfur and carbon species predominate (Fig. 1A) or when reduced sulfur and oxidised carbon are predominant (Fig. 2A). If $\Sigma C$ concentrations are high enough (or $a_{FeCO3}$ is low enough), the two fields may merge, but will still 'wrap' around the pyrite field (Fig. 1B and 2B) due to the change in sulfur speciation. The presence of siderite or ferroan carbonate therefore has the potential to help understand the genesis of sediment hosted Pb–Zn deposits, because it can form in oxidised environments in association with pyrite and/or hematite,

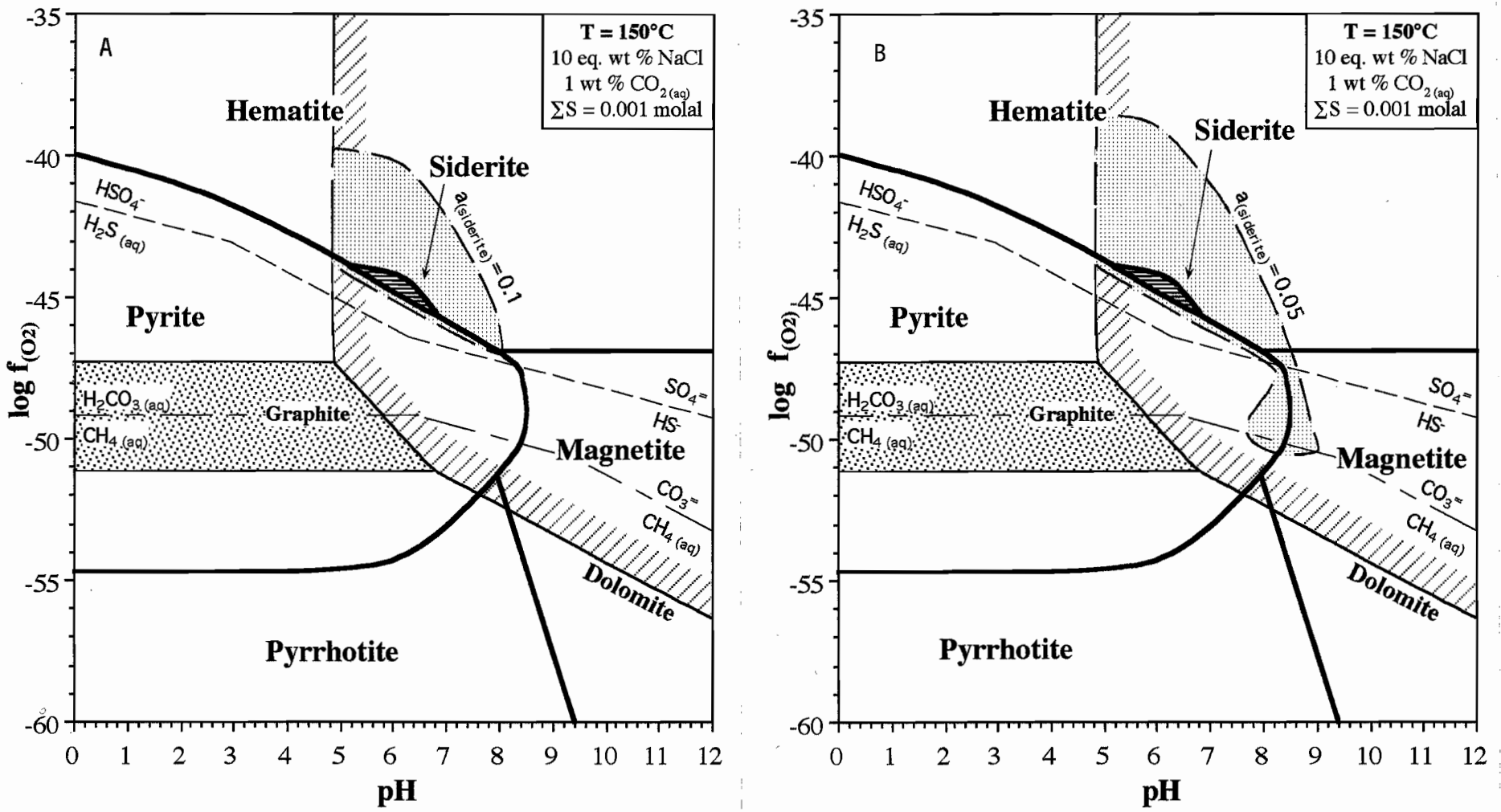


*Figure 1 — Log $f_{O2}$-pH diagram showing the stability fields of the common Fe-O-S minerals (hematite, magnetite, pyrite, pyrrhotite) together with the predominance boundaries between oxidised and reduced sulfur species, and oxidised and reduced carbon species at 150 °C. A: stability fields for pure siderite and ferroan carbonate ($a_{FeCO3} = 0.1$). B: stability field of ferroan carbonate ($X_{FeCO3} = 0.05$). These diagrams have been constructed for 10 eq. wt. % NaCl solutions that contain 0.001 molal ΣS, 0.256 molal ΣC (≈ 1 wt. % $CO_{2\,(aq)}$), 1 wt. % $CaCl_2$ and 36 ppm Mg (the same conditions assumed for the hypothetical fluids used by Cooke (1993a, b) for numerical simulations of mineral deposition from sedimentary brines).*

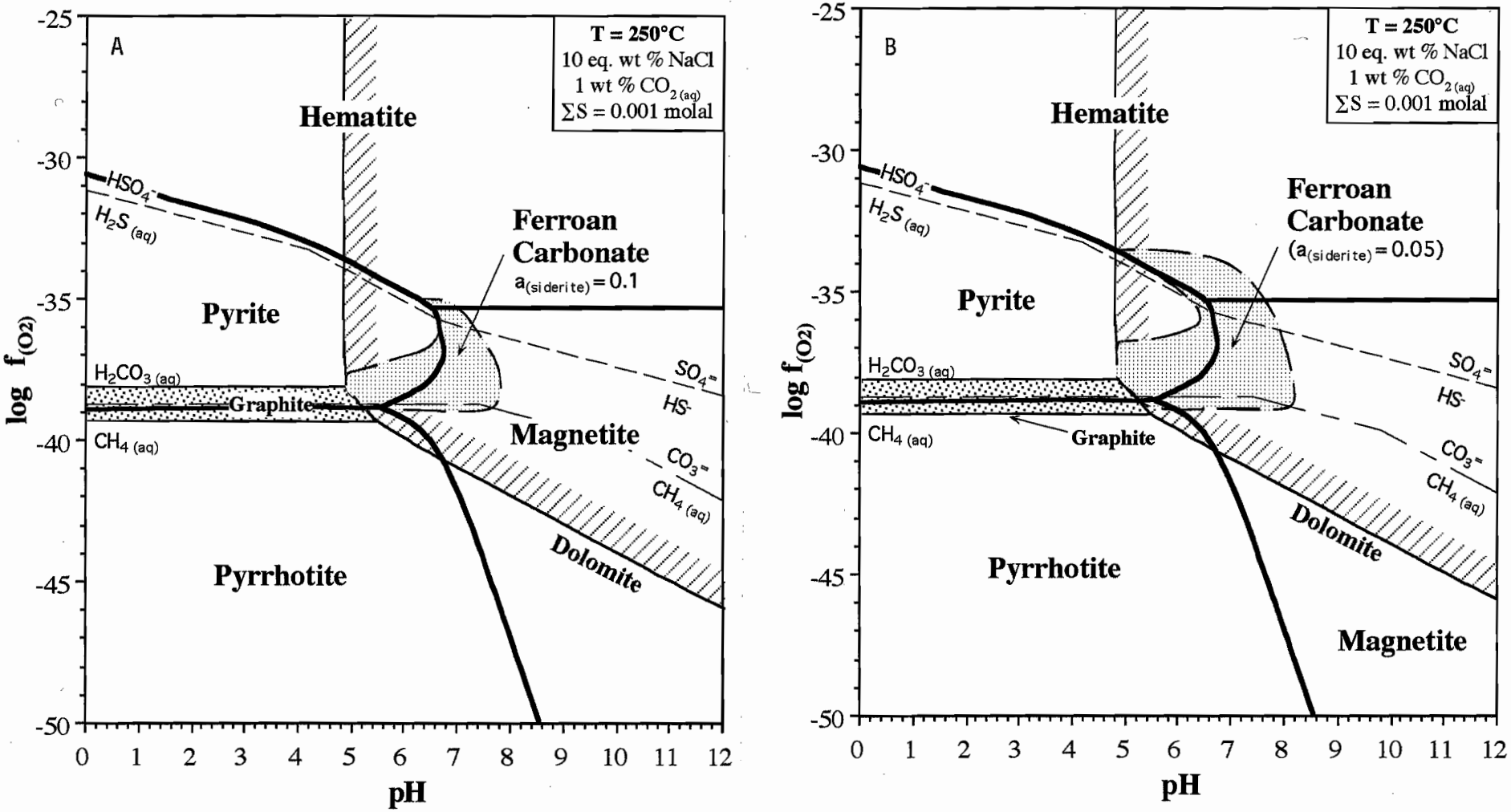


*Figure 2: Log $f_{O2}$-pH diagram showing the stability fields of the common Fe-O-S minerals (hematite, magnetite, pyrite, pyrrhotite) together with the predominance boundaries between oxidised and reduced sulfur species, and oxidised and reduced carbon species at 250 °C. A: stability field for ferroan carbonate ($a_{FeCO3}$ = 0.1). B: stability field of ferroan carbonate ($X_{FeCO3}$ = 0.05). These diagrams have been constructed for 10 eq. wt. % NaCl solutions that contain 0.001 molal ΣS, 0.256 molal ΣC (≈ 1 wt. % $CO_{2\,(aq)}$), 1 wt. % $CaCl_2$ and 36 ppm Mg (the same conditions assumed for the hypothetical fluids used by Cooke (1993A and B) for numerical simulations of mineral deposition from sedimentary brines). Pure siderite is not stable under these conditions.*

or in reduced environments in association with magnetite, pyrite and/or pyrrhotite.

## Controls on siderite and ferroan carbonate deposition

To investigate the controls on ferroan carbonate deposition, four log $f_{(O2)}$–pH diagrams have been constructed that portray the stability fields of the common Fe–O–S minerals (hematite, magnetite, pyrite, pyrrhotite) together with the predominance boundaries between oxidised and reduced sulfur species, and oxidised and reduced carbon species (Figs 1A, 1B, 2A and 2B). Figures 1A and 2A show the stability fields for pure siderite and ferroan carbonate ($a_{FeCO3}$ = 0.1) at 150° and 250°C respectively. Figures 1B and 2B show the stability fields of ferroan carbonate ($X_{FeCO3}$ = 0.05) at 150° and 250°C respectively. These diagrams have been constructed for 10 eq. wt. % NaCl solutions that contain 0.001 molal ΣS, 0.256 molal ΣC (≈ 1 wt. % $CO_{2\,(aq)}$), 1 wt. % $CaCl_2$ and 36 ppm Mg; the same conditions assumed for the hypothetical fluids used by Cooke (1993a, b) for numerical simulations of mineral deposition from sedimentary brines. The dolomite field has also been overlain on these diagrams for reference purposes.

### Aqueous $CO_2$ concentrations

Carbonates require high $CO_2$ partial pressures to be stabilised in hydrothermal systems. For example, calcite forms in 'gas-rich' subaerial geothermal systems such as Broadlands, New Zealand ($m_{CO2}$ = 0.15 molal; Henley, 1984) due to the 'high' $CO_2$ concentrations of the fluids (Note that 'gas-rich' in the near-surface environment can refer to $CO_2$ concentrations of less than 0.5 wt. % $CO_2$ — considerably lower than what metamorphic petrologists consider $CO_2$-rich!). In contrast, gas-poor systems such as Wairakei ($m_{CO2}$ = 0.01 molal; Henley, 1984) precipitate calc-silicate minerals such as epidote and calcium-bearing zeolites rather than carbonates because the solutions are $CO_2$-deficient.

As for calcite, Fe-rich carbonates require high $CO_{2\,(aq)}$ concentrations to be stabilised over the naturally abundant Fe-oxide, sulfide and silicate minerals. While other variables such as temperature and pH play significant roles, $CO_2$ concentrations are probably the most important control on siderite stability in hydrothermal systems, because without sufficient $CO_2$, carbonates cannot form. Equations 1.1 to 1.3 illustrates the importance of $CO_{2\,(aq)}$ (as $H_2CO_3$) in stabilising siderite over pyrite, hematite and magnetite:

$$FeS_{2\,(s)} + H_2CO_{3\,(aq)} + H_2O_{(l)} \Leftrightarrow FeCO_{3\,(s)} + 2\,H_2S_{(aq)} + 0.5\,O_{2\,(g)} \quad (1.1)$$

$$Fe_2O_{3\,(s)} + 2\,H_2CO_{3\,(aq)} \Leftrightarrow 2\,FeCO_{3\,(s)} + 2\,H_2O_{(l)} + 0.5\,O_{2\,(g)} \quad (1.2)$$

$$Fe_3O_{4\,(s)} + 3\,HCO_3^-{}_{(aq)} + 3\,H^+{}_{(aq)} \Leftrightarrow 3\,FeCO_{3\,(s)} + 3\,H_2O_{(l)} + 0.5\,O_{2\,(g)} \quad (1.3)$$

In each of these reactions, increasing $a_{(H2CO3)}$ or $a_{(HCO3-)}$ stabilises siderite at the expense of the relevant iron oxide or sulfide phase. This type of reaction is important for controlling siderite deposition in many hydrothermal environments. For reduced systems, where $CH_{4\,(aq)}$ is the dominant carbon-bearing species, increasing $a_{(CH4)}$ stabilises siderite over reduced Fe-bearing minerals (e.g. pyrrhotite):

$$FeS_{(s)} + CH_{4\,(aq)} + 2\,O_{2\,(g)} \Leftrightarrow FeCO_{3\,(s)} + H_2S_{(aq)} + H_2O_{(l)} \quad (1.4)$$

Such reactions are of minimal importance, however, because of the high solubility of carbonates under reduced ($CH_4$ predominant) conditions.



### Carbonate composition ($X_{FeCO3}$)

Between 150° and 250°C, pure siderite is only stabilised by high $CO_{2\,(aq)}$ concentrations (± low total sulfur concentrations — see below) in the hydrothermal fluid. This is reflected by the small siderite field on Figure 1, and the complete absence of siderite on Figure 2. However, impure siderite (ferroan carbonate) is stable over a much broader range of conditions (Figs 1 and 2). Decreasing $a_{FeCO3}$ has essentially the same effect as increasing $\Sigma C$ concentrations in the fluid, and comparing the ferroan carbonate fields in Figures 1A and 1B, and 2A and 2B provides some insights to the effects of increasing $\Sigma C$ at 150° and 250°C. Although the substitution of minor amounts of Fe into carbonates can occur over a broad range of conditions compared to the formation of pure siderite, Fe contents of carbonates still provides useful information on conditions of formation, as seen from Figures 1 and 2.

### Temperature

At constant $\Sigma C$ concentrations, increasing temperatures destabilise pure siderite (Figs 1A and 2A). Siderite is therefore more likely to occur at lower temperatures, provided $CO_{2\,(aq)}$ concentrations are sufficiently high. The abundance of siderite at Century (Waltho and Andrews, 1993) suggests that Century may have formed from lower temperature solutions than the HYC or Mt Isa deposits.

Temperature has a second, indirect effect on siderite and ferroan carbonate stability. Pyrite is stable over a broader range of $f_{(O2)}$ and pH conditions at lower temperatures and constant $\Sigma S$ (compare Figs 1 and 2). The expanded pyrite field at lower temperatures means that siderite is more easily stabilised under relatively oxidised to oxidised conditions (Fig. 1). As the pyrite field contracts with increasing temperature, siderite will be able to form more readily under reduced conditions (Fig. 2).

### Oxygen fugacity

Siderite will be stabilised somewhere along the margins of the pyrite field, potentially forming a boomerang-shaped stability field in $f_{(O2)}$–pH space (e.g. Fig. 2B). As discussed in the previous section, ferroan carbonates and siderite are more easily stabilised under oxidised conditions at low temperatures (i.e. between pyrite and hematite; Fig 1), and reduced conditions at higher temperatures (between pyrite and magnetite, or pyrite and pyrrhotite; Fig. 2). The oxidised and reduced domains for ferroan carbonates can meet at the oxidised/reduced sulfur boundary, but the transition from oxidised to reduced sulfur can cause the ferroan carbonate field to almost pinch out, before expanding again at lower $f_{(O2)}$ values (eg. Fig. 1B). Siderite/ferroan carbonates therefore have potential as indicators of redox conditions in SHMS systems, and can help understand metal transport and depositional processes (discussed below).

### pH

Although the ferroan carbonate fields are shown to terminate at the dolomite boundary on Figures 1 and 2, they can extend to lower pH values depending on the stability range of the host carbonate phase. Because of the close association with pyrite, pure siderite appears to be mostly restricted to weakly acidic to weakly alkaline conditions (Fig. 1A). This pH range has important implications for base and precious metal transport, because Cooke (1993a, b) has demonstrated that reduced, weakly alkaline brines are not capable of transporting significant quantities of base metals (see below).

### $\Sigma S$

Total sulfur concentrations affects the stability of siderite with respect to iron sulfides. Equations 1.1 and 1.4 illustrate that decreasing $\Sigma S$ concentrations (as $H_2S_{(aq)}$) will stabilise siderite at the expense of pyrite and pyrrhotite. These effects have not been quantified to date, and will be the subject of further research.

### Salinity

Salinity has an indirect effect on the siderite and ferroan carbonate stability fields, because the ionic strength of the solution controls the position of the predominance field boundaries around which the mineral fields deflect (Figs 1 and 2). Salinity controls on siderite stability are likely to be minor compared to other factors (e.g. $\Sigma C$ and $\Sigma S$ concentrations, temperature, etc.), but have not been quantified to date.

### $a_{(Fe^{+2})}$, $a_{(Ca^{+2})}$ and $a_{(Mg^{+2})}$

Siderite will be stabilised over calcite and dolomite in hydrothermal environments by high Fe/Ca and Fe/Mg ratios. Because most sedimentary brines contain abundant $Ca^{+2}$ and $Mg^{+2}$ compared to $Fe^{+2}$, conditions favourable for siderite formation will be rare. It may be that siderite can only form in rock-buffered environments where $Fe^{+2}$ is abundant relative to other cations. Further research is planned to quantify the effects of Fe/Ca and Fe/Mg ratios on siderite stability.

## Discussion

### Depth of formation for sediment-hosted Pb–Zn deposits

The high $CO_{2\ (aq)}$ concentrations required to stabilise siderite over Fe-oxide, sulfide and silicate phases have important implications for depths of formation of SHMS deposits. Figure 3 shows boiling point–depth curves for pure and saline waters. For pure water at 150°C, boiling will only occur at depths shallower than 40 m. In contrast, for a 150°C fluid that contains 1 wt % $CO_2$, depths of at least 250–500 m below sea level (in submarine settings) or below the paleowater table (in subaerial settings) are required to prevent boiling, due to the high gas concentrations (Cooke, 1993b). If siderite in the Century and Lady Loretta deposits formed at the same time as lead–zinc mineralisation, then mineralisation could not have formed at shallow depths because of the complete absence of mineralogical and textural evidence for boiling (eg. bladed carbonates, phreatic brecciation, etc.). This is contrary to the claims of Carr (1981) and McGoldrick (1993), who proposed that Lady Loretta formed at depths of less than 10 m, based on the presence of stromatolites and desiccation features in the ore horizon and footwall dolomitic unit.

The relative timing of siderite with respect to base metal mineralisation is a crucial question that needs to be resolved. At Century, Waltho & Andrews (1993) have reported fine grained sphalerite intergrown with fine grained siderite aggregates, or "more commonly in the cuspate interstices between siderite aggregates", suggesting that some sphalerite deposition accompanied siderite formation. They also note that "textures suggesting replacement of siderite by sphalerite are commonly developed at boundaries between sideritic siltstone and mineralised black shale environments". If siderite formed prior to base metal mineralisation,

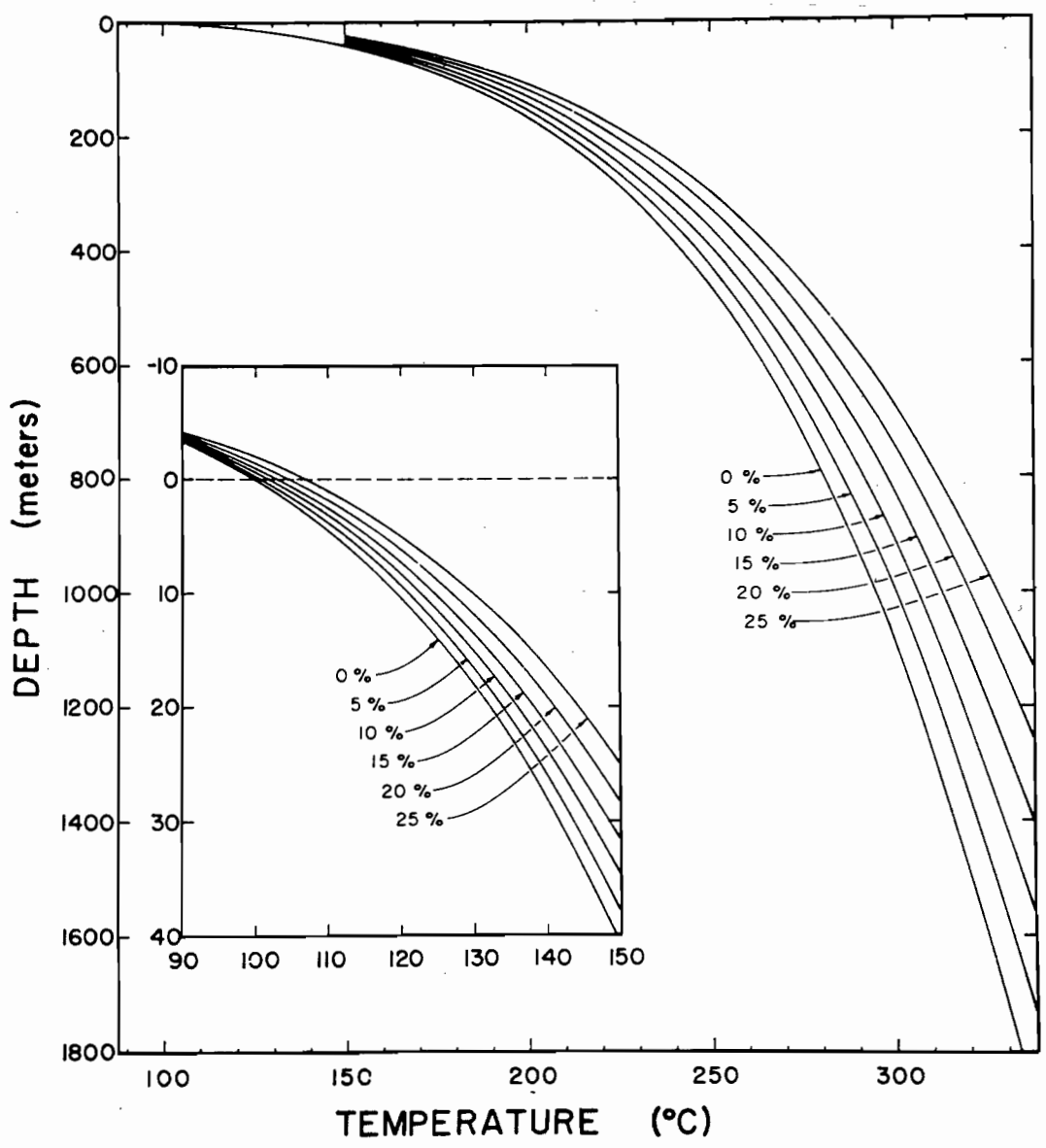


*Figure 3: Boiling point-depth curves for pure water and 5, 10 15, 20 and 25 wt % NaCl solutions (after Henley, 1984). $CO_2$-rich solutions comence boiling at much greater depths (e.g. 250–500 m for a 150°C fluid that contains 1 wt % $CO_2$)*

then rather than providing us with information concerning the depth of formation of base metal mineralisation, the presence of siderite merely indicates the depths at which diagenetic replacement of dolomite occurs. However, it would imply that siderite formation occurred after the sediments of Lady Loretta were buried to depths of 250–500 m, thereby implying a later diagenetic replacement origin for Pb–Zn mineralisation.

There is a possibility that some siderite represents a late diagenetic overprint on sulfide mineralisation, with the abundant pre-existing iron sulfides providing a local source of Fe that helped to stabilise siderite over dolomite. However, until more detailed paragenetic and microprobe studies are undertaken on carbonates from Lady Loretta, Century and other SHMS deposits, this possibility will remain untested.

### Base and precious metal transport

Cooke (1993a, b) has demonstrated that reduced acid brines and oxidised brines of any pH are capable of transporting significant quantities of base metals and silver as chloride complexes, and could form economic massive sulfide mineralisation given the right chemical trap. In contrast, reduced alkaline brines can only transport trace amounts of base metals, but may be capable of carrying significant quantities of Au and Ag as bisulfide complexes.

The reduced ferroan carbonate domain shown on Figure 2 is coincident with high precious metal and low base metal solubilities. The oxidised ferroan carbonate domain on Figure 1 is coincident with high Zn, Pb and Ag solubilities as chloride complexes, and low Au solubilities. Assuming that siderite and ferroan carbonate are related to base metal mineralisation, the scarcity of Au in SHMS deposits suggests that ferroan carbonates and base metal mineralisation formed under conditions constrained within the oxidised ferroan carbonate domain, and sulfur will be transported primarily as sulfate in the mineralising solutions. These hypotheses are the subject of on-going research and will be discussed further in the next report.

## Summary

- Siderite and ferroan carbonate are stabilised by high $\Sigma C$ and low $\Sigma S$ concentrations in hydrothermal solutions. Lower temperatures will stabilise siderite at constant $a_{(CO2\ aq)}$. $CO_2$ concentrations are probably the dominant control on carbonate formation.

- Aqueous carbon and sulfur species are involved in reactions between siderite and other Fe-sulfide and oxide minerals. This allows the formation of two distinct domains (oxidised and reduced) for ferroan carbonates in $f_{(O2)}$–pH space

- Ferroan carbonates that form under relatively oxidised to oxidised conditions in association with pyrite or hematite are favoured by lower temperatures and/or high $\Sigma S$ concentrations, and have the potential to be associated with base metal-rich solutions.

- Ferroan carbonates precipitated from reduced solutions are more likely to form at higher temperatures and/or low $\Sigma S$ concentrations, and will be associated with base metal-deficient but possibly precious metal-rich solutions.

- Detailed petrographic and electron microprobe studies are required to establish the paragenetic relationships between pyrite, base metal sulfides, dolomite and siderite at Lady Loretta, Century and other siderite-bearing SHMS deposits. If siderite and base metal mineralisa-



tion are synchronous, then depths of formation (either in a replacement or sedimentary-exhalative setting) must have been at least several hundred metres below the surface/ paleowater table.

## References


Carr, G.R., 1981. The mineralogy, petrology and geochemistry of the zinc–lead–silver ores and host sedimentary rocks at Lady Loretta, northwest Queensland. Unpublished PhD thesis, The University of Wollongong: 431 p.

Carr, G.R., 1984. Primary geochemical and mineralogical dispersion in the vicinity of the Lady Loretta Zn–Pb–Ag deposit, Northwest Queensland. *J. Geochem. Expl.* 22: 217–238.

Cooke, D.R., 1993a. Transport and deposition of base metals from high temperature (250°C) sedimentary brines. AMIRA/ARC Project P384, unpublished report No. 4: 111–130.

Cooke, D.R., 1993b. Transport and deposition of base metals from low temperature (150°C) sedimentary brines. AMIRA/ARC Project P384, unpublished report No. 4: 131–139.

Eldridge, C.S., Williams, N., and Walshe, J.L., 1993. Sulfur isotope variability in sediment-hosted massive sulfide deposits as determined using the ion microprobe SHRIMP:II A study of the HYC deposit at McArthur River, N.T., Australia. *Econ. Geol.* 88: 1–26.

Henley, R.W. 1984. Hydrolysis reactions in hydrothermal fluids. *In* R.W. Henley, A.H. Truesdell and Barton, P.B. Jr. (Editors) – Fluid–mineral equilibria in hydrothermal systems. *Rev. Econ. Geol.* 1: 65–82.

Lambert, I.B., and Scott, K.M., 1973. Implications of geochemical investigations of sedimentary rocks within and around the McArthur zinc–lead–silver deposit, Northern Territory. *J. Geochem. Expl.* 2: 307–330.

Large,R.R., and McGoldrick, P.J., 1993. Deposit halos 5: Primary geochemical halos related to Proterozoic sediment-hosted Pb–Zn deposits and applications to exploration. AMIRA/ ARC Project P384, unpublished report No. 3: 63–126.

McGoldrick, P.J., 1993. Deposit halos 3: Geology of the Lady Loretta deposit: review, new developments, and implications for ore genesis. AMIRA/ARC Project P384, unpublished report No. 3: 1–30.

Waltho, A.E., and Andrews, S.J., 1993. The Century zinc–lead deposit, Northwest Queensland. AusIMM Centenary Conference: 41–61.

# Analysis of fluid flow during late stage wrenching of the Tawallah Fault system, southern McArthur Basin, Northern Territory: a fluid inclusion approach

**Jamie Rogers**
*CODES Key Centre*

## Summary

A fluid inclusion study of the quartz–hematite hydraulic breccias along the Tawallah Fault system indicates that hot (~210°C), saline, oxidised fluids passed through the fault during late-stage wrench movements associated with post-Roper deformation. Enthalpy–chlorite plots suggest that the hot fluids were boiling, and mixing with colder fluids during hematite–quartz deposition. High-heat-producing granites are proposed as a heat source for the fluids, as the system was active well after rifting and volcanism had ceased.

The presence of hot, saline, oxidised fluids lend great potential for mineralisation throughout the entire history of the southern McArthur Basin along the Tawallah Fault and similar fault systems where reduced (graphite and/or pyrite bearing) sediments are juxtaposed against the structure. The results may also provide an insight into processes that occurred along the Emu Fault system during the formation of base metal mineralisation at McArthur River.

## Introduction

This paper summarises preliminary results of a fluid inclusion study conducted on the Tawallah Fault system in the southern McArthur Basin, Northern Territory. Analyses of inclusions from hydraulic fault breccias associated with the post-Roper deformation are presented with the aims of determining fluid processes and tracing fluid sources. The results of these analyses are used in conjunction with the fluid geochemical modelling of Cooke (1993) to model the fluids that have been channelled during the late stage wrench movements on the Tawallah Fault.

### Aims of the research

The primary aims of this fluid inclusion study are to:

1. Characterise the fluids in the Tawallah Fault system;
2. Investigate fault-controlled thermal anomalies in the "unmetamorphosed" McArthur Basin;
3. Investigate processes which have led to hematite–quartz precipitation along the faults;
4. Estimate possible depths of formation;
5. Suggest a possible heat source for the fluids.

### The Batten Range: Background Geology

The Batten Range, located approximately 50 km west of the McArthur River deposit, is bounded by the Tawallah Fault along its eastern margin (Fig. 1). The Tawallah Fault and the Emu Fault to the east



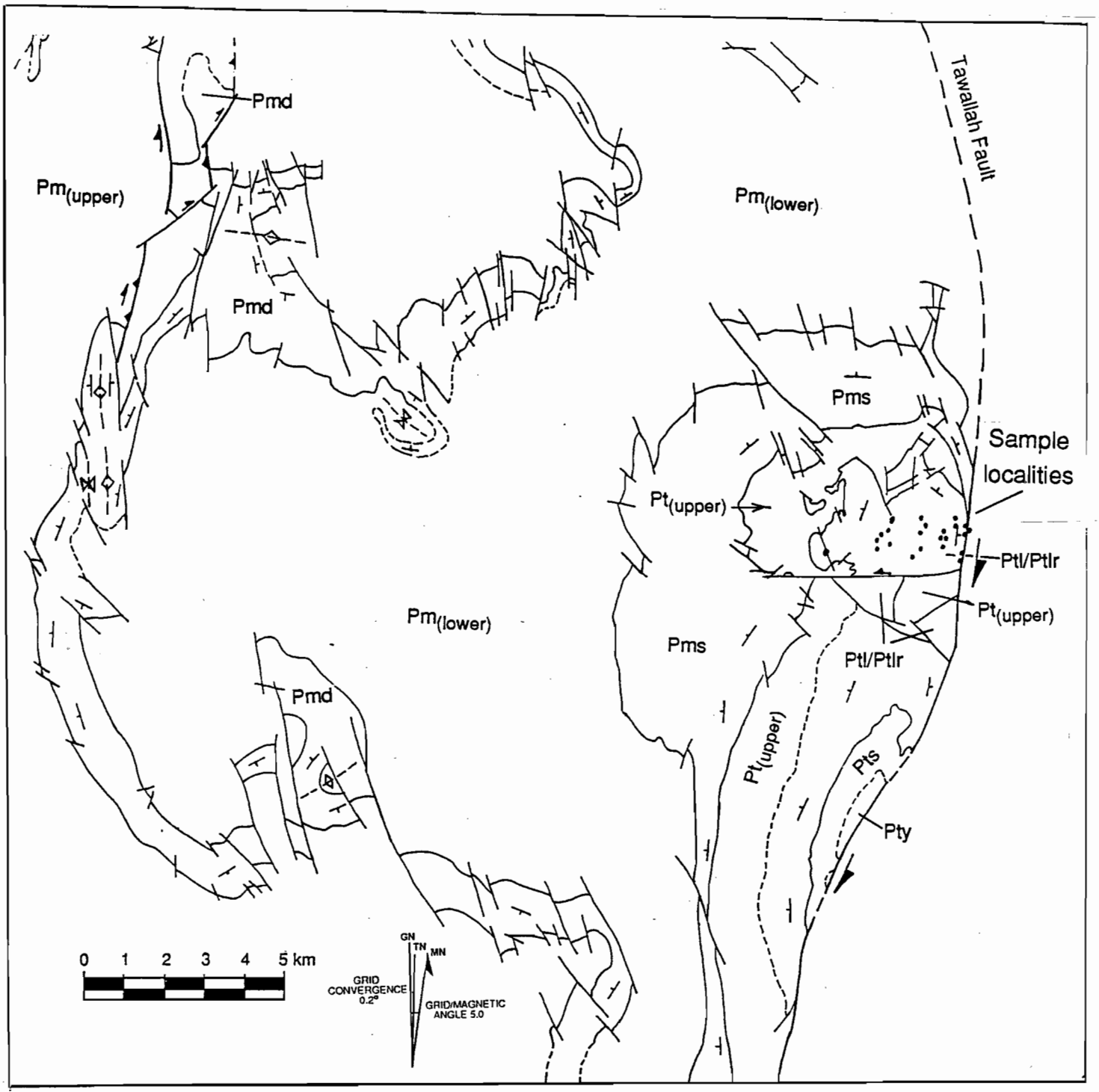


Stratigraphic nomenclature

- $Pm_{(upper)}$ - undivided upper McArthur Group
- Pmd - Tatoola Sandstone
- $Pm_{(lower)}$ - undivided lower McArthur Group
- Pms - Masterton Sandstone
- $Pt_{(upper)}$ - undivided upper Tawallah Group
- Ptl/Ptlr - Sly Ck./Rosie Ck. Sandstone
- Pts - Seigal Volcanics
- Pty - Yiyintyi Sandstone

*Figure 1 — Sample localities in the Batten Range.*

are early basin forming structures that have been reactivated as dextral wrench systems. The major difference between the two fault systems is that the Tawallah Fault has undergone several periods of inversion during its history so that the oldest sedimentary units of the basin (Tawallah Group) and parts of the basement (Scrutton Volcanics) are currently exposed along the western side of the structure. This provides an excellent window into the lower parts of the stratigraphy and also to processes that may have taken place beneath the McArthur River Pb–Zn deposit.

In the Batten Range, the lowermost units of the Tawallah Group up to and including the Settlement Creek Volcanics are exposed, which are in turn overlain by basal McArthur Group sediments. The fault block that includes the Batten Range was a positive topographic feature during the early evolution of the southern McArthur Basin, being structurally emplaced by the "Mid-Tawallah" basin inversion event (Rogers, 1993). The extensional phase that followed early inversion saw the uplifted fault block acting as a source for clastic alluvial/fluvial sediments of the upper Tawallah Group and lower McArthur Group (Bull, 1993; Rogers, 1993) and was associated with bimodal and felsic volcanism. With the cessation of extension (perhaps during a NW–SE directed compressional event at some stage during McArthur Group time; Keele, 1993), suppression of relief led to continued deposition of the carbonate-dominated McArthur and Nathan Groups in a sag-type environment (Bull, 1993). The uppermost unit of the McArthur Basin, the sandstone-dominated Roper Group, may have developed in response to another as yet unrecognised compressional tectonic event (Bull, 1993). The major structural event to affect the southern McArthur Basin was a NE–SW directed compression post-dating all sedimentary deposition and may represent final basin closure. This event, termed the post-Roper Inversion (Rogers, 1993) saw the reactivation of early segmented basinal structures to wrench or thrust fault geometries depending on initial orientation.

In summary, the Batten Range has undergone a complex structural history involving multiple periods of high level brittle deformation with dextral wrench faulting associated with the post-Roper Inversion particularly well recorded. The structural position of the Batten Range is fortuitous for high levels of fluid flow as it is situated at a transtensional position along the Tawallah Fault, on the inside of a fault bend.

### Fault Breccias

A characteristic feature of primary and secondary brittle structures in the clastic units of the Tawallah Group (particularly the Sly Creek Sandstone) is hydraulic brecciation. The Sly Creek Sandstone was (diagenetically ?) silicified early in the development of the basin (Rogers, 1993; Bull, 1993), providing a favourable unit for the development of hydraulic brecciation. Consequently, this study has focussed on the breccias from the Sly Creek Sandstone in the Batten Range (see Figure 1 for sample locations).

Breccias textures vary from jigsaw-fit clast-supported through to matrix-supported breccias with random clast orientation (Fig. 2a.). These two textural end members are referred to hereafter as fracture and open breccias respectively. The matrix is predominantly comprised of hematite and quartz, with the breccia clasts composed of wall rock fragments (Fig. 2b.).

## Fluid inclusions

Thirty-three doubly polished plates were prepared from fault breccia samples associated with the post-Roper wrench movement on the Tawallah Fault. Fault types sampled included the primary Tawallah

Fault and secondary NNW dextral, NW sinistral, SW dextral/normal and SSW dextral structures. The data is discriminated by distance away from the Tawallah Fault and data populations generated may include one or more of the secondary fault types mentioned above. From these samples, measurements of liquid–vapour homogenisation temperatures, freezing point depressions and first melting temperatures were made on 101 chips using the standard heating and freezing procedures of Roedder (1984). Salinities were calculated from freezing point depression measurements assuming an NaCl–$H_2O$ system and using the algorithms provided in Hall *et al.* (1988). Of the 800 inclusions measured, only 65% yielded both freezing point depressions and homogenisation temperatures as small inclusion size (5–20 μm) limits optical viewing conditions during the freezing procedure.

Fluid inclusions mostly occur within breccia clasts as trails along healed tension fractures in individual quartz grains and are virtually all secondary in origin (Figs 2c, 2d, 2e). The development of tension fracturing is assumed to be a product of the hydraulic brecciation process (Sibson, 1989). The fluid inclusions developed along the fractures may therefore represent the entrapment of fluids present in the system during brittle rupturing on the Tawallah Fault.

Two inclusion populations are recognised in secondary trails. Population I is dominated by secondary inclusions with constant liquid/vapour ratios (90–95%; Fig. 2c), while population II represents trails of inclusions with variable liquid–vapour ratios (Figs 2d, 2e). The latter have similar homogenisation temperatures from both liquid and vapour rich inclusions and are interpreted to represent the entrapment of a fluid undergoing phase separation (boiling; Roedder & Bodnar, 1980). The inclusions invariably contain no visible $CO_2$, and daughter minerals are rare.

## Assumptions

Interpretation of the fluid inclusion data has been made using four major assumptions:

1. Faults are roughly synchronous to each other and to the dextral wrench movement on the Tawallah Fault (i.e., they are all post-Roper in age);
2. Breccias are all developed during this deformation (i.e., none of the breccias are derived from older, reactivated structures;
3. Secondary inclusions are trapped during or shortly after the brecciation process;
4. The fossil geothermal system, although initially under lithostatic conditions during brecciation, was driven to hydrostatic conditions once permeability and fluid flow became established.

### Temperature and Salinity

Homogenisation temperatures for both populations range from 90° to 400°C, although most are between 120° and 220°C. Salinities for population I are mostly between 0.0 and 5.0 eq. wt.% NaCl while population II inclusions record higher values of 10 to 20 eq. wt.% NaCl. Although this is generally the case, there is some overlap in measured salinity, particularly for homogenisation temperatures over 250°C where values for both populations are mostly between 8 and 13 eq. wt.% NaCl.

Figure 3 shows homogenisation temperatures in secondary faults as a function of increasing distance from the Tawallah Fault. With a mean homogenisation temperature of 210°C, the Tawallah Fault population is markedly hotter than inclusions from all secondary structures which have mean homogenisation temperatures around 160°C. Figure 4 suggests a systematic decrease in temperature away from the Tawallah Fault. The spread of data above the mean value in Figure 4 is probably due to mixed entrapment of both liquid and vapour

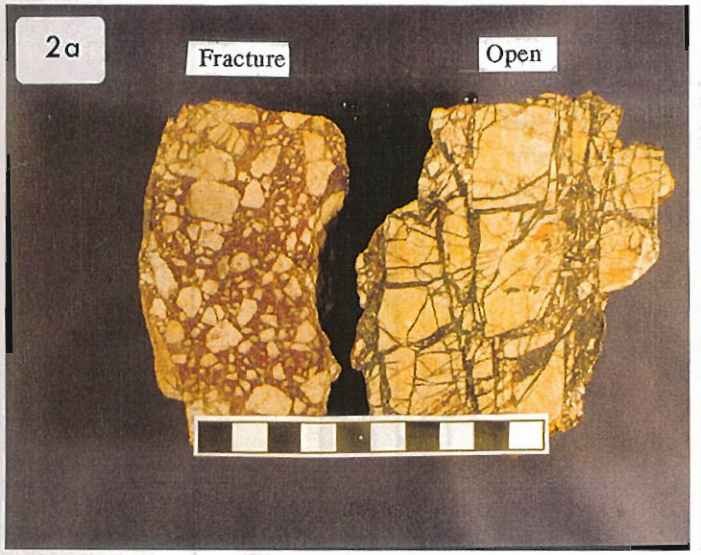


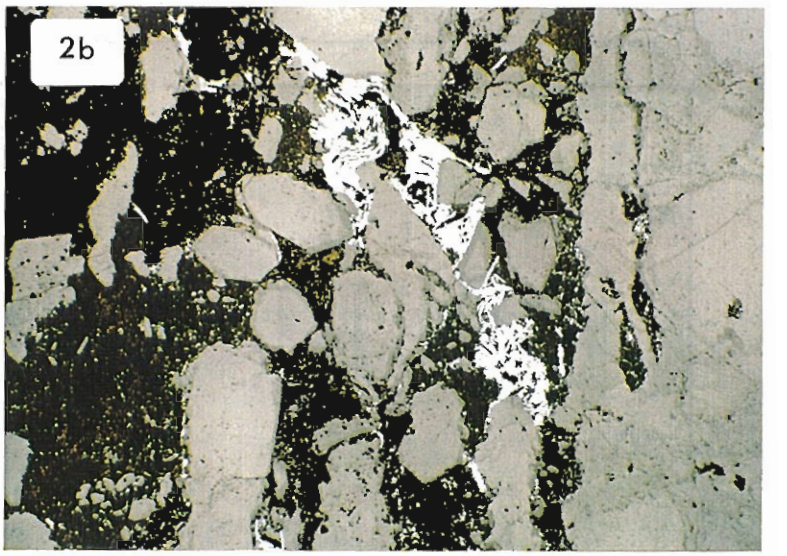



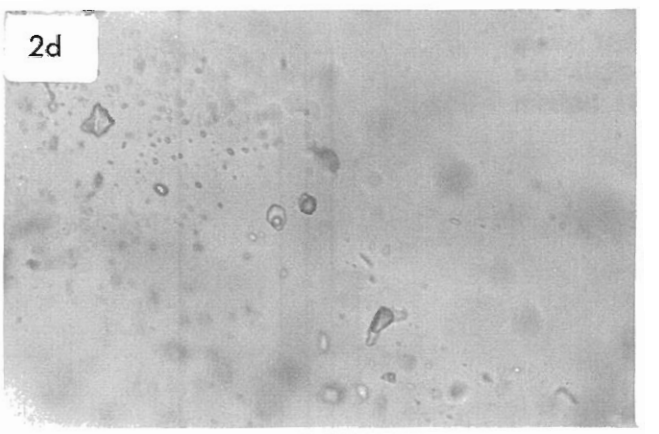



*Figure 2a — Breccia textures developed in primary and secondary brittle structures in the Sly Creek Sandstone. Fracture breccias show jigsaw-fit clast-supported textures while open breccias are matrix supported with random clast orientation.*

*Figure 2b — Photomicrograph of hydraulic breccia developed in the Sly Creek Sandstone. The breccia matrix is predominantly comprised of primary hematite and quartz plus minor limonite, leucoxene and goethite. The breccia clasts are unimodal and are derived from the Sly Creek Sandstone wall rock (scale: × 5).*

*Figure 2c — Photomicrograph of population I secondary inclusion trails. Constant liquid/vapour ratios which characterise population I inclusions are mostly between 90 and 95% (scale: × 40)*

*Figures 2d and 2e — Photomicrographs of population II secondary inclusion trails. Variable liquid/vapour ratios define population II inclusions. Similar homogenisation temperatures from both liquid and vapour rich inclusions and represent the entrapment of a fluid undergoing phase separation (boiling; Roedder and Bodnar, 1980) (scale: × 40).*

fig. 2 reverse

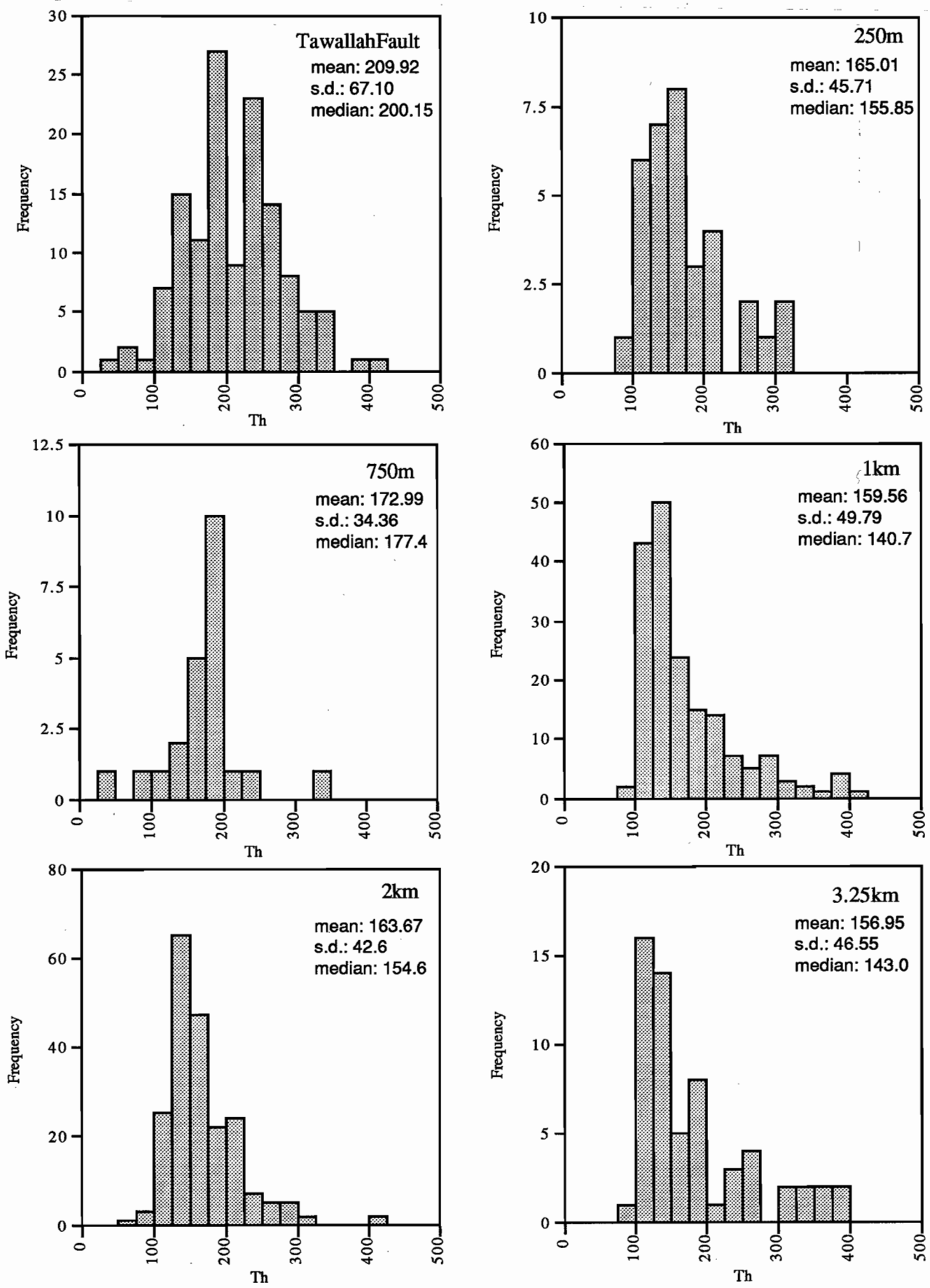


*Figure 3 — Homogenisation temperatures of inclusion populations with increasing distance from the Tawallah Fault.*

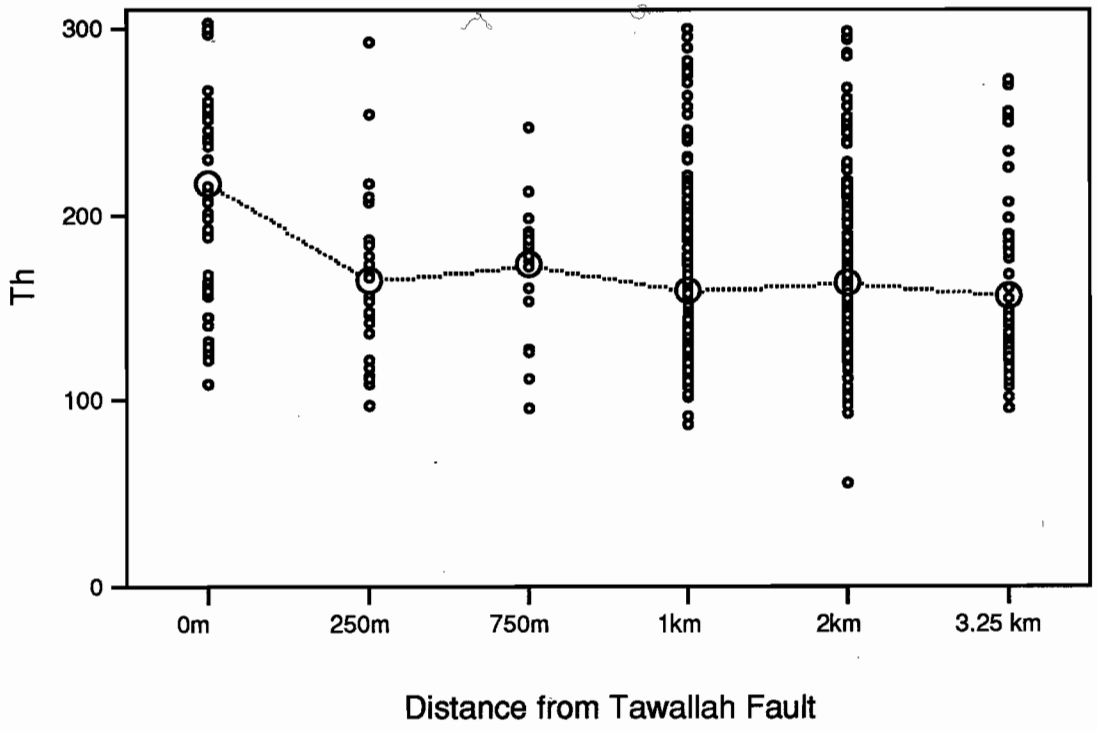


*Figure 4 — Homogenisation temperatures of inclusions with increasing distance from the Tawallah Fault. Large circles represent the mean value for each population.*

phases during boiling rather than a single homogenous phase as this would *"yield higher, and spurious, Th values"* (Roedder & Bodnar, 1980).

Figure 5 depicts the salinities of inclusions with increasing distance away from the Tawallah Fault. The salinity data suggests that there is a bimodal population of inclusions, a low salinity population (0–5 eq. wt.% NaCl) and a high salinity population (10–20 eq. wt.% NaCl). with the exception of the Tawallah Fault which, in addition, has recorded fluids with intermediate salinities (8–12 eq. wt.% NaCl).

Homogenisation temperatures and salinities of fluid inclusions hosted by the different breccia types discussed previously are displayed in Figure 6. The most noticeable feature of this comparison is that the clast supported, fracture type breccias contain a higher proportion of saline inclusions.

### Enthalpy-chloride diagrams

Henley *et al.* (1984) state that three principle processes are responsible for decreasing temperature in a rising fluid: (1) boiling, whereby heat is transferred to a vapour phase that separates from an ascending fluid upon reaching a critical level in the crust. The specific depth at which boiling will occur is governed by the hydrostatic pressure imposed on the fluid; (2) dilution by mixing with cool groundwaters (which may also prevent the uprising fluid from boiling); (3) conductive loss of heat to the surrounding wall rock. These processes acting on a hot, saline brine will result in different final fluid chemistries. It is therefore, theoretically possible to discern which fluid processes have been operative in a fossil hydrothermal system. Boiling of a hot, saline brine will effectively concentrate salts into solution, progressively increasing the salinity of the residual fluid (Henley *et al.*, 1984). In contrast, dilution due to mixing of a hot, saline brine with a relatively cool groundwater generally leads to a salinity decrease in the resultant hybrid fluid (Fournier, 1979). With loss of heat by conduction, the salinity of a fluid during cooling would remain fairly constant (Fournier, 1979).

To trace possible depositional processes, the fluid inclusion data is presented on enthalpy–chloride diagrams where enthalpy is the heat of the fluid (taken from the steam tables of Haas (1976)) and chloride is a measure of salinity.

Enthalpy–chloride diagrams were chosen to represent the data because they allow for the prediction of boiling and mixing relationships (Fournier, 1979) and simple calculations when modelling trends in the data (Henley *et al.*, 1984). Figure 7 shows enthalpy–chloride diagrams for the Tawallah Fault and also for associated secondary faults at specific distances from the primary structure. For the Tawallah Fault, two rough trends may be present; a boiling trend towards higher chloride concentrations and a mixing trend towards decreased chloride concentrations. These trends become more distinct with increasing distance away from the Tawallah Fault, although the high enthalpy (high temperature) values are absent.

To model this data, a fluid with a given temperature (300°C) and salinity (8.06–12.75 eq. wt.% NaCl) was cooled to 100°C by boiling and to 80°C by mixing with a cooler, lower salinity fluid (eg. heated ground water at 80°C, 0.5–5.0 eq. wt.% NaCl).

Using the following formulae (Henley *et al.*, 1984), steam factors that separate during boiling (Table 1) can be calculated:

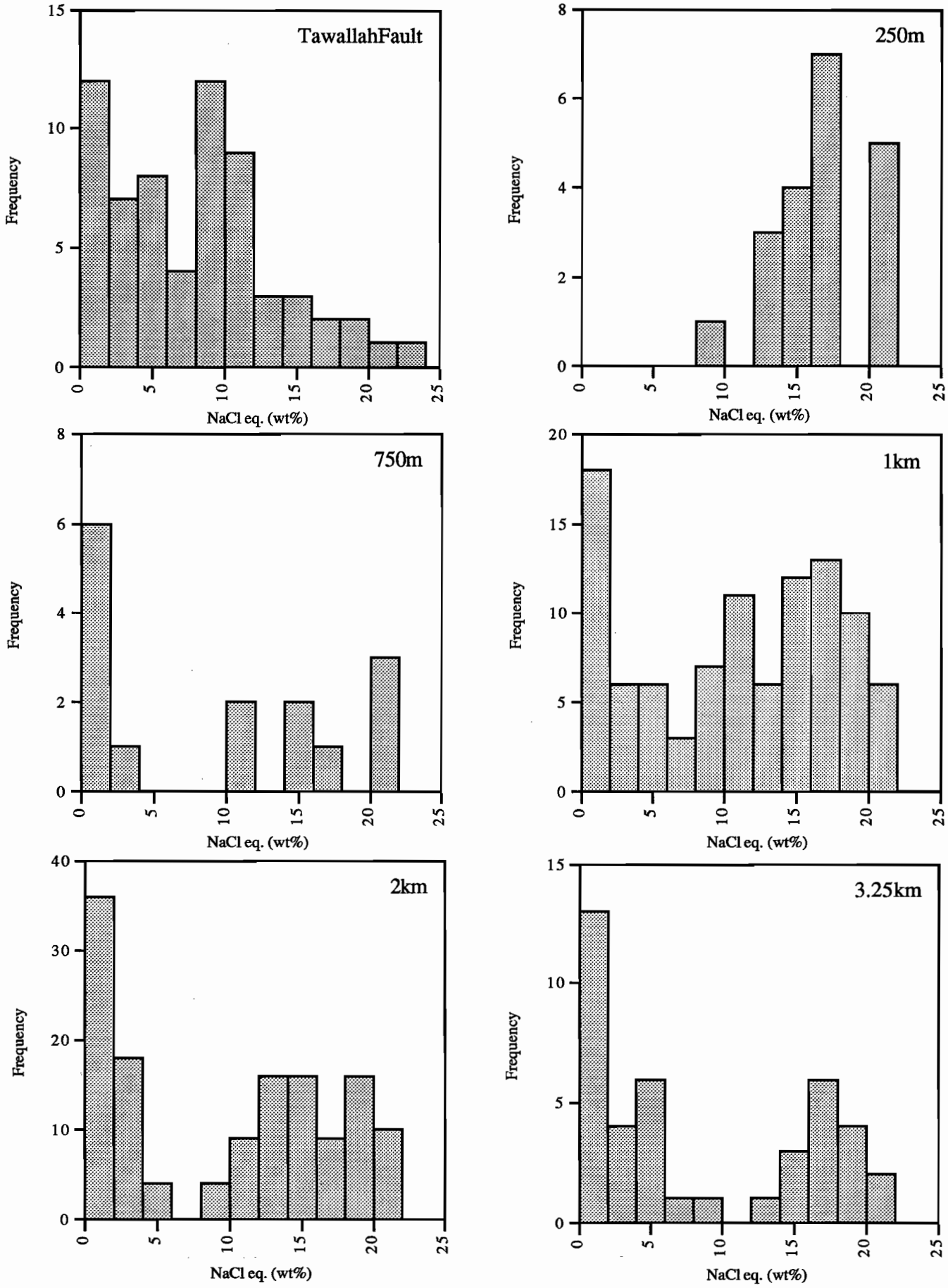


*Figure 5 — Salinity of inclusion populations with increasing distance from the Tawallah Fault.*

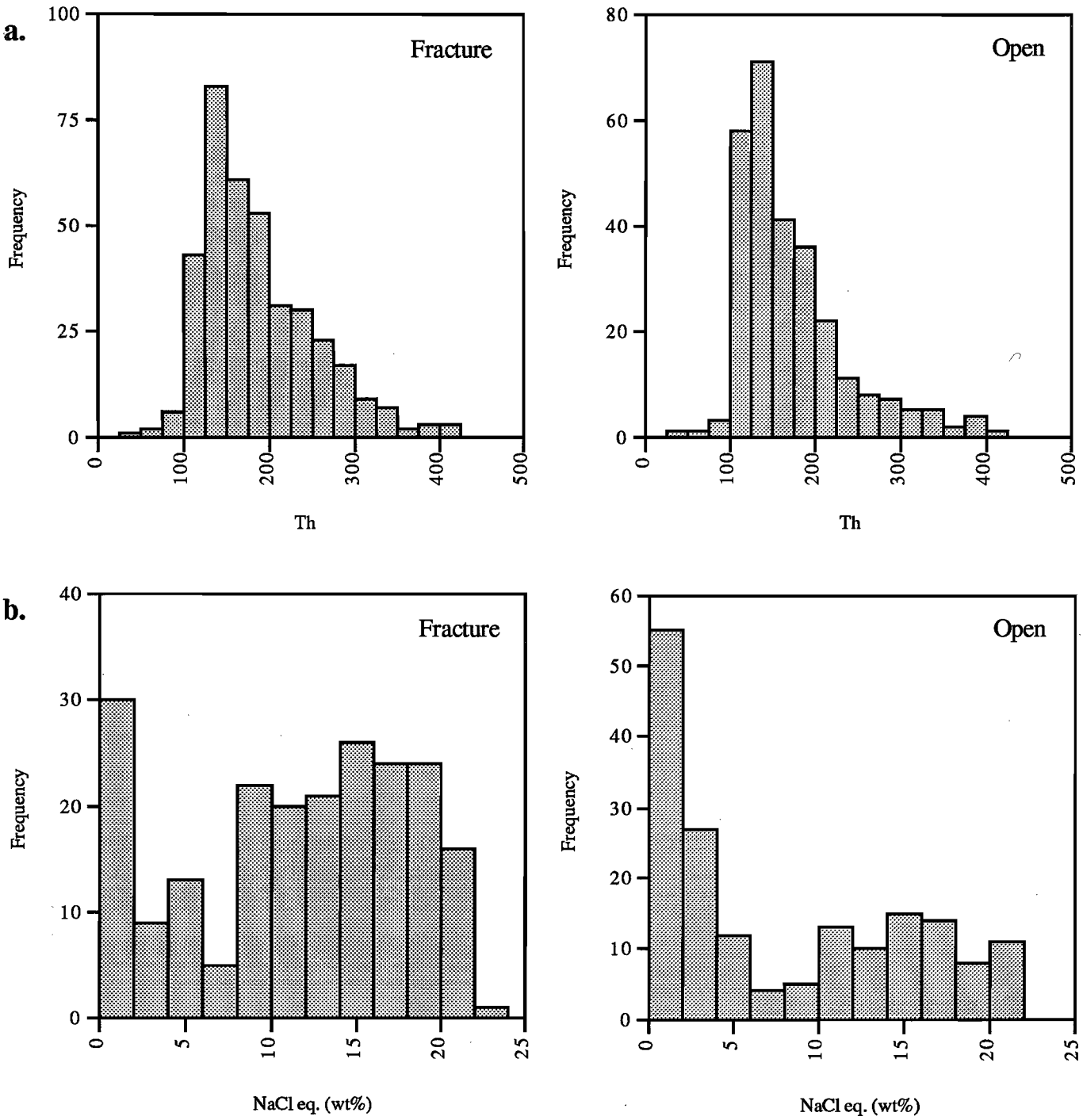


*Figure 6 — (a) Homogenisation temperatures and (b) salinities of inclusion populations from the different fault breccia textures (see fig. 1 and text for texture descriptions).*

$$y = \frac{H_{L(300°C)} - H_{L(100°C)}}{H_{V(100°C)} - H_{L(100°C)}}$$

$$C_{Cl(100°C)} = \frac{C_{Cl(300°C)}}{(1-y)}$$

Where $H$ = specific enthalpy (gained from standard steam tables, e.g. Haas, 1976), $C_{Cl}$ = concentration of chloride, $y$ = mass fraction of initial liquid which turns to steam, and subscripts $L$,t and $V$,t refer to liquid and vapour phases at the specified temperature.

Mixing trends have been calculated (Table 2) assuming infinite dilution of the initial fluid at 80°C by (1) seawater (5.0 eq. wt.% NaCl) and (2) pure (meteoric) water (0.5 eq. wt.% NaCl).

*Table 1 — Calculated enthalpy and chloride values for boiling-induced cooling of a 300°C fluid to 100°C. Superscripts 1 and 2 represent initial salinities of 8.06 and 12.75 eq. wt.% NaCl respectively.*

| Temperature (°C) | enthalpy[1] (J/mol) | chlorinity[1] (mol/kg) | enthalpy[2] (J/mol) | chlorinity[2] (mol/kg) |
|---|---|---|---|---|
| 300 | 23825 | 1.5 | 23509 | 2.5 |
| 175 | 13241 | 2.18 | 13178 | 3.68 |
| 100 | 7507 | 2.66 | 7490 | 4.55 |

*Table 2 — Enthalpy and chloride values calculated for mixing of a 300°C fluid with an 80°C heated groundwater. Superscript 1 represents an initial 8.06 eq. wt.% NaCl fluid mixing with a 0.5 eq. wt.% NaCl groundwater, superscript 2 represents an initial 12.75 eq. wt.% NaCl fluid mixing with a 5.0 eq. wt.% NaCl. groundwater.*

| Temperature (°C) | enthalpy[1] (J/mol) | chlorinity[1] (mol/kg) | enthalpy[2] (J/mol) | chlorinity[2] (mol/kg) |
|---|---|---|---|---|
| 300 | 23825 | 1.5 | 23509 | 2.5 |
| 80 | 6005 | 0.086 | 6005 | 0.90 |

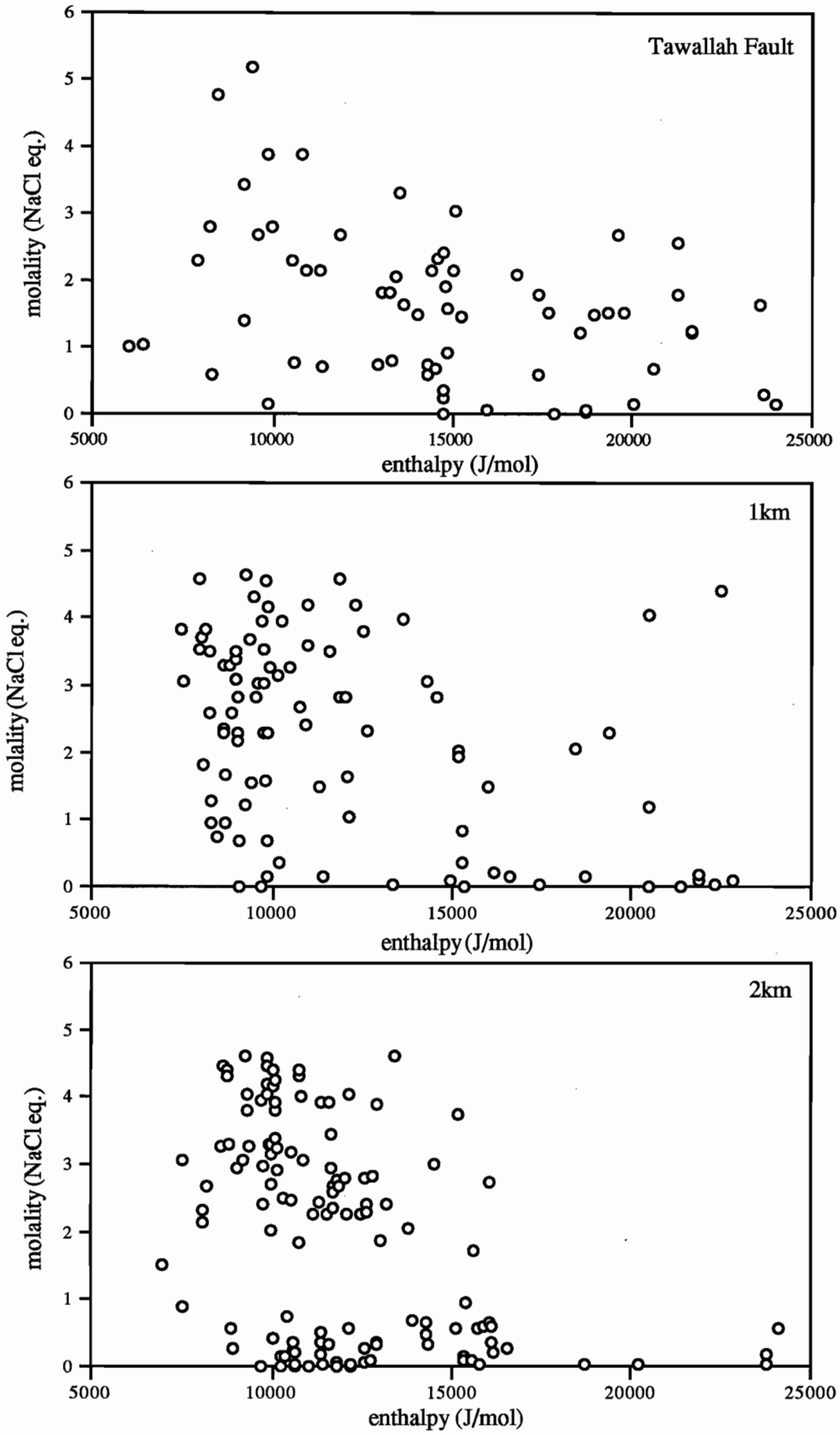


*Figure 7 — Enthalpy-chloride mixing diagrams for inclusion populations with increasing distance from the Tawallah Fault.*

Figure 8 shows the calculated boiling and mixing trends for initial 300°C fluids with salinities of 8.06 and 12.75 eq. wt.% NaCl. Boiling can account for the cooler, high salinity population, whereas mixing with heated seawater or meteoric water accounts for the rest of the low salinity population. These cooling trends also provide a reasonable fit to the total data collected for the Tawallah Fault system (Fig. 9).

There are many other possible starting fluid compositions that could have been chosen. Each would provide a set of cooling trends, and by choosing several starting fluids, the data could be accounted for by combinations of conductive cooling, boiling and mixing. However, to avoid complexity and considering that one fluid cooling by two simple processes adequately explains the data, these options are not discussed further.

Numerical modelling by Cooke (1993) predicted the effects of cooling an oxidised, 250°C and 10 eq. wt.% NaCl brine by boiling, mixing with seawater, and calculated the precipitation sequences when the fluid interacts with a hematitic quartz sandstone. Boiling-induced and conductive cooling to 100°C resulted in the precipitation of hematite and silica with traces of muscovite, chalcocite and (very) minor gold. The ubiquitous hematite–quartz assemblages in the Tawallah Fault breccias and also within stockwork veins close to the Tawallah Fault are consistent with precipitation from an oxidised boiling brine. Furthermore, Cooke (1993) suggests that *"oxidised metalliferous brines can travel significant distances along structures, cooling and/or boiling along the way, without dumping their metal load provided that no reactive lithology or subsurface groundwater is encountered"*. This statement, together with the results of this study, lend great potential for mineralisation throughout the entire history of the southern McArthur Basin along the Tawallah Fault and similar fault systems where reduced (graphite and/or pyrite bearing) sediments are juxtaposed against the structure. The results may also provide an insight into processes that occurred along the Emu Fault system during the formation of base metal mineralisation at McArthur River.

### Depth of the system

The depth of formation for hematite–quartz mineralisation during wrenching on the Tawallah Fault can be determined from boiling inclusion populations by assuming open system behaviour. By plotting homogenisation temperature directly onto a boiling point–depth curve (Roedder & Bodnar, 1980), a maximum depth of 210 m beneath the paleo water table is estimated for hydrostatic conditions.

Estimates of depth from surface are purely speculative as thickness of the palaeo water table and sediment above the system is unknown. Groundwater in the Cypress Plain fluid flow system operative in the Mesozoic Western Canada Sedimentary Basin reaches depths of 500 m (Toth & Corbet, 1987; Fig. 11). Using this system as an example, it is conceivable that hematite–quartz mineralisation in the Tawallah Fault system occurred at 700 m below surface.

There are several lines of evidence that support shallow-level deposition of the hematite–quartz breccias. In the Tawallah Fault system, crustiform veins are abundant close to the major primary structure in the southern parts of the Batten Range. In addition, boiling populations 3 km from the Tawallah Fault indicate that boiling was not induced during seismic rupturing and related dilational pumping in a sub-hydrostatic environment as this process is restricted to within several hundred meters of the structure (Gray *et al.*, 1994).

Figure 10 shows two possible paths that a 300°C, 8.06–12.75 eq. wt.% NaCl fluid may have taken to

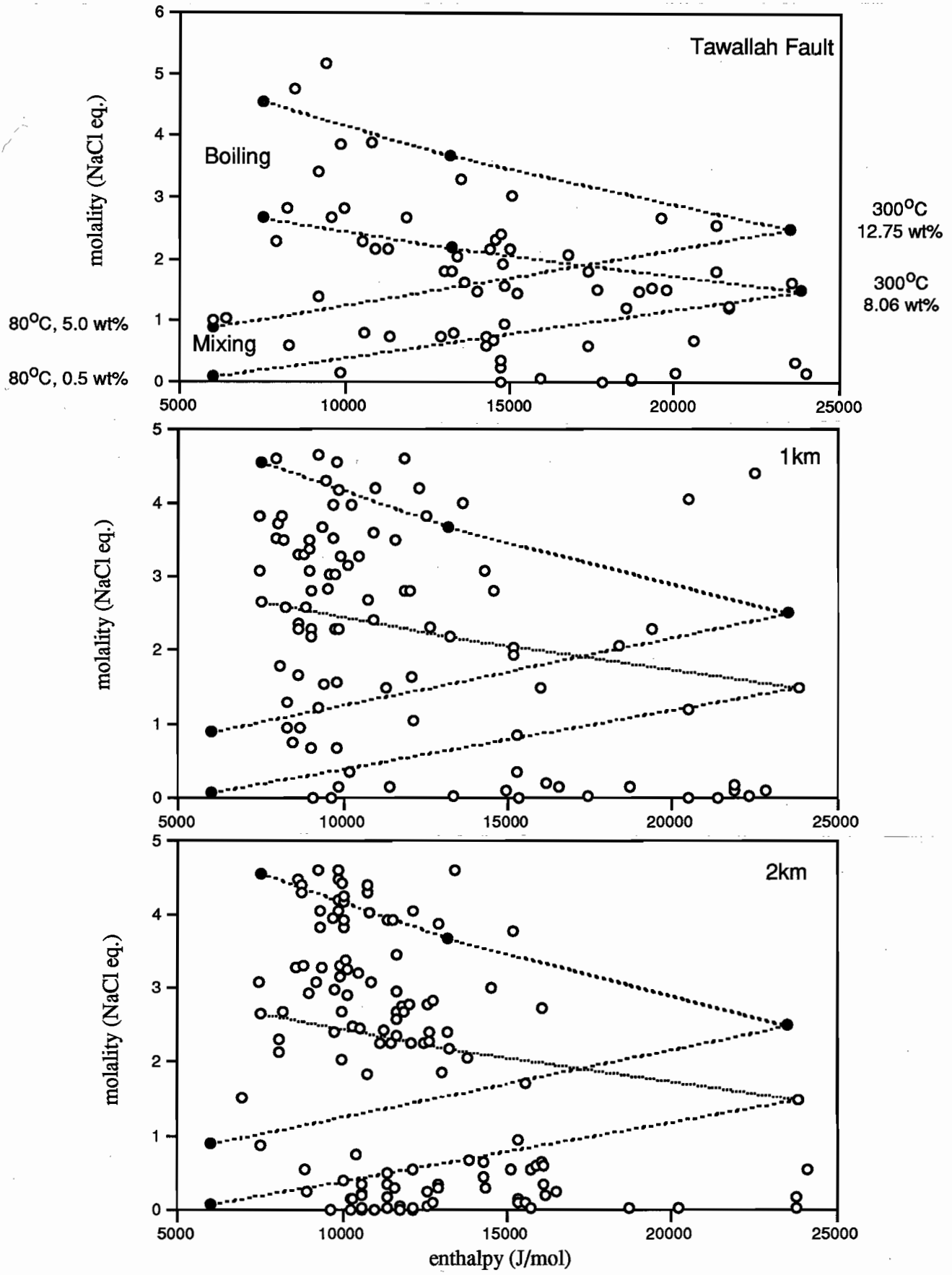


*Figure 8 — Enthalpy-chloride mixing diagrams and boiling/mixing curves for inclusion populations with increasing distance from the Tawallah Fault. Curves are calculated for a 300°C, 8.06–12.75 wt.% NaCl initial fluid. Mixing is assuming maximum dilution with a 80°C, 0.5–5.0 wt.% NaCl heated groundwater.*

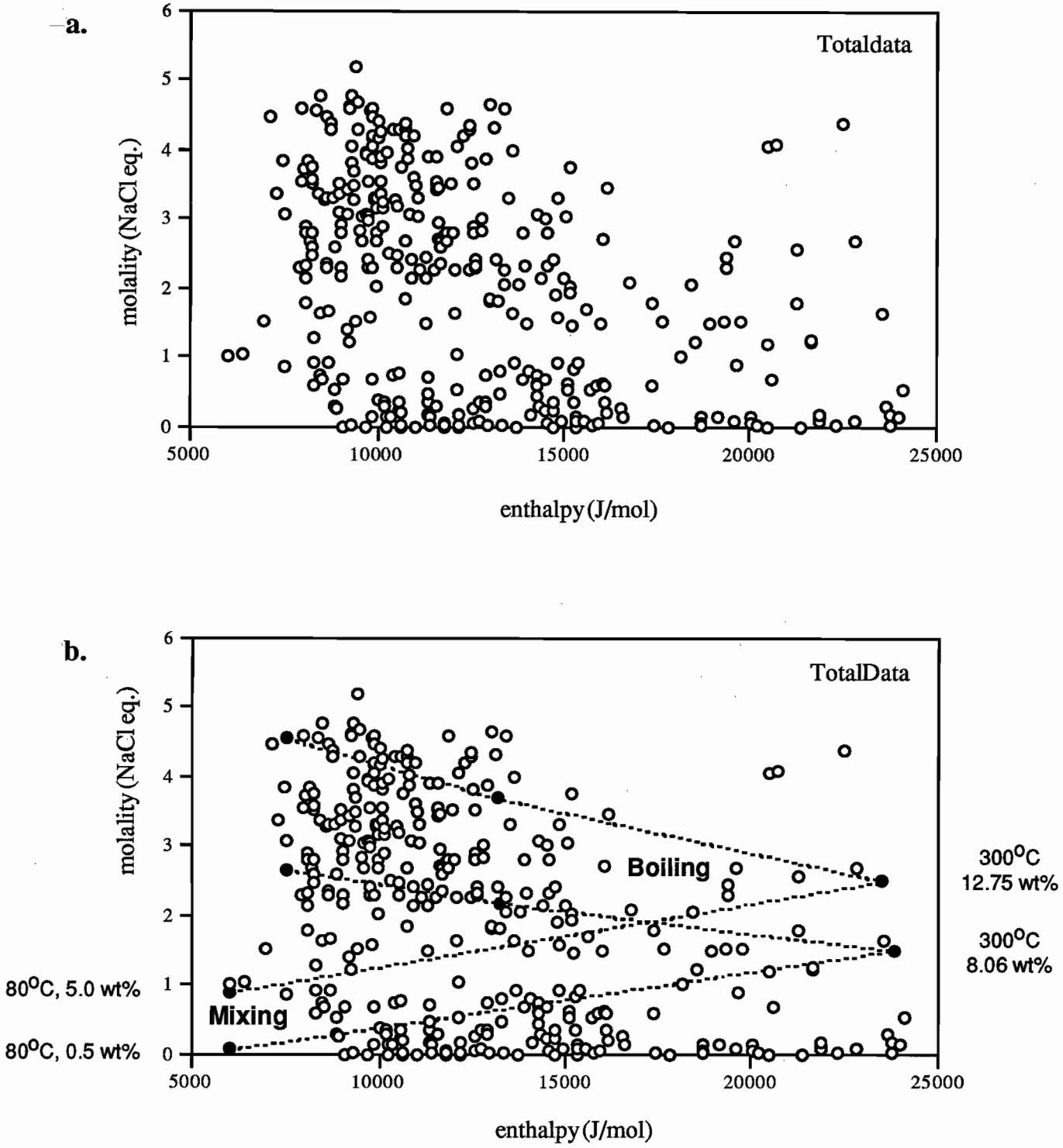


*Figure 9 — Enthalpy-chloride mixing diagram for the Tawallah Fault system (total data). (a) Raw data, and (b) with boiling/mixing curves of figure 8.*

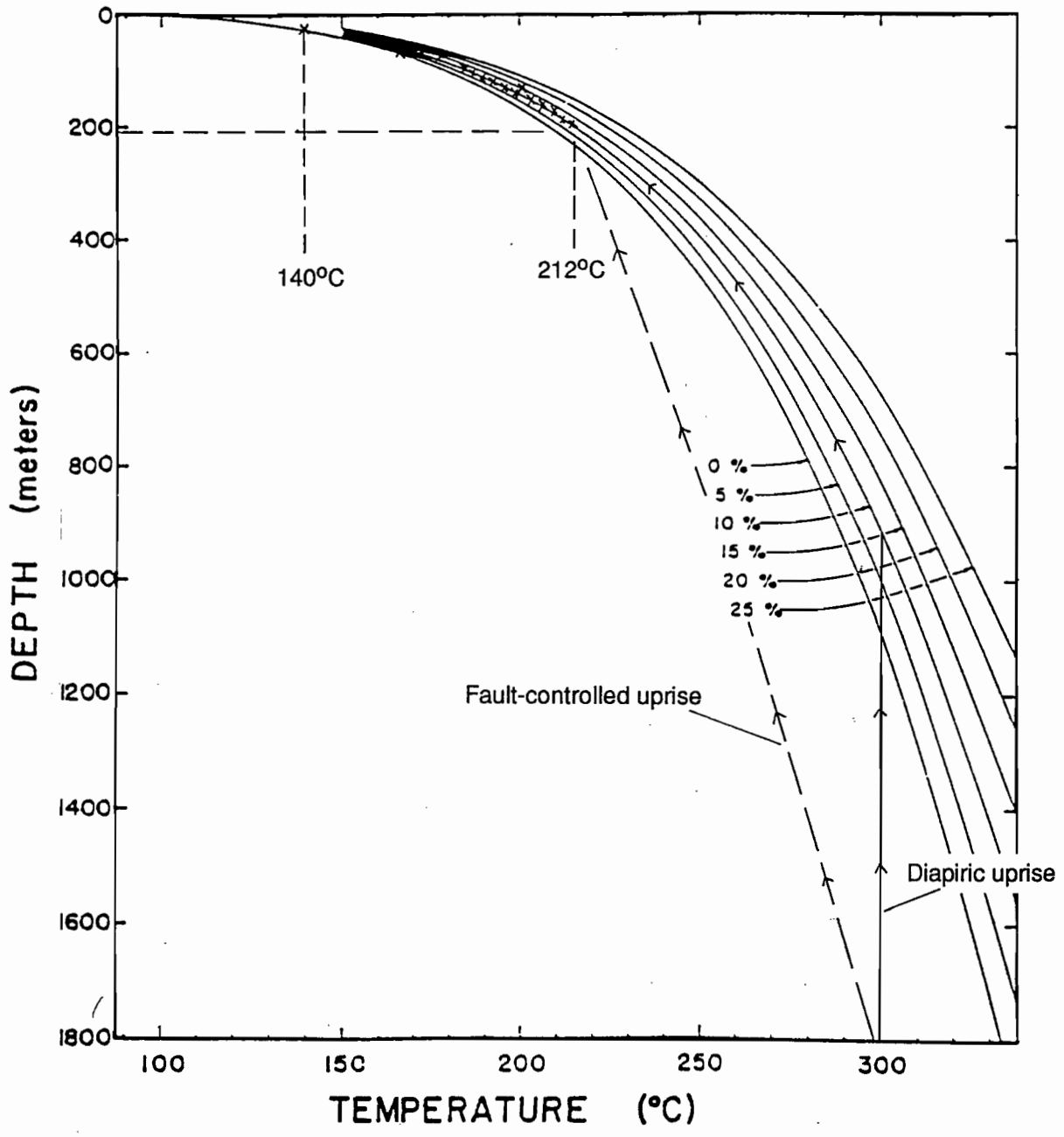


*Figure 10 — Boiling point-depth curves for varying fluid salinities (after Haas, 1971). Boiling populations of inclusions from the Tawallah Fault system define a maximum depth of boiling at 210 m. Source fluids at 300°C may migrate to these depths via two paths, diapiric uprise (heavy line) or fault-controlled uprise (dashed line).*

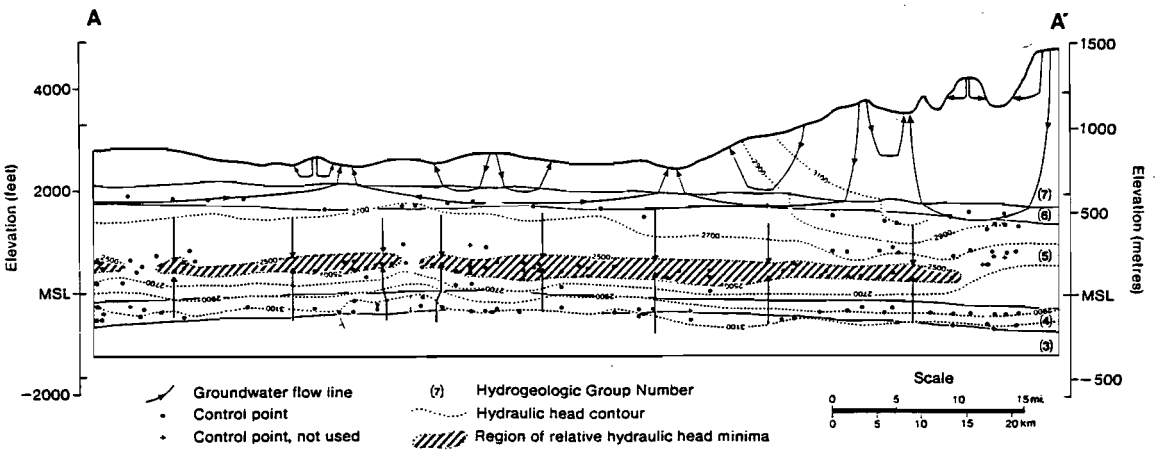


*Figure 11 — Hydraulic cross section of the Cypress Plain fluid flow system showing groundwater flow patterns and depth of groundwater system (from Toth & Corbet, 1987).*

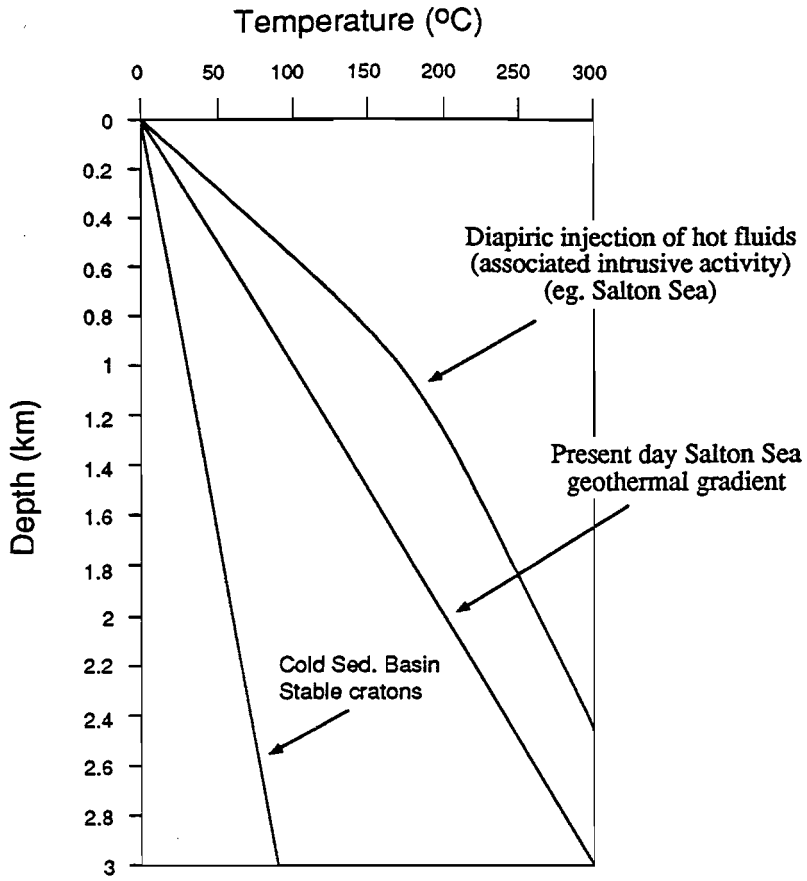


*Figure 12 — Range of possible geothermal gradients for sedimentary basins. Salton Sea examples after McKibben* et al. *(1988), cold sedimentary basin example after Fyfe* et al. *(1978).*

reach these depths. The path depicting diapiric uprise of the fluid would necessitate boiling at just over 1 km depth and so an alternate path, via the Tawallah Fault, is inferred to enable the hot fluid to reach shallow levels before boiling. The source fluids are therefore suggested by Figure 12 to have travelled from depths in the order of 2–3 km.

### Heat source

Known geothermal gradients from a variety of sedimentary basins are shown on Figure 12. The fluids in the Tawallah Fault system define a geothermal gradient akin to that of the present day Salton Sea system, rather than a cool cratonic basin. However, the Salton Sea geothermal gradient is elevated due to widespread intrusive activity in an active extensional environment (McKibben *et al.*, 1988). As previously discussed, the Tawallah Fault was activated as a wrench fault system some time after the cessation of sedimentation associated with Mid-Proterozoic rifting and related volcanism, and so magmatic input of heat is unlikely.

An alternate heat source for the fluids in the Tawallah Fault system could be high-heat-producing granites in the Early Proterozoic basement. Solomon and Heinrich (1992) have suggested that the McArthur River deposit may have formed from basement fluids driven by high heat flow associated with long-lived radiogenic heat production from U–Th enriched Lower Proterozoic granites. Their rationale is that *"the rate of decay of high initial geothermal gradients related to initial extension, crustal thinning and magmatism of the McArthur Basin is probably too fast to have persisted through to ore forming time"*. McNaughton *et al.* (1993) suggest that high-heat-producing granites *"may maintain temperatures of >200°C "indefinitely" (e.g. $10^9$ years) if their U–Th–K contents are sufficiently high and they are blanketed by a few kilometres of insulating or heat-producing cover"*.

Considering that the Tawallah Fault wrench system has been active after the cessation of sedimentation, there is less than 2 km to the basement, and that there is still warm spring activity 25 km to the west at the Nathan Group/Roper Group unconformity, the notion of high-heat-producing granites elevating fluid temperatures at depth is not unreasonable.

Another alternative is that wrench movement on the Tawallah Fault was not related to the Post-Roper Inversion, but occurred during active extension and related volcanism earlier in basin evolution. However, the findings of Rogers (1993) suggests that this option is not likely.

## Fluid flow model

A schematic model (Fig. 13) is proposed to explain the fluid dynamics during late stage wrenching of the Tawallah Fault system based on the fluid inclusion data and on the numerical modelling studies of Cooke (1993).

In the initial stages, deep saline oxidised formation waters within the basal clastic Tawallah Group became heated by high-heat-producing granites in the Early Proterozoic basement. Rupture propagation during wrench movement on the Tawallah Fault is arrested at the transtensional (dilational) position along the structure, in the Batten Range. Enhanced fracture permeability was created and localised pressure imbalances adjacent to the fault lead to the development of hydraulic implosion breccias (Sibson, 1989). Deep, heated fluids ascend towards the surface along the Tawallah Fault and the network of secondary structures, boiling and precipitating hematite–quartz assemblages in breccia matrices and dilational veins. The fluids also mix with cooler, less saline meteoric or connate waters which filter into the system.

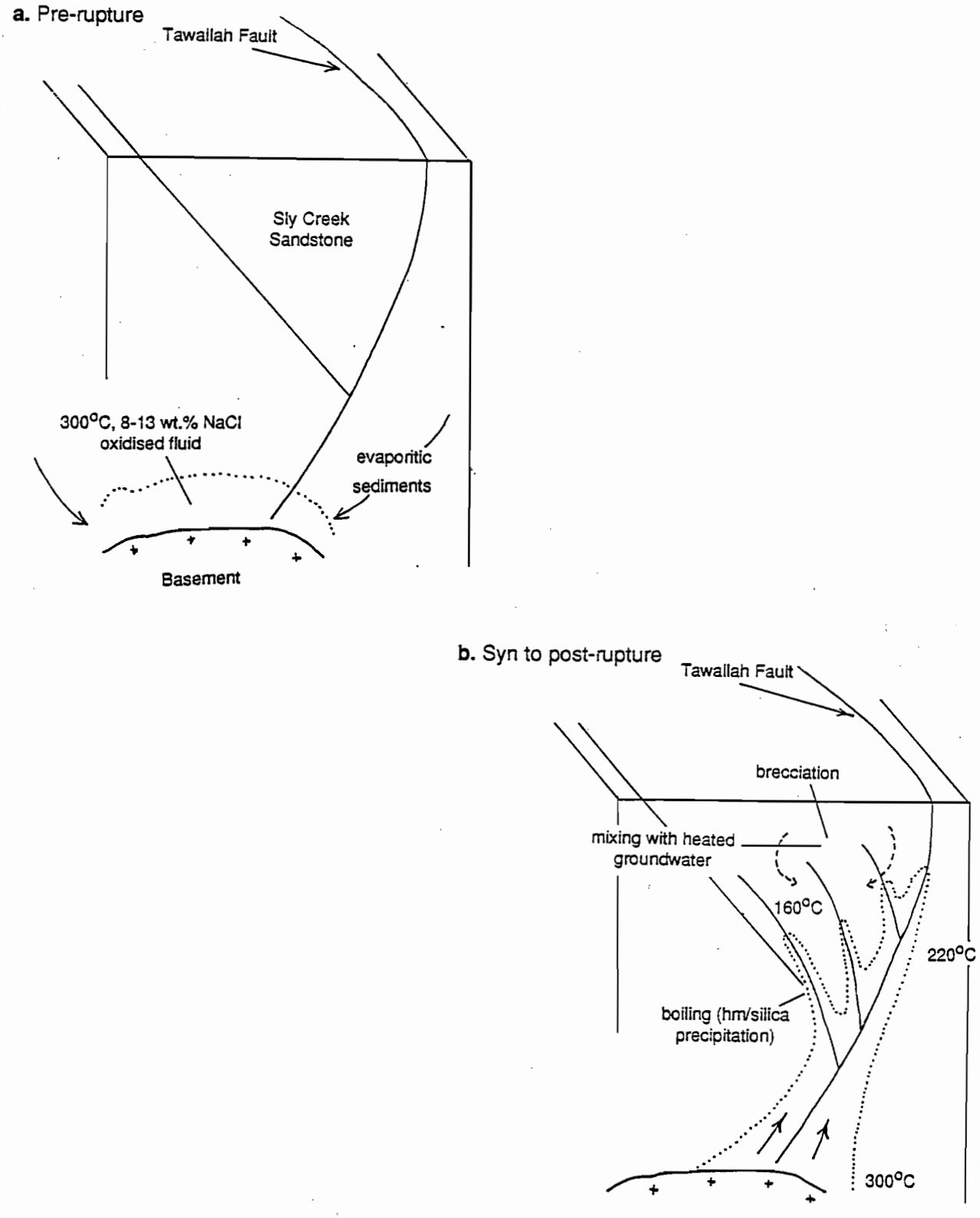


*Figure 13 — Fluid flow model for post-Roper wrench movements on the Tawallah Fault system. (a) Pre-rupture: accumulation of deep, saline fluid reservoir heated by high-heat-producing granites in the basement, (b) syn- to post-rupture: fluid migration through the system.*

The observed systematic decrease in temperature away from the Tawallah Fault may be predicted by this model as fluids migrating out along secondary structures probably cooled quicker due to lower fluid/rock ratios and may have mixed with cooler local groundwaters. The inclusions within the Tawallah Fault that record moderate salinity values (8–12 eq. wt.% NaCl) and high temperatures may also be explained in this way.

This model is proposed for an episode of fluid flow and related mineral precipitation during a single rupturing event. In reality, multiple seismic ruptures could be expected during post-Roper evolution of the Tawallah Fault that may or may not be associated with fluid influx. However, the mechanisms that induce fluid flow and the physical processes associated with fluid influx will be similar for successive rupture events along a structure (Sibson, 1989). As the fluid inclusion data remains fairly consistent over the study area, it is conceivable that multiple fluid generations could be represented, provided that a similar source was utilised during each rupture event.

## Conclusions

1. The fluids that passed through the Tawallah Fault system during late stage wrench movement are characterised by moderate to high temperatures and bimodal salinities.

2. The Tawallah Fault saw significantly hotter fluids (210°C) than did its associated secondary structures (≈160°C).

3. Enthalpy/chloride plots suggest that cooling by boiling and by mixing of a hot (300°C), moderately saline (8–13 eq. wt.% NaCl) fluid generated the spread in salinity data. A combination of boiling and mixing processes were responsible for the deposition of the hematite-quartz mineralisation found in the fault breccias (assuming an initial oxidised fluid).

4. Homogenisation temperatures from boiling populations of inclusions reflect a maximum depth for boiling at 200 m (assuming an open system). The source fluids are suggested to have been generated at depths of 2–3 km.

5. High-heat-producing granites are required for a heat source as the system was active well after rifting and volcanism had occurred.

6. The presence of hot, saline oxidised fluids lend great potential for mineralisation throughout the entire history of the southern McArthur Basin along the Tawallah Fault and similar fault systems where reduced (graphite and/or pyrite bearing) sediments are juxtaposed against the structure.

7. The results may also provide an insight into processes that occurred along the Emu Fault system during the formation of base metal mineralisation at McArthur River.

## References

Bull, S., 1993. Unpublished rogress report — sedimentology and volcanology of the southern McArthur Basin. *AMIRA/ARC project 384, unpublished report no.* 4: 33–53.

Cooke, D.R., 1993. Transport and deposition of base metals from high temperature (250°C) sedimentary brines. *AMIRA/ARC project P.384, unpublished report no. 4* : 111–130.

Fournier, R.O., 1979. Geochemical and hydrologic considerations and the use of enthalpy-chloride diagrams in the prediction of underground conditions in hot-spring systems. *J. Volcan. Geotherm. Res., 5* : 1–16.



Fyfe, W.S., Price, N.J. and Thompson, A.B., 1978. *DEVELOPMENTS IN GEOCHEMISTRY 1: FLUIDS IN THE EARTH'S CRUST.* Elsevier: Amsterdam: 383 pp.

Gray, D.R., Gregory, R.T. and Durney, D.W., 1994. Vein and fabric development within quartzo-feldspathic turbidite successions: implications for the role of fluid during deformation. *Geol. Soc. Aust. (abs)*, 36 : 56.

Haas, J.L., Jr., 1971. The effect of salinity on the maximum thermal gradient of a hydrothermal system at hydrostatic pressure. *Econ. Geol.* 66 : 940–946.

Haas, J.L., Jr., 1976. Physical properties of the coexisting phases and the thermochemical properties of the $H_2O$ component in boiling NaCl solutions. *U.S. Geol. Surv. Bull. 1421-A*: 73 pp.

Hall, D.L., Sterner, S.M. and Bodnar, R.J., 1988. Freezing point depression of NaCl-KCl-$H_2O$ solutions. *Econ. Geol.*, 83: 197–202.

Henley, R.W., Truesdell, A.H. and Barton, P.B., Jr., 1984. Fluid-mineral equilibria in hydrothermal systems. *Rev. Econ. Geol.* 1: 267.

Keele, R.A., 1993. The histories of some faults in the southern McArthur Basin: evidence for an end-Tawallah uplift and a preliminary analysis of stress related to post-McArthur and post-Roper compressions. AMIRA/ARC project 384, unpublished report 4: 55–86.

McKibben, M.A., Andes, J.P., Jr. and Williams, A.E., 1988. Active ore formation at a brine interface in metamorphosed deltaic sediments: the Salton Sea geothermal system, California. *Econ. Geol.* 83: 511–523.

McNaughton, N.J., Pollard, P.J., Stacey, J., Groves, D.I. and Taylor, R.G., 1993. An extreme high-heat producing Sn–W granite from the Bushveld Complex: evidence for a long-lived hydrothermal system. *Geol. Soc. Aust. (abs)* 34: 46–47.

Plumb, K.A., Ahmad, M. and Wygralak, A.S., 1990. Mid-Proterozoic basins of the North Australian Craton — regional geology and mineralisation, *In* F.E. Hughes (Ed.): Geology of the Mineral Deposits of Australia and Papua New Guinea. The Australasian Institute of Mining and Metallurgy, Melbourne: 881–902.

Roedder, E., 1984. *FLUID INCLUSIONS. Rev. in Mineral.* 12 : 644 pp.

Roedder, E. and Bodnar, R.J., 1980. Geologic pressure determinations from fluid inclusion studies. *Ann. Rev. Earth Planet. Sci.* 8 : 263–301.

Rogers, J.R., 1993. The structural setting of the Tawallah Group, southern McArthur Basin, Northern Territory: implications for an early tectonic event. AMIRA/ARC Project P.384, unpublished report No. 4: 17–31.

Sibson, R.H., 1989. *STRUCTURE AND MECHANICS OF FAULT ZONES IN RELATION TO FAULT HOSTED MINERALISATION.* Dept. Geol. Sci. Uni. Calif.: Aust. Min. Foundation: 66 pp.

Solomon, M. and Heinrich, C.A., 1992. Are high-heat-producing granites essential to the origin of giant lead–zinc deposits at Mount Isa and McArthur River, Australia? *Explor. Mining Geol. 1 (1)* : 85–91.

Toth, J. and Corbet, T., 1987. Post-Palaeocene evolution of regional groundwater flow systems and their relation to petroleum accumulations, Taber Area, southern Alberta, Canada. *In* Goff J.C. and Williams B.P.J. (Eds.): *Fluid flow in sedimentary basins and aquifers.* Geol. Soc. Spec. Publ. 34: 45–77.

# Alteration vectors applied to the Mount Isa Pb-Zn system: a review of existing data

**Peter McGoldrick**

## Summary

This presentation will review some of the published available whole rock geochemical data for the Mount Isa mineralised sequence and associated Mount Isa Group sedimentary rocks.

The data comprise:

(i) a large (>1,000 samples) multi-element suite from Smith and Walker (1970); these data were measured by carbon-rod spark-source emission spectroscopy at the BMR in the late 1960s;
(ii) twenty-seven samples from Scott & Taylor (1979);
(iii) eighty-seven samples from McGoldrick (1986); these latter two sample sets were analysed by XRF and AAS techniques at CSIRO North Ryde and University of Melbourne, respectively, and will be dealt with separately from the older data of Smith and Walker (1970).

The Smith & Walker (1970) data set has a wider (both spatial and stratigraphic) coverage than the other two sets but the quality of much of it is difficult to assess. Nevertheless, the elements required to calculate the Alteration Index and $MnO_D$ (Large and McGoldrick, 1993) appear to have been measured well enough for useful comparisons to be made. Their data came from the following diamond drill holes:

- **NL21/21A** drilled through the Hilton orebodies

- **Quartzite No.1** in barren Mount Isa Group sediments (Spear/Kennedy Siltstone and Urquhart Shale) about 5 km south of Hilton

- **Biotite No 2** in metamorphosed/metasomatised Native Bee Siltstone south of the Crystallena Block, 10 km south of Isamine

- **Mount Novit No. 1** in Moondarra Siltstone at the north end of the Mt Novit gossans about 15 km south of Isamine.

Three underground and a surface hole from Mt Isa:

- **G27W** unmineralised Urquhart Shale up-dip from 1100 Cu orebody
- **W23W** drilled through the outer silica-dolomite envelope of 1100 orebody
- **PE365** Native Bee siltstone in the footwall of 1100 orebody
- **W26W** a surface hole through Spear/Kennedy Siltstone and Urquhart Shale inthe hangingwall of 1100 orebody.

The two newer data sets are a combination of grab samples from drill-core and underground samples and most are precisely located in relation to mineralisation. The data from McGoldrick (1986) includes samples collected along strike within

12 orebody and across strike encompassing mineralisation and barren inter-ore beds between 5 orebody and 14/80 orebody.

Analyses of the Smith & Walker (1970) data indicate that anomalous A1 and $MnO_D$ are present as an envelope around the Hilton orebodies, and suggest the position of the Mt Novit mineralisation south of Mt Novit No. 1. Their Isa mine samples show a variable AI and $MnO_D$ enrichment and a simple interpretation of these results is difficult. The proximity of many of the samples to the 1100 orebody silica–dolomite alteration envelope may account for this.

The newer data, however, display a strong AI and Zn relationships, similar to the Lady Loretta trend and elevated $MnO_D$ values $\geq 1.0\%$ persist in barren inter-ore beds. Graphs summarising these relationships will be presented at the meeting.

## References

Large, R.R. & McGoldrick, P.J., 1993. Deposit Halos 5. Primary geochemical halos related to Proterozoic sediment hosted Pb–Zn deposits and applications to exploration, CODES: AMIRA/ARC Project P384, unpublished report no. 3: 31–62.

McGoldrick, P.J., 1986. Volatile and precious metal geochemistry of the Mt Isa ores and their host rocks. Unpubl. PhD thesis, University of Melbourne.

Scott, K.M. & Taylor, G.F., 1977. Geochemistry of the Mammoth copper deposit, NW Queensland. *Aust. J. Geochem. Explor.* 8: 1`53–168.

Smith S.E. & Walker, K.R., 1970. Mt Isa geochemical project — analyses of core samples. *BMR Record* 47.